

**KARADENİZ TECHNICAL UNIVERSITY
THE GRADUATE SCHOOL OF NATURAL AND APPLIED SCIENCES**

DEPARTMENT OF PHYSICS

**GENERAL NEUTRINO INTERACTIONS WITHIN COHERENT ELASTIC NEUTRINO-NUCLEUS
SCATTERING**

MASTER THESIS

MUHAMMAD FAUZI MUSTAMIN

**JUNE 2021
TRABZON**



KARADENİZ TECHNICAL UNIVERSITY
THE GRADUATE SCHOOL OF NATURAL AND APPLIED SCIENCES

DEPARTMENT OF PHYSICS

**GENERAL NEUTRINO INTERACTIONS WITHIN COHERENT ELASTIC
NEUTRINO-NUCLEUS SCATTERING**

Muhammad Fauzi MUSTAMIN

**This thesis is accepted to give the degree of
"MASTER OF SCIENCE"**

**By
The Graduate School of Natural and Applied Sciences at
Karadeniz Technical University**

The Date of Submission : 17 / 05 / 2021

The Date of Examination : 21 / 06 / 2021

Supervisor : Assoc. Prof. Dr. Mehmet DEMİRCİ

Trabzon 2021

PREFACE

Neutrino interaction with matter has reached one of its great triumphs as its coherent interaction with the nucleus was successfully witnessed. This event assigns a milestone to neutrino physics and will be paved to a more comprehensive study to better understand other nature unexplained phenomena. One of the possible ways is by introducing a general form of interactions, which is the objective of this manuscript. Further advancement of the process may be conducted in other studies, such as neutrino magnetic moment, dark matter direct detection, etc.

During the completion of this work, I would like to deliver my heartfelt respect to my supervisor, Assoc. Prof. Mehmet Demirci. It is a great privilege for me to be advised by him. I have gained a lot from his knowledge and wide horizon on high energy physics as well as his wise advice on academia and beyond. His dedication and encouragement have shaped my path in doing research independently. I also express my gratitude to Prof. Ahmet Hakan Yılmaz for sharing his experience and meaningful suggestions.

Furthermore, my sincere gratitude is toward the "Presidency of Turks Abroad and Related Communities (YTB)" for introduced the magnificent Trabzon and granted the opportunity to conduct my Postgraduate study at Karadeniz Technical University. I extend this to my Indonesian companions, as well as those from other continents who have made a vibrant environment during my study period.

Last but not least, I would like to thank my beloved mother Bahjah, my father Mustamin, my brother Mukram and my sisters Nadhrah and Nihlah. They are the supporting system from afar during my journey in Anatolia. I finally thank the Almighty, which only with His benevolence all particles and forces could form perfect harmony in the observed, as well as in the yet unobserved universe.

Trabzon, May 2021

Muhammad Fauzi MUSTAMIN

STATEMENT OF ETHICS

I declare this thesis entitled "General Neutrino Interactions within Coherent Elastic Neutrino-Nucleus Scattering" is original research. It is conducted by me under the supervision of Assoc. Prof. Mehmet Demirci and has not been submitted to any previous university or published in any institution. I confirm that the work submitted is my own work. The data and information from other researches have been cited in the reference section. Publication ethics and rules have been obeyed during the completion of this work and I am fully responsible for every possible outcome of this work. 21/06/2021

Muhammad Fauzi MUSTAMIN

CONTENTS

	<u>Page No.</u>
PREFACE	III
STATEMENT OF ETHICS	IV
CONTENTS	VI
SUMMARY	VII
ÖZET	VIII
LIST OF FIGURES	X
LIST OF TABLES	XI
ABBREVIATIONS	XII
1. INTRODUCTION	1
1.1. The Early Era of Neutrino	1
1.2. Neutrino Sources	3
1.3. Neutrinos in the Standard Model	7
1.4. Neutrino Properties	10
1.4.1. Neutrino Flavors	10
1.4.2. Chirality and Helicity	11
1.4.3. Dirac and Majorana Neutrinos	13
1.4.4. Neutrino Oscillation	16
1.5. Outline of Thesis	17
2. COHERENT ELASTIC NEUTRINO-NUCLEUS SCATTERING	19
2.1. Theoretical Formulation of CEvNS	19
2.1.1. Spinless Nucleus	20
2.1.2. Dirac Nucleus	24
2.2. Criteria of Coherency	26
2.3. Event Rates and Number of Events	27
2.4. CEvNS Observations	28

3.	GENERAL NEUTRINO INTERACTIONS	32
3.1.	Non-standard Interactions of Neutrino	32
3.2.	Simplified Model	34
3.2.1.	Matching the nucleus current	35
3.2.1.1.	Scalar Interaction	35
3.2.1.2.	Pseudoscalar Interaction	36
3.2.1.3.	Vectorial Interaction	38
3.2.1.4.	Axial-vector Interaction	39
3.2.1.5.	Tensorial Interaction	41
3.2.2.	Differential cross-section	42
3.2.2.1.	Scalar Contribution	43
3.2.2.2.	Pseudoscalar Contribution	44
3.2.2.3.	Vector Contribution	45
3.2.2.4.	Axial-vector Contribution	48
3.2.2.5.	Tensor Contribution	51
3.3.	Summary of Generalized Interactions	52
4.	NUMERICAL RESULTS AND DISCUSSIONS	53
4.1.	Kinematics and Form Factor Effect	53
4.2.	Standard Model	55
4.3.	Non-Standard Interactions	56
4.4.	Simplified Model	59
4.5.	Analysis of COHERENT Data	61
4.5.1.	Non-Standard Neutrino Interactions	63
4.5.2.	Simplified Model	64
5.	CONCLUSIONS	67
6.	REFERENCES	69
7.	APPENDICES	75
7.1.	CONVENTION AND NOTATION	75
7.2.	RELATED FEYNMAN RULES	76
7.3.	KINEMATICS	76
	CURRICULUM VITAE	

Master Thesis
Summary

GENERAL NEUTRINO INTERACTIONS WITHIN COHERENT ELASTIC
NEUTRINO-NUCLEUS SCATTERING

Muhammad Fauzi MUSTAMIN

Karadeniz Technical University
The Graduate School of Natural and Applied Sciences
Physics Graduate Program, High Energy and Plasma Physics
Supervisor: Assoc. Prof. Mehmet DEMİRCİ
2021, 80 pages

In this work, we investigate the effect of general neutrino interactions within the Coherent Elastic Neutrino Nucleus Scattering (CEvNS). In this process, neutrino collides with the nucleus via a neutral boson exchange as a whole. We give the standard model (SM) formulation of the process by considering the nucleus as spin-0 and spin-1/2. Coherent criteria of the interaction are also discussed by showing the form factor effect for several target nuclei. For the general interaction, we consider two models: non-standard interactions (NSI) and a simplified model. We show the differential cross-section effect of each model with the SM predictions to look for new physics behaviors. Indication of new physics from the NSI is presented in a parameter space of interaction strength of flavor conserving and flavor violation case. Recent values of interaction strength for the NSI for both considerations are used to show the difference from the SM. The simplified model consists of all the possible invariant bilinear combinations; scalar, pseudoscalar, vectorial, axial-vector, and tensorial interactions. We consider low energy scale approximation in the calculation of new physics contributions so that the momentum transfer term in the propagator is included. The constraints on free parameters of both models, namely interaction strength for NSI and coupling-mass for the simplified model, are given with 68% and 90% CL using data from the COHERENT experiment.

Keywords: Neutrino, CEvNS, General neutrino interactions, NSI.

Yüksek Lisans Tezi
ÖZET

KOHERENT ELASTİK NÖTRİNO-ÇEKİRDEK SAÇILMASI İLE GENEL NÖTRİNO
ETKİLEŞMELERİNİN İNCELENMESİ

Muhammad Fauzi MUSTAMIN

Karadeniz Teknik Üniversitesi
Fen Bilimleri Enstitüsü
Fizik Anabilim Dalı, Yüksek Enerji ve Plazma Fiziği
Danışman: Doç. Dr. Mehmet DEMİRCİ
2021, 80 sayfa

Bu çalışmada, genel nötrino etkileşimlerinin Koherent Elastik Nötrino Çekirdek Saçılması (CEvNS) üzerindeki etkisini inceliyoruz. Bu süreçte, nötrino, çekirdeğin yapısını bozmaksızın, bir nötr bozon değiş-tokuşu aracılığıyla çekirdekten saçılır. Çekirdeği hem spin-0 hem de spin-1/2 olarak dikkate alarak, standart model (SM)'de CEvNS için tüm formülasyonu türetiyoruz. Ayrıca, birkaç hedef çekirdek için form faktörü etkisi üzerinden koherentlik kriterini tartışıyoruz. Bu bağlamda, genel nötrino etkileşmelerini iki farklı yoldan ele alıyoruz: Standart Olmayan Nötrino Etkileşmeleri (NSI) ve Basitleştirilmiş model. SM ötesi Yeni Fizik davranışlarını incelemek için her modelin diferansiyel tesir kesitini SM tahminleriyle karşılaştırıyoruz. NSI'den gelen Yeni Fizik katkıları, çeşni korumlu ve çeşni ihlali durumları için çiftlenim parametrelerinin uzayında sunuluyor. Burada, SM'den sapmayı göstermek için parametrelerin güncel değerleri kullanılmıştır. Basitleştirilmiş model çerçevesinde, tüm olası invaryant bilinear kombinasyonları, yani; skaler, pseudoskaler, vektör, aksiyel-vektör ve tensör etkileşmeleri inceliyoruz. Yeni fizik katkılarını düşük enerji ölçeğinde hesaplıyoruz. Sonuç olarak her iki model için, COHERENT deneyi verilerini kullanarak serbest parametreler uzayı (NSI için etkileşme parametreleri ve basitleştirilmiş model için çiftlenim-kütle parametre uzayı) üzerindeki kısıtlamaları %68 ve %90 güvenirlilik düzeyinde elde ediyoruz.

Anahtar Kelimeler: Nötrino, CEvNS, Genel nötrino etkileşmeleri, NSI.

LIST OF FIGURES

	<u>Page No.</u>
Figure 1. β -decay with Four-fermion coupling.....	1
Figure 2. Experimental consideration of β -decay of ^{60}Co into $^{60}\text{Ni}^*$, e_L^- and $\bar{\nu}_R$	3
Figure 3. The neutrino spectrum from various sources.	4
Figure 4. Process of the proton-proton cycle and CNO cycle inside the sun	6
Figure 5. The $\sin^2 \theta_W$ as a function of energy scale μ	9
Figure 6. β -decay in the SM with mediator W^-	10
Figure 7. Helicity interpretation of neutrino and antineutrino.....	13
Figure 8. CEvNS process in the SM.....	19
Figure 9. Various processes involving neutrino.....	20
Figure 10. Behavior of α and ξ for several targets with neutrino flux from π -DAR, reactor and solar neutrino (Sharma <i>et. al.</i> , 2021).	27
Figure 11. Neutrino flux from π -DAR source with $\eta = 1$	29
Figure 12. CEvNS with scalar mediator.....	43
Figure 13. CEvNS with pseudoscalar mediator.....	45
Figure 14. CEvNS with vectorial mediator.....	46
Figure 15. CEvNS with axial-vector mediator.....	48
Figure 16. CEvNS with tensorial mediator.....	51
Figure 17. Behavior of T_{max} for some different nucleus (left). Effect of T_{max} for high E_ν (right).....	54
Figure 18. T -dependent (left) and Q -dependent of the Helm form factor (right).....	54
Figure 19. SM CEvNS differential (left) and its total cross-section spectrum (right) for five nucleus targets.....	55
Figure 20. Differential rate of SM CEvNS for five nucleus targets.....	56
Figure 21. CEvNS differential cross section with recent NSI parameters.	57
Figure 22. Bound prediction of the NSI parameters in CEvNS process.	58
Figure 23. The differential cross-section for CEvNS process with the simplified model.	60
Figure 24. Predicted CEvNS event per 2 PE at COHERENT.	62
Figure 25. $\Delta\chi^2$ corresponds to 1-bin analysis of COHERENT data.	62

Figure 26. Allowed regions of the NSI FC (upper) and FV (lower) parameter space with 68% (red) and 90% (blue) CL from COHERENT data.	63
Figure 27. Lower exclusion bound on parameter space of $g_S^2 - m_S$ (left) and $g_S - m_S$ (right) with 68% (red) and 90% (blue) CL.....	64
Figure 28. Same as Figure 27 for pseudoscalar mediator.	65
Figure 29. Same as Figure 27 for vector mediator.	65
Figure 30. Same as Figure 27 for axial-vector mediator.	66
Figure 31. Same as Figure 27 for tensor mediator.	66
Figure 32. Framework of kinematics for CEvNS process.....	77



LIST OF TABLES

	<u>Page No.</u>
Table 1. Irreducible representation of the SM $(d_{SU(3)}, d_{SU(2)})_Y$	9
Table 2. Some suitable experiments around the globe for detecting CEvNS.	31
Table 3. Summary of quantities from simplified model.....	52
Table 4. Key properties from several experiments.....	53
Table 5. Considered NSI parameters for plotting.....	56
Table 6. Values of the simplified parameters.	59
Table 7. Significance value and its corresponding degree of freedom.	61

ABBREVIATIONS

ARIANNA	Antarctic Ross Ice-Shelf Antenna Neutrino Array
BBN	Big-bang nucleosynthesis
BSM	Beyond standard model
CC	Charged current
CE ν NS	Coherent elastic neutrino-nucleus scattering
CKM	Cabibbo-Kobayashi-Maskawa
CNB	Cosmic neutrino background
CNO	Carbon-Nitrogen-Oxygen
CONUS	COherent Neutrino nUcleus Scattering
DAR	Decay at rest
DM	Dark matter
DSNB	Diffuse supernova neutrino background
EW	Electroweak
FC	Flavor-conserving
FV	Flavor-violating
GUNS	Grand Unified Neutrino Spectrum
KARMEN	KAllsruhe Rutherford Medium energy Neutrino experiment
LSND	Liquid scintillator neutrino detector
NC	Neutral current
NSI	Non-standard interaction
QCD	Quantum Chromodynamics
QED	Quantum electrodynamics
RENO	Reactor experiment for neutrino oscillation
SM	Standard model
SNS	Spallation Neutron Source
TEXONO	Taiwan EXperiment On Neutrino
WIMP	Weakly interacting massive particle

1. INTRODUCTION

1.1. The Early Era of Neutrino

In the year 1930, a neutral particle was hypothesized by W.Pauli to address unknown missing energy in the β -decay. He proposed the existence of a weakly interacting fermion with the scale of the electron mass that responsible for this phenomenon. E. Fermi in 1932 then termed this elusive particle *neutrino* and considered it to be massless and neutrally charged (Fermi, 1934). The general form of the β -decay process that produces this particle can be written as

$$X(A,Z) \rightarrow Y(A,Z+1) + e^- + \bar{\nu}_e. \quad (1.1)$$

The initial atom X , with the atomic number Z and mass number A , decays into the final atom Y accompanied with an electron and an electron anti-neutrino. This process can be viewed at the nucleon level as neutron changes to a proton

$$n \rightarrow p + e^- + \bar{\nu}_e, \quad (1.2)$$

where the diagram describing this three-body decay mode can be pictured as a four-fermion vertex as in Figure 1. The amplitude of this process can be interpreted using the prescription

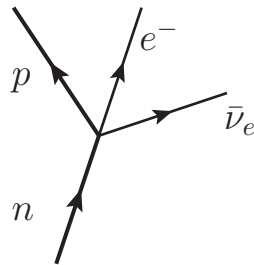


Figure 1. β -decay with Four-fermion coupling.

of quantum electrodynamic (QED) by introducing a coupling G_F to the interaction vertex,

$$\mathcal{M} = G_F(\bar{p}\gamma^\mu n)(\bar{e}\gamma_\mu \nu_e), \quad (1.3)$$

where p, n, e , and ν_e are spinors of proton, neutron, electron, and electron neutrino, respectively. In writing amplitude, we note that only particle spinor is entered so when we encounter an antiparticle, we can reverse the momentum to obtain particle spinor.

The amplitude in Eq.(1.3) which is a product of two currents in the same point in space-time is known as an effective theory. This four-point interaction, proposed by Fermi (Fermi, 1934), had been driven by many experimental attempts to explain the full features of the β -decay phenomena. The cross-section of the hypothetical neutrino was predicted to be $\sigma_{\bar{\nu}} \leq 10^{-44} \text{ cm}^2$ with energy $E_{\bar{\nu}} \approx 2 \text{ MeV}$ (Bethe and Peierls, 1934). The first detection was succeeded from the proton inverse β -decay experiment in a ton-mass scale Savannah River detector (Cowan *et al.*, 1956), which match the theoretical prediction. Their attempts became not only the first successful observation of anti-neutrinos but also the inspiration for the development of neutrino detectors. Since then, the β -decay experiments intensified to study the full physics of the phenomenon.

The general set-up of the β -decay experiments was aimed to observe emitted electron angle using specific nuclei under the influence of an external magnetic field, such that the nuclear spin-polarized along the field. The triumph of this experiment happened as Wu and her team (Wu *et al.*, 1957), using ^{60}Co ($J = 5$) nucleus, found a signature of maximal *parity violation* since the emitted electrons in their observation prefer the opposite direction from the nucleus spin. Figure 2 represents the experimental setting as well as the consequence of the process. Since the total spin $J = L + S$, where the angular momentum L does not change under parity, only the spin S can be in an arbitrary direction under the parity transformation. It implies that antineutrinos should be emitted in the same direction as the nuclear spin. With this observation, the emitted electron antineutrinos that accompanying electrons then should have the right helicities, a parameter that will be discussed further. This conclusion is achieved from the massless consideration of neutrino. This is the reason why neutrino (antineutrino) was considered to carry no mass and left-handed (right-handed) chirality.

The four-fermion interaction needs to be modified to accommodate this parity vio-

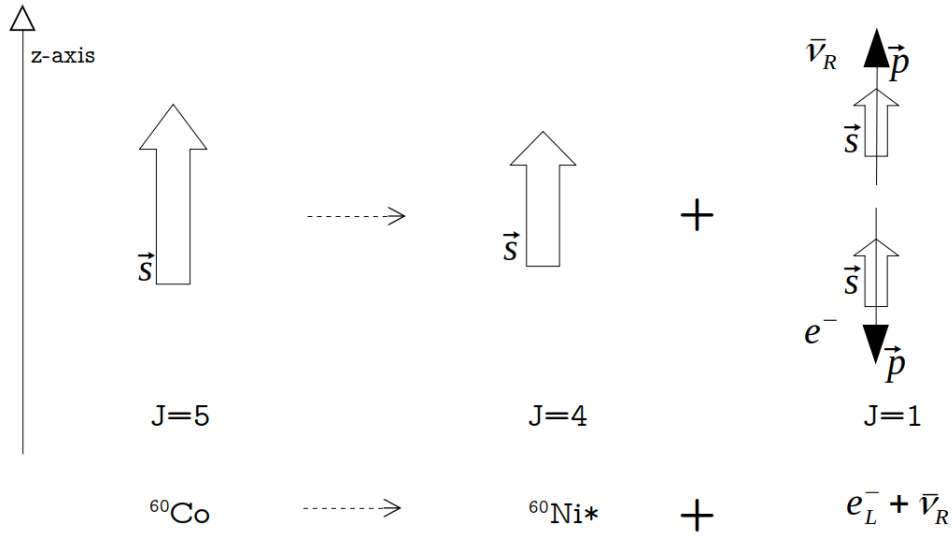


Figure 2. Experimental consideration of β -decay of ${}^{60}\text{Co}$ into ${}^{60}\text{Ni}^*$, e_L^- and $\bar{\nu}_R$.

lation. This was achieved by introducing a simple form of vector–axial-vector, $V - A$, to the weak current (Feynman and Gell-Mann, 1958; Sudarshan and Marshak, 1958; Sakurai, 1958). Hence, for the case of electron and its antineutrino

$$j_{\bar{\nu}_e e}^\mu = \bar{e} \gamma^\mu (1 - \gamma^5) \nu_e. \quad (1.4)$$

We can then write the previous amplitude, neglecting nucleon structure, as

$$\mathcal{M} = \frac{G_F}{\sqrt{2}} [\bar{p} \gamma^\mu (1 - \gamma^5) n] [\bar{e} \gamma_\mu (1 - \gamma^5) \nu_e]. \quad (1.5)$$

The factor $1/\sqrt{2}$ is conventional to compensate the new form of interaction so that the value of G_F stay still. The updated value of this coupling is $1.1663787(6) \times 10^{-5} \text{GeV}^{-2}$ (Zyla *et al.*, 2020). The scale of this coupling indicates a necessity for a new interaction at that time, a weak interaction.

1.2. Neutrino Sources

Neutrinos are available abundantly around us since they are fabricated from many sources. Neutrally charge, tiny mass (even considered massless), and only interact weakly with other particles made neutrinos unobserved with human's sense organs. Extremely sen-

sitive and generally large detector size is needed to detect neutrinos from their source, which can come from natural and artificial agents. The spectrum of neutrinos that pass through the earth is shown in Figure 3, an updated version for Grand Unified Neutrino Spectrum (GUNS) at the earth so far (Vitagliano *et al.*, 2020). Some of them are briefly discussed below.

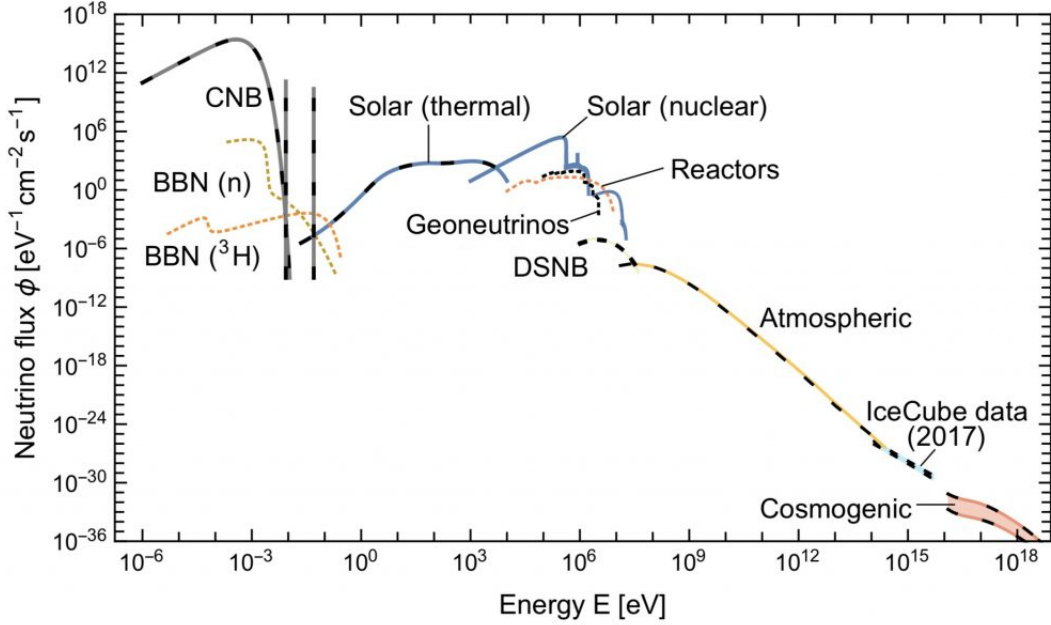


Figure 3. The neutrino spectrum from various sources on the surface of the Earth, taken from the improvement of GUNS (Vitagliano *et al.*, 2020). In this improved version, neutrino comes from CNB, BBN, and DSNB, as well as from cosmogenic sources have been included.

- **Relic Neutrino:** Relic neutrinos come from the early universe before the expansion period. In this phase, neutrinos together with photons were trapped as hot-plasma in an equilibrium state by electroweak interactions. They were exist through $\gamma\gamma \rightarrow \nu\bar{\nu}$ or $e^-e^+ \leftrightarrow \nu\bar{\nu}$, detected as cosmic neutrino background (CNB), and $n \rightarrow p + e^- + \bar{\nu}_e$ during the big-bang nucleosynthesis (BBN). When the temperature decrease, neutrinos decoupled and filled the universe as hot relics. Neutrinos then dominated dynamics of the early stage and structure formation of the universe as they have tiny masses. Cross-section of this case is predicted to be $\sigma \sim 10^{-56} \text{ cm}^2$ (Gelmini, 2004).
- **Cosmogenic:** Cosmogenic events have been recorded an ultra-high-energy cosmic rays up to 10^{20} eV (Bird *et al.*, 1994). This is the most energetic neutrino source had ever been observed, yet with the lowest flux. What kind of event-triggered this

acceleration still remains unanswered. Some candidates for this process are gamma-ray burst, a remnant of supernovae, and cosmic rays with Greisen-Zatsepin-Kuzmin (GZK) cutoff (Greisen, 1966; Zatsepin and Kuzmin, 1966). Detection of this event has been driving the development of the so-called neutrino telescope, such as IceCube (Aartsen *et al.*, 2015) in the South Pole and Antarctic Ross Ice-Shelf Antenna Neutrino Array (ARIANNA) (Barwick *et al.*, 2015) in the Antarctica.

- **Supernova:** Supernovas produce a high-flux neutrino when a core of a massive star collapse. The collapse occurs just in a small fraction of a second, however able to separate iron nuclei in the core into its nucleons components which then undergoes neutronization as free protons favored to capture electrons followed by neutrino product and formed what is called a protoneutron star. There is an exchange of energy from $p + e^- \rightleftharpoons n + \nu_e$ reactions. Neutrinos produced during this procedure rapidly escape the star core which now mostly composed of the neutron as burst. Only about 1% of energy in this process produce visible electromagnetic radiation, while the rest is radiated away as neutrinos. Supernova explosion was detected with 24 events of ν_e when the explosion of the Supernova 1987A reached earth in 1987; 11 at Kamiokande-II (Hirata *et al.*, 1987), 8 at Irvine-Michigan-Brookhaven (IMB) (Bionta *et al.*, 1987), and 5 at Baksan (Alekseev *et al.*, 1987). This is the first detection of neutrino from such a process so far. Additionally, this supernova explosion also produces the diffuse supernova neutrino background (DSNB) which has lower flux and weakly glow in the MeV scale (Horiuchi *et al.*, 2018). The aim of detecting this phenomenon is still in advancement.
- **Stars:** Stars that undergo thermonuclear reaction in their core produce neutrinos with large flux, especially the electron neutrino. As for our solar system, neutrinos appear as a product of nuclear fusion inside the core of the sun. Fusion reaction of hydrogen classified from pp chain (Bethe and Critchfield, 1938) as well as carbon-nitrogen-oxygen (CNO) cycle (Bethe, 1939) which can be expressed as $4p + 2e^- \rightarrow {}^4\text{He} + 2\nu_e + \text{energy}$. The released energy is $4m_p + 2m_e - m_{{}^4\text{He}} = 26.731$ MeV, where $4m_p = 28.296$ MeV, $m_e = 0.511$ MeV, and $m_{{}^4\text{He}} = 2(m_n - m_p) = 2(939.565 - 938.272)$ MeV. Schematic diagrams for both process are shown in Figure 4. Neutrinos from this source are termed solar neutrinos, which has been integrated in the standard solar model (SSM)

(Bahcall *et.al.*, 2000). Neutrinos reach the surface of the sun much earlier than pho-

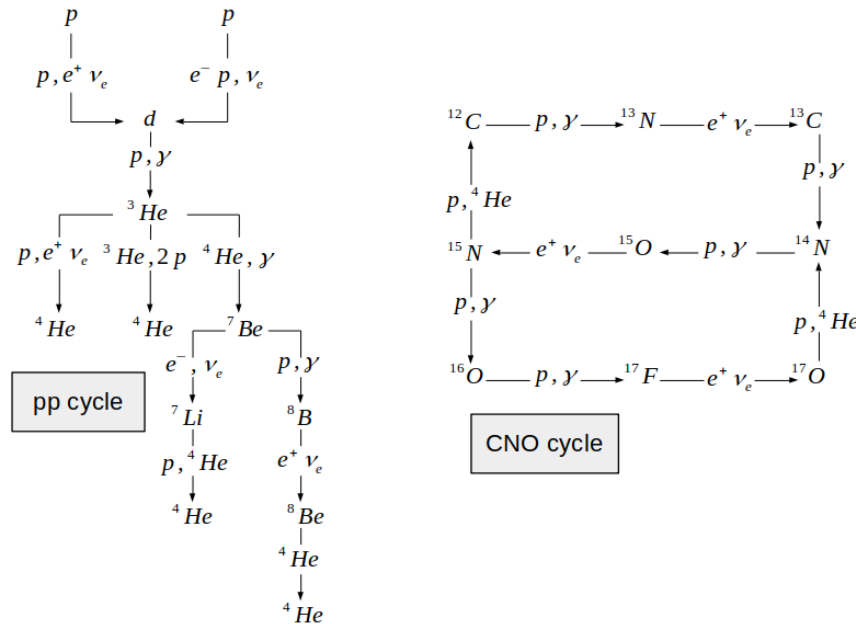


Figure 4. Process of the proton-proton cycle and CNO cycle inside the sun.

tons since only interact weakly, so that understanding solar neutrino is important to learn the interior of the sun. Despite availability, they arrive at the Earth's surface with relatively small energy.

- **Atmospheric Neutrino:** In the outer atmosphere of the earth, interactions of cosmic ray particles such as the proton, helium, or other massive nuclei, with atoms that construct the atmospheric layer generate short-lived mesons such as kaon or pion (Gaisser and Honda, 2002). Neutrinos commonly occur as a product of pion ($\pi^+ \rightarrow \mu^+ + \nu_\mu$) and kaon ($K^- \rightarrow \mu^- + \bar{\nu}_\mu$) decays, which then lead to muon decay ($\mu^- \rightarrow e^- + \bar{\nu}_e + \nu_\mu$, $\mu^+ \rightarrow e^+ + \nu_e + \bar{\nu}_\mu$). Neutrinos from this process are termed atmospheric neutrinos and arrive at the Earth's surface with relatively large energy, but smaller flux compared to the previous sources.
- **Earth Radioactivity:** Neutrinos are also produced beneath the Earth from the existing radioactive materials. The neutrino fluxes are mostly originated from the decay of Uranium and Thorium isotopes on the crust layer, only available as $\bar{\nu}_e$. The main reactions which produce this geoneutrinos can be expressed as $^{238}\text{U} \rightarrow ^{206}\text{Pb} + 8\alpha + 8e^- + 6\bar{\nu}_e + 51.7 \text{ MeV}$ or $^{232}\text{Th} \rightarrow ^{208}\text{Pb} + 6\alpha + 4e^- + 4\bar{\nu}_e + 42.7 \text{ MeV}$ (Fiorentini *et. al.*,

2007). Detection of these neutrinos can be conducted by observing their interactions with protons that followed by neutron capture, $\bar{\nu}_e + p \rightarrow n + e^+$. Since the elements responsible for its decay have a comparable lifetime with Earth's age, geoneutrinos provide useful information about geological activities, the generation of the magnetic field as well as the evolution of the Earth.

- **Particle Accelerator:** Neutrinos from particle accelerator can be obtained mostly from pion decays, which is produced from the collision of the proton beam with a fixed heavy target such as graphite. Massive target enables the produced decaying pion to come at rest. This is the reason this kind of accelerator is termed a decay at rest (DAR) experiment. With this procedure, all SM neutrino flavors can be produced. Such experiments have been used by Karmen (Armbruster *et al.*, 2002) and LSND (Athanasopoulos *et al.*, 1997) for studying, for example, neutrino oscillation, the weak form factor of nuclei, neutral current universality, and astrophysical neutrinos.
- **Nuclear Reactor:** Produced energy from nuclear power plants contains neutrino within a few MeV scale. Typically, $\bar{\nu}_e$ type is detected since the core of reactors undergo β -decay from the nuclear fission process. Nuclei with rich neutron become the main source of the fuel such as ^{235}U , ^{239}Pu , ^{238}U , and ^{241}Pu . Hence, a steady-state single flavor neutrino is produced from a nuclear reactor. Neutrinos detected from reactor based on proton's inverse β -decay $\bar{\nu}_e + p \rightarrow n + e^+$. Some of the nuclear reactors that aim to observe mixing angle and the possible appearance of sterile neutrino are Double CHOOZ (Abe *et al.*, 2012), RENO (Ahn *et al.*, 2012), and Daya Bay (An *et al.*, 2012).

1.3. Neutrinos in the Standard Model

The Standard Model (SM) is the state-of-the-art theory that explains all fundamental particles and their interactions. The model is constructed from a gauge theory of $SU(3)_C \times SU(2)_L \times U(1)_Y$ local symmetry (Glashow, 1961; Weinberg, 1967; Salam, 1968). The subscripts C, L , and Y stand for color, left-hand chirality, and hypercharge, respectively. The $SU(3)_C$ describes color charges from Quantum Chromodynamics (QCD), a model that explains the dynamics of quarks inside nucleons together with their binding gluons. The $SU(2)_L \times U(1)_Y$ is the group transformation that is obeyed by all the particles, quarks and

leptons, correspond to the electroweak interactions. After spontaneous symmetry breaking, the electroweak-interaction Lagrangian reads the following form (Zyla *et al.*, 2020):

$$\begin{aligned} \mathcal{L}_{SM(int)} = & -e \sum_i Q_i \bar{\psi}_i \gamma^\mu \psi_i A_\mu - \frac{g_W}{2\sqrt{2}} \sum_i \bar{\Psi}_i \gamma^\mu (1 - \gamma^5) (T^+ W_\mu^+ + T^- W_\mu^-) \Psi_i \\ & - \frac{g_W}{2 \cos \theta_W} \sum_i \bar{\psi}_i \gamma^\mu (g_V^i - g_A^i \gamma^5) \psi_i Z_\mu + \sum_i \bar{\psi}_i \left(i \not{\partial} - m_i - \frac{m_i}{v} H \right) \psi_i. \end{aligned} \quad (1.6)$$

This Lagrangian describes both quarks and leptons with their electroweak interactions with photon $A_\mu \equiv B_\mu \cos \theta_W + W_\mu^3 \sin \theta_W$, charged bosons $W_\mu^\pm \equiv (W_\mu^1 \mp W_\mu^2)/\sqrt{2}$, neutral boson $Z_\mu \equiv -B_\mu \sin \theta_W + W_\mu^3 \cos \theta_W$, and the Higgs boson H . Here θ_W denotes the weak mixing angle. Fermions are denoted by ψ_i , while its doublet representation Ψ stands for either quark $\begin{pmatrix} u_i \\ d_i' \end{pmatrix}$ or lepton $\begin{pmatrix} \nu_i \\ l_i \end{pmatrix}$. Note that $d' = \sum_j V_{ij} d_j$ where V_{ij} is known as Cabibbo-Kobayashi-Maskawa (CKM) matrix, responsible for quark flavor-mixing under the influence of weak interactions.

The first term in the Lagrangian describes electromagnetic interaction, where e stands for positron electric charge and Q for its sign. The next two terms are for weak interaction. It contains the electroweak coupling $g_W = e/\sin \theta_W$ with T^\pm stand for the weak isospin raising and lowering operators, and also the coupling of vector and axial-vector structure, defined as

$$g_V^i = T_3 - 2Q_i \sin^2 \theta_W, \quad g_A^i = T_3. \quad (1.7)$$

Here, T_3 and Q_i are respectively the weak isospin third component and the charge of fermion- i . The last component in the Lagrangian describes fermion kinetic and mass term, as well as its coupling to Higgs boson. The parameter $v \approx 246$ GeV is the vacuum expectation value (vev) of the Higgs field. The effective value of the sinus square of the weak angle is $\sin^2 \theta_W = 0.23153(4)$ (Zyla *et al.*, 2020). This value changes according to the energy scale as depicted in Figure 5, where results from various experiments are shown.

The elementary particles of the SM can be summarized as the gauge group irreducible representation in Table 1. It shows the fermions quantum numbers for each gauge group transformations. It can be seen that neutrinos are doublets under $SU(2)$ transformation, singlets in $SU(3)$, and own $-1/2$ hypercharge. Their electric charge vanishes since $Q = T_3 + Y$, where their weak isospin T_3 is $1/2$.

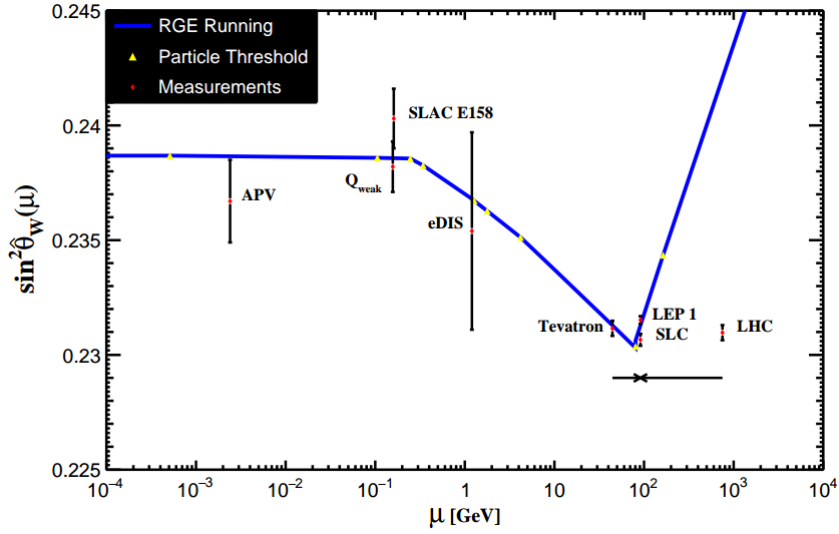


Figure 5. The $\sin^2 \theta_W$ as a function of energy scale μ , adapted from (Zyla *et al.*, 2020).

Table 1. Irreducible representation of the SM $(d_{SU(3)}, d_{SU(2)})_Y$.

$(\mathbf{1}, \mathbf{2})_{-1/2}$	$(\mathbf{3}, \mathbf{2})_{-1/6}$	$(\mathbf{1}, \mathbf{1})_{-1}$	$(\mathbf{3}, \mathbf{1})_{-2/3}$	$(\mathbf{3}, \mathbf{1})_{-1/3}$
$\begin{pmatrix} \nu_e \\ e \end{pmatrix}_L$	$\begin{pmatrix} u^i \\ d^i \end{pmatrix}_L$	e_R	u^i_R	d^i_R
$\begin{pmatrix} \nu_\mu \\ \mu \end{pmatrix}_L$	$\begin{pmatrix} c^i \\ s^i \end{pmatrix}_L$	μ_R	c^i_R	s^i_R
$\begin{pmatrix} \nu_\tau \\ \tau \end{pmatrix}_L$	$\begin{pmatrix} t^i \\ b^i \end{pmatrix}_L$	τ_R	t^i_R	b^i_R

Considering only neutrinos, where $g_V^i = g_A^i = 1/2$, the Lagrangian becomes

$$\mathcal{L}_{int}^{(\nu)} = -\frac{g}{2\sqrt{2}} \sum_{\alpha} \bar{\nu}_{\alpha} \gamma_{\mu} (1 - \gamma^5) l_{\alpha} W_{\mu}^{+} - \frac{g}{4 \cos \theta_W} \sum_{\alpha} \bar{\nu}_{\alpha} \gamma_{\mu} (1 - \gamma^5) \nu_{\alpha} Z_{\mu} + h.c., \quad (1.8)$$

with i runs up to the third lepton family and $h.c.$ stands for Hermitian conjugate. The Lagrangian shows that the neutrino interaction with lepton needs to be mediated by either W^{\pm} or Z^0 boson. Both mediators are respectively responsible for the standard charged and neutral current interactions. It can be seen clearly that the electroweak current has $V - A$ structure. This also indicates that neutrinos are left-handed in the SM, as have shown in Table 1.

The Fermi interaction from the previous β -decay then being resolved by the appear-

ance of a massive W boson as in Figure 6. The corresponding amplitude of this process can

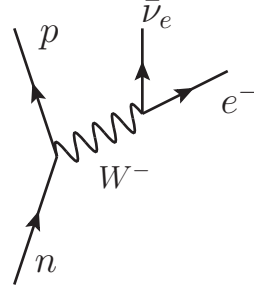


Figure 6. β -decay in the SM with mediator W^- .

be obtained from Feynman rules Appendix 7.2. as

$$\mathcal{M}_\beta = \frac{g_W^2}{8m_W^2} [\bar{p}\gamma^\mu(1-\gamma^5)n][\bar{e}\gamma_\mu(1-\gamma^5)v_e]. \quad (1.9)$$

Comparing to the G_F form, it is found that $\frac{G_F}{\sqrt{2}} = \frac{g_W^2}{8m_W^2}$. The mass of the W^\pm boson is about 80.4 GeV, hence using the value of G_F the weak coupling is $g_W = 0.65$.

1.4. Neutrino Properties

1.4.1. Neutrino Flavors

It is known that neutrinos come in three flavors. They correspond to each lepton type, e^- , μ^- , and τ^- . The ν_e type occurs in the β -decay process as mentioned previously in Eq.(1.2). The other two types were discovered from different channels. Possible processes of these are the pion decay for ν_μ and the leptonic-tau decay for ν_τ , respectively given in the following reactions

$$\pi^+ \rightarrow \mu^+ + \nu_\mu, \quad \tau^- \rightarrow \nu_\tau + e^- + \bar{\nu}_e. \quad (1.10)$$

These processes obey lepton number conservation, $L = 1$ for lepton, $L = -1$ for antilepton, and $L = 0$ for non-leptonic particle. Moreover, there are also number conservation for each generation denoted by L_e, L_μ , and L_τ which can have value of 1 for particle and -1 for antiparticle. Both reactions above and the β -decay for example obey this lepton conservation.

The restriction of three generations in the electroweak theory is determined from Z boson decay. The decay width consists of the summation of visible hadrons, e^-e^+ , $\mu^-\mu^+$, and $\tau^-\tau^+$, as well as invisible process widths. The branching ratio of the invisible final states for SM consideration would be due to the number of the light neutrino species N_ν . Therefore, the branching ratio of the invisible decay would be $\Gamma_{\text{inv}} = N_\nu\Gamma_{\nu\bar{\nu}}$ and from combined LEP observations (Schael *et al.*, 2006), the number of light neutrino species, excluding non-standard possibilities, is $N_\nu = 2.984 \pm 0.0082$. Hence, the SM should contain three neutrino flavors.

1.4.2. Chirality and Helicity

Concept of chirality comes from the chiral matrix γ^5 in the $V - A$ structure of weak interactions. It gives rise to two possible chiral operators, right and left projection, respectively defined as

$$P_R = \frac{1}{2}(1 + \gamma^5), \quad P_L = \frac{1}{2}(1 - \gamma^5). \quad (1.11)$$

The γ^5 matrix itself consists of the other γ -matrices

$$\gamma^5 = \gamma_5 = i\gamma^0\gamma^1\gamma^2\gamma^3 = \begin{pmatrix} 0 & 1 \\ 1 & 0 \end{pmatrix}. \quad (1.12)$$

The left(right)-handed operator belongs to $-1(+1)$ eigenvalue of the $P_L(P_R)$ operator for particle spinor and reversed case for antiparticle, since $\gamma_5^2 = 1$. Both operators satisfy the following properties

$$P_L + P_R = 1, \quad P_L P_R = P_R P_L = 0, \quad P_{R,L}^2 = P_{R,L}. \quad (1.13)$$

With these operators, any fermion and anti-fermion spinor can be decomposed respectively as

$$f_{R,L} = P_{R,L} f, \quad \bar{f}_{R,L} = P_{L,R} \bar{f}. \quad (1.14)$$

The weak current in Eq. (1.4) clearly contain left-handed chirality if factor 1/2 attached. Furthermore, we may calculate this current form to show that

$$\bar{e}\gamma^\mu \frac{1}{2}(1 - \gamma^5)v_e = \bar{e}\gamma^\mu P_L^2 v_e = \bar{e}P_R\gamma^\mu P_L v_e = \bar{e}_L\gamma^\mu v_{eL}. \quad (1.15)$$

It then appears that in the weak interactions, involved particles participate only with L -component spinor. This is in fact a direct implication of the parity violation, observed in the β -decay experiment.

Another important quantity in the electroweak process is the helicity of a particle. Helicity is defined as the projection of particle spin to its momentum, i.e. direction of particle motion. As for massless particle, or at least moves at the speed of light, helicity is equivalence with chirality. We can show this by firstly notice that the Dirac Lagrangian

$$\mathcal{L} = \bar{\psi}(i\partial - m)\psi, \quad (1.16)$$

gives the following equation of motions as a right or left-handed spinor

$$i\cancel{\partial}\psi_{R,L} = m\psi_{R,L}. \quad (1.17)$$

Since the four-momentum operator obeys $i\partial_\mu = p_\mu$, then $\cancel{p} = \gamma^\mu p_\mu = \gamma^0 E - \gamma^i p^i$. So for massless case, $|\vec{p}| = E$ and by multiplying $\gamma^5 \gamma^0$ from the left we have

$$(\gamma^5 \gamma^0 |\vec{p}| - \gamma^5 \gamma^0 \gamma^i p^i)\psi_{R,L} = 0. \quad (1.18)$$

Using the representation of the spin matrix

$$\Sigma^i = \gamma^0 \gamma^i \gamma^5 = \begin{pmatrix} \sigma^i & 0 \\ 0 & \sigma^i \end{pmatrix}, \quad (1.19)$$

we find that

$$\gamma^5 \psi_{R,L} = \frac{\vec{\Sigma} \cdot \vec{p}}{|\vec{p}|} \psi_{R,L} \equiv h \psi_{R,L}, \quad (1.20)$$

which shows that the chirality is the same with helicity for massless particle.

Recognizing the difference between chirality and helicity can be seen from the pion decay process to $\mu^+ \nu_\mu$ or to $e^+ \nu_e$. Spinless pion at initial set the decay products to have opposite spins. Since (ν_μ, ν_e) is left-handed in helicity, with the same chirality, the (μ^+, e^+) also need to have the left-handed helicity to preserve angular momentum conservation. But this requirement is forbidden as anti-particle must be in right-handed helicity. The process then contains a mixture of left-handed helicity for a right-handed chirality state (Naumov, 2011). This behavior can be depicted as in Figure 7.

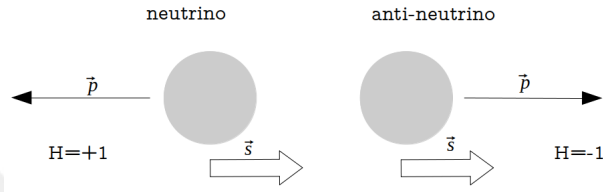


Figure 7. Helicity interpretation of neutrino and antineutrino.

In short, the $V - A$ structure of the weak process in the SM only couples left-handed neutrino and right-handed antineutrino as a consequence of $(1 - \gamma^5)$ correction in Eq.(1.4) from the initial proposed model that violates parity. Therefore, only

$$\nu_L = \frac{1}{2}(1 - \gamma^5)\nu, \quad \bar{\nu}_R = \frac{1}{2}(1 + \gamma^5)\bar{\nu}, \quad (1.21)$$

states are allowed in the SM framework.

1.4.3. Dirac and Majorana Neutrinos

Neutrinos appear to have a tiny mass as indicated from neutrino oscillation experiment. It makes neutrinos unique from other particles in the SM which are considered as Dirac type. The latest conducted experiments give the upper bound limits with 90% Confidence Level (CL) of their masses (Zyla *et al.*, 2020) :

$$m_{\nu_e}^{eff} < 1.1\text{eV}, \quad m_{\nu_\mu}^{eff} < 190\text{keV}, \quad m_{\nu_\tau}^{eff} < 18.2\text{MeV}. \quad (1.22)$$

In its early stage, neutrinos were considered as Dirac particles in the same spirit as the

other fermions. The process of weighting a Dirac particle can be made by introducing the following mass term

$$\mathcal{L}_m = -m\bar{\psi}\psi = -m(\overline{\psi_L + \psi_R})(\psi_L + \psi_R) = -m(\bar{\psi}_L\psi_R + \bar{\psi}_R\psi_L). \quad (1.23)$$

It shows that massive particle must have both left and right-handed components. But this adding by hand process is simply not allowed since it breaks gauge symmetry. The field ψ_L is a doublet in $SU(2)_L$ while ψ_R is a singlet $U(1)$. For this reason, fermion mass needs to be generated spontaneously with the Higgs mechanism (Higgs, 1964; Englert and Brout, 1964; Guralnik *et. al.*, 1964).

If neutrinos are considered to be the same as the other SM particles, we need three right-handed neutrinos. So that its mass term can be introduced by introducing Yukawa interaction

$$\mathcal{L}_Y^{Dirac} = -\bar{L}g_V\phi_c\nu_R - \bar{\nu}_Rg_V\phi_c^\dagger L \quad (1.24)$$

with L is a doublet $\begin{pmatrix} \nu_L \\ e_L \end{pmatrix}$, ν_R is a singlet, and $\phi_c = i\sigma_2\phi^*$ is a Higgs doublet conjugate, which

after spontaneous symmetry breaking becomes $\phi_c = \frac{1}{\sqrt{2}}\begin{pmatrix} v+h \\ 0 \end{pmatrix}$ with h is the Higgs field.

With this procedure, we obtain the Yukawa Lagrangian as

$$\mathcal{L}_Y^{Dirac} = -\frac{vg_V}{\sqrt{2}}(\bar{\nu}_L\nu_R + \bar{\nu}_R\nu_L) - \frac{g_V}{\sqrt{2}}(\bar{\nu}_L\nu_R + \bar{\nu}_R\nu_L)h. \quad (1.25)$$

The mass term of neutrino is then

$$m_\nu^{Dirac} = g_V \frac{v}{\sqrt{2}}. \quad (1.26)$$

Assuming $m_{\nu_e} < 1$ eV and since $v = 242$ GeV, we would then have $g_{\nu_e} < 10^{-11}$. This is bothering since for the other fermion, for example, $m_e \sim 0.5$ MeV $g_e \sim 10^{-6}$. This is in fact a hierarchy problem, why the same mechanism of obtaining mass lead to different coupling scale?

Experiments have been showing that they only appear as left-handed (right-handed)

particles (anti-particles). However, the $\bar{\nu}_e$ products of beta decay are not observed in the reaction with incoming ν_e and imply that both particles may be the same entities. If neutrinos are equal with their antiparticles, they are categorized as *Majorana* particles. The massiveness of neutrino is also accounted for with this Majorana proposal. This model could be sensitively observed from the neutrinoless double beta decay ($0\nu\beta\beta$) process.

If neutrinos are Majorana particles, the right-handed neutrinos should be the conjugate of the left-handed ones so that neutrinos are nothing but their own anti-neutrinos. For this purpose, we need a conjugate field

$$\psi^c = C\gamma^0\psi^* = C\bar{\psi}^T, \quad (1.27)$$

where C denotes the charge conjugation operator with properties $C = -C^{-1} = -C^\dagger = -C^T$ so that $\psi_R = \psi_L^c$. With this, a field then can be composed as $\psi = \psi_L + \psi_L^c$ and hence $\psi = \psi^c$. With this prescription, we may try to construct Yukawa interaction for this case by writing

$$\begin{aligned} \mathcal{L}_Y^{Majorana} &= -\bar{L}\phi_c g_\alpha (C(\bar{L}\phi_c)^T) + \text{h.c.} \\ &= -\bar{L}\phi_c g_\alpha C\bar{\phi}_c^T \bar{L}^T + \text{h.c.} \end{aligned} \quad (1.28)$$

where we have used $\bar{L} \rightarrow \bar{L}\phi^c$ to get singlet transformation (Hernandez, 2015), where g_α refers to Weinberg coupling. After breaking the symmetry we find

$$\mathcal{L}_Y^{Majorana} = -\frac{1}{2}g_\alpha v^2 \bar{\nu}_L \nu_L^c + \text{interaction term} + \text{h.c.} \quad (1.29)$$

The conventional form of Majorana mass term is

$$\mathcal{L}_m^{Majorana} = \frac{1}{2}(m\bar{\psi}\psi^c + m\bar{\psi}^c\psi), \quad (1.30)$$

so that the mass of Majorana neutrino is predicted to be

$$m_\nu^{Majorana} = g_\alpha v^2. \quad (1.31)$$

Since the field in Eq.(1.28) has $[M]^5$, the coupling g_α should have $[M]^{-1}$. We can relate this coupling with the neutrino as $g_\alpha = g_\nu/\Lambda$, where Λ is the place new physics enters. If there is

a Λ with a scale much greater than the ν , the hierarchy problem can emerge naturally through this Majorana mechanism.

1.4.4. Neutrino Oscillation

In its early stage, neutrinos are concerned massless with three distinct flavors. However, possible anomalies from solar and atmospheric neutrino observations (Fukuda *et al.*, 1998; Ahmad *et al.*, 2002) indicate that neutrinos possess to be massive. The two experiments showed that over a large distance, neutrinos undergo flavor transformation. It had been anticipated theoretically by B. Pontecorvo (Pontecorvo, 1957) and then later on elaborated by Maki, Nakagawa, and Sakata (Maki *et al.*, 1962). This phenomenon is known as neutrino oscillation.

In the formulation of neutrino oscillation, the mass and the flavor eigenstates are not identical. Three eigenstates, correspond to lepton family ν_e, ν_μ, ν_τ , can be connected with mass eigenstate ν_1, ν_2, ν_3 (or matter waves) by

$$\begin{pmatrix} \nu_e \\ \nu_\mu \\ \nu_\tau \end{pmatrix} = U_{PMNS} \begin{pmatrix} \nu_1 \\ \nu_2 \\ \nu_3 \end{pmatrix}. \quad (1.32)$$

U_{PMNS} denotes the commonly used mixing matrix in the lepton flavor sector (PMNS comes from the initial name of the above-mentioned scientists that built its foundation). Explicitly, each element of this matrix can be expressed generally as (Thomson, 2013)

$$U_{PMNS} = \begin{pmatrix} 1 & 0 & 0 \\ 0 & c_{23} & s_{23} \\ 0 & -s_{23} & c_{23} \end{pmatrix} \begin{pmatrix} c_{13} & 0 & s_{13}e^{-i\delta} \\ 0 & 1 & 0 \\ -s_{13}e^{i\delta} & 0 & c_{13} \end{pmatrix} \begin{pmatrix} c_{12} & s_{12} & 0 \\ -s_{12} & c_{12} & 0 \\ 0 & 0 & 1 \end{pmatrix}, \quad (1.33)$$

where, $c_{ab} = \cos \theta_{ab}$, $s_{ab} = \sin \theta_{ab}$, with $\theta_{12}, \theta_{13}, \theta_{23}$ are the mixing angles between flavors, and δ represents phase of charge and parity (CP)-violation. Using this unitary matrix,

generic formula to account probability oscillation of ν_a to ν_b is given by

$$P(\nu_a \rightarrow \nu_b) = \sum_{j,k} U_{aj}^* U_{bj} U_{ak} U_{bk}^* e^{-i \frac{\Delta m_{jk}^2 L}{2|\mathbf{p}|}}, \quad (1.34)$$

where $\Delta_{jk}^2 \equiv m_j^2 - m_k^2$ is the squared mass difference of the state ν_j and ν_k , U_{aj} is the a, j element of the U_{PMNS} matrix, L is the distance traveled by neutrino from its source to a detector (or simply baseline), and $|\mathbf{p}|$ is the momentum of the neutrino.

In its observation, neutrinos from a source (sun, μ -decay, nuclear reaction, etc.) are produced and then are detected after traveling a distance L . During propagation, neutrinos experience a weak process in combination with flavor states and randomly distributed in space-time. It implies a slightly different velocity phase, hence there is a non-zero probability of obtaining a different state between the detected and produced neutrinos.

1.5. Outline of Thesis

Having briefly described the development of neutrino physics in the previous pages, what follows will be focused on discussing the coherent interaction of a neutrino with a nucleus, the main objective of this thesis. Neutrino interaction with the nucleus is important as neutrinos available in the universe in a gigantic amount while the nucleus constructs every macroscopic matter. In this work, we are focusing on a coherent process, meaning that neutrinos scatter with the nucleus as a whole via neutral boson exchange in low energy without changing their internal structure. It is commonly known as coherent elastic neutrino-nucleus scattering. The process plays role in many physical phenomena, such as dark matter probes, supernova physics, neutrino electromagnetic, nuclear physics, and new neutrino interactions.

The discussion will be conducted in the framework of SM as well as beyond. For the latter, generalized new interactions from two models are considered: non-standard interaction and simplified model. Both of them are important to study possible new neutrino interaction which is indicated from various observations. The phenomenology of both models will be studied by including their possible effect on the SM predictions.

We describe the formulation of the neutrino coherent interaction with the nucleus within the SM in Chapter 2. Both spin-0 and spin-1/2 cases will be discussed. We also

give the formulation of its event rate as well as the number of events in this chapter. In addition, we will briefly describe how this process is observed, particularly in the COHERENT experiment whom the results we concern. Chapter 3 will discuss the theoretical formulation of the generalized neutrino interaction from non-standard interactions and a simplified model. Numerical results of the SM process, as well as from these models, will be elaborated in Chapter 4. We firstly present the kinematics of the process and its standard model differential cross-section in the SM, non-standard interaction, and simplified model for five nucleus target. For the SM, we also provide the total cross-section and also the differential rate from COHERENT experiment. Afterwards, by performing single-bin χ^2 -analysis, we present the constraint of each parameter from both considered models. Finally, we will conclude this Master thesis and give further suggestions in Chapter 5.

2. COHERENT ELASTIC NEUTRINO-NUCLEUS SCATTERING

Since neutrinos in the universe available in gigantic amounts, their interaction with the nucleus has been considered an advancement for investigating new physics. One proposed a tree-level process of this kind called coherent elastic neutrino-nucleus scattering (CEvNS) in which Neutral-Current (NC) interaction happens between neutrinos with quarks inside the nucleus of an atom. The proposal (Freedman, 1974) had been hanging up for a few decades after first its confirmation in recent years by COHERENT experiment (Akimov *et al.*, 2017). In what follows, we first examine the theoretical formulation of the process and then present some appropriate attempts to detect this neutral interaction.

2.1. Theoretical Formulation of CEvNS

CEvNS reaction can be depicted as neutrinos interact with a nucleus coherently via neutral boson exchange in low energy. Coherent here means that neutrinos are capable to reach the nucleus structure without breaking it. The implication of this is that the complexity of strong interaction can be attached to a nuclear form factor. Through this procedure, properties of neutrinos when they mingle with matters in low momentum transfer can be investigated. Feynman diagram showing CEvNS process is shown in Figure 8. It shows

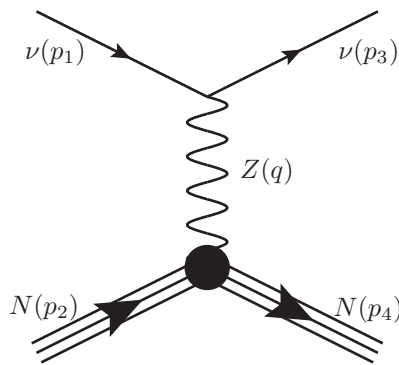


Figure 8. CEvNS process in the SM.

a neutrino interacting with the nucleus as a whole by exchanging neutral boson. So far, CEvNS is a process with the largest cross-section involving neutrinos as shown in Figure 9.

In this work, the CEvNS is generally studied to show the differential cross-section predictions for the cases of SM and beyond, considering the effect of general new interactions. For this purpose, we consider NSI and a simplified model. In doing so, we approach the nucleus as a spinless or a Dirac particle.

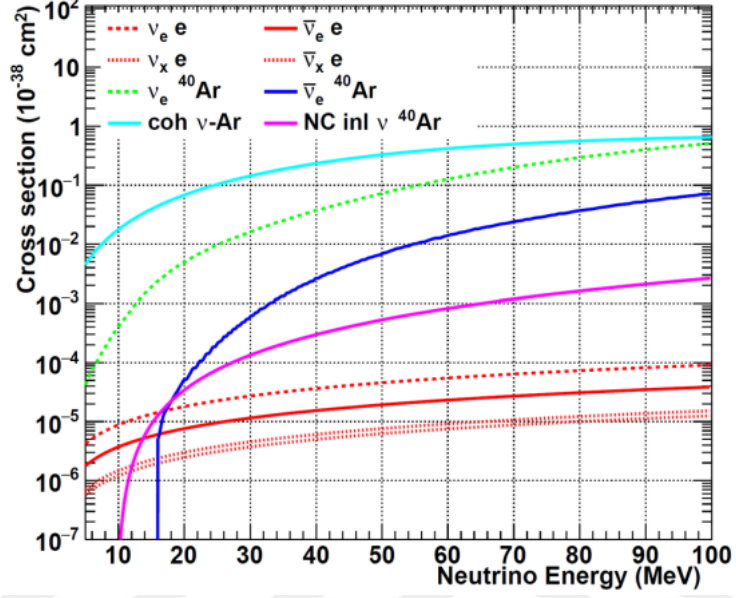


Figure 9. Various processes involving neutrino, adapted from (Sinev, 2020).

2.1.1. Spinless Nucleus

The scattering amplitude for the process of

$$\nu(p_1) + N(p_2) \rightarrow \nu(p_3) + N(p_4), \quad (2.1)$$

while assuming the nucleus as a spinless particle can be calculated as

$$\begin{aligned} -i\mathcal{M} = & \left[-i \frac{g}{2 \cos \theta_W} \bar{\nu}(p_3) g_L^{\nu} \gamma^{\mu} (1 - \gamma^5) \nu(p_1) \right] \left[-i \frac{(g_{\mu\nu} - p_{\mu} p_{\nu} / m_Z^2)}{q^2 - m_Z^2} \right] \\ & \times \left[-i \frac{g}{2 \cos \theta_W} \langle N(p_4) | J_{NC}^{\nu} | N(p_2) \rangle \right], \end{aligned} \quad (2.2)$$

and for $q^2 \ll m_Z^2$, we have

$$\begin{aligned} \mathcal{M} &= \frac{g^2}{4m_Z^2 \cos^2 \theta_W} \bar{\nu}(p_3) g_L^{\nu} \gamma^{\mu} (1 - \gamma^5) \nu(p_1) \langle N(p_4) | J_{NC\mu} | N(p_2) \rangle \\ &= \frac{2G_F}{\sqrt{2}} g_L^{\nu} \bar{\nu}(p_3) \gamma^{\mu} (1 - \gamma^5) \nu(p_1) \langle N(p_4) | J_{NC\mu} | N(p_2) \rangle \end{aligned} \quad (2.3)$$

where we have used $G_F/\sqrt{2} = g^2/8m_W^2$ and $m_W = m_Z \cos \theta_W$. The $|N\rangle$ represents that the nucleus is composed of quarks. Since the nucleus consists of the proton (uud) and neutron (udd), which then also composed of quarks, the nucleus NC term can be written using Eq.(1.7) as

$$\begin{aligned} \langle N(p_4) | J_{NC\mu} | N(p_2) \rangle &= 2 \langle N(p_4) | g_L^u \bar{u}_L \gamma^{\mu} u_L + g_R^u \bar{u}_R \gamma^{\mu} u_R \\ &\quad + g_L^d \bar{d}_L \gamma^{\mu} d_L + g_R^d \bar{d}_R \gamma^{\mu} d_R | N(p_2) \rangle \\ &= 2 \langle N | (g_L^u + g_R^u) \bar{u}_L \gamma^{\mu} u_L + (g_L^d + g_R^d) \bar{d}_L \gamma^{\mu} d_L | N \rangle, \end{aligned} \quad (2.4)$$

where the u and d quarks considered to conserve parity. For a nucleus with a large mass number, the ratio of the up and down quarks related to the proton number, \mathcal{Z} , and neutron number, \mathcal{N} , which is related by the atomic mass number $\mathcal{A} = \mathcal{Z} + \mathcal{N}$, is given by

$$\frac{\langle N | \bar{u} \gamma^{\mu} u | N \rangle}{\langle N | \bar{d} \gamma^{\mu} d | N \rangle} = \frac{\langle p | \bar{u} \gamma^{\mu} u | p \rangle + \langle n | \bar{u} \gamma^{\mu} u | n \rangle}{\langle p | \bar{d} \gamma^{\mu} d | p \rangle + \langle n | \bar{d} \gamma^{\mu} d | n \rangle} = \frac{2\mathcal{Z} + \mathcal{N}}{\mathcal{Z} + 2\mathcal{N}}. \quad (2.5)$$

From this relation, the EM property can be attached by defining f^{μ} to each quark as (Lindner *et al.*, 2017)

$$\langle N | \bar{u} \gamma^{\mu} u | N \rangle = (2\mathcal{Z} + \mathcal{N}) f^{\mu}, \quad \langle N | \bar{d} \gamma^{\mu} d | N \rangle = (\mathcal{Z} + 2\mathcal{N}) f^{\mu}. \quad (2.6)$$

We know that the EM charge of u and d are $Q_u = 2/3$ and $Q_d = -1/3$, respectively. From the EW Lagrangian, the EM current for quarks in a nucleus is

$$J_{EM}^{\mu} = \frac{2}{3} \bar{u} \gamma^{\mu} u - \frac{1}{3} \bar{d} \gamma^{\mu} d. \quad (2.7)$$

Then for the whole nucleus, we have

$$\langle N(p_4) | J_{EM}^{\mu} | N(p_2) \rangle = \frac{2}{3} (2\mathcal{Z} + \mathcal{N}) f^{\mu} - \frac{1}{3} (\mathcal{Z} + 2\mathcal{N}) f^{\mu} = \mathcal{Z} f^{\mu}. \quad (2.8)$$

Comparing this with the case of scalar QED (Appendix 7.2.),

$$\langle N(p_4) | J_{EM}^\mu | N(p_2) \rangle = -Q_{nucl} (p_4^\mu + p_2^\mu) F(q^2), \quad (2.9)$$

where we have defined form factor $F(q^2)$ to take into account nucleus structure, we can see that

$$Q_{nucl} = \mathcal{Z}, \quad f^\mu = -(p_4^\mu + p_2^\mu) F(q^2). \quad (2.10)$$

Since we have

$$\langle N | \bar{u}_L \gamma^\mu u_L | N \rangle = \frac{1}{2} \langle N | \bar{u} \gamma^\mu u | N \rangle - \frac{1}{2} \langle N | \bar{u} \gamma^\mu \gamma^5 u | N \rangle, \quad (2.11)$$

$$\langle N | \bar{d}_L \gamma^\mu d_L | N \rangle = \frac{1}{2} \langle N | \bar{d} \gamma^\mu d | N \rangle - \frac{1}{2} \langle N | \bar{d} \gamma^\mu \gamma^5 d | N \rangle, \quad (2.12)$$

and the fact that the QED nature is independent of $\gamma^\mu \gamma^5$ terms, we can split the nucleus current as

$$(g_L^u + g_R^u) \langle N(p_4) | \bar{u}_L \gamma^\mu u_L | N(p_2) \rangle \equiv g_V^u \frac{1}{2} \langle N | \bar{u} \gamma^\mu u | N \rangle = \frac{1}{2} g_V^u (2\mathcal{Z} + \mathcal{N}) f^\mu, \quad (2.13)$$

and

$$(g_L^d + g_R^d) \langle N(p_4) | \bar{d}_L \gamma^\mu d_L | N(p_2) \rangle \equiv g_V^d \frac{1}{2} \langle N | \bar{d} \gamma^\mu d | N \rangle = \frac{1}{2} g_V^d (\mathcal{Z} + 2\mathcal{N}) f^\mu, \quad (2.14)$$

hence the nucleus current becomes

$$\begin{aligned} \langle N(p_4) | J_{NC_\mu} | N(p_2) \rangle &= - \left[\mathcal{Z} (2g_V^u + g_V^d) + \mathcal{N} (g_V^u + 2g_V^d) \right] (p_4^\mu + p_2^\mu) F(q^2) \\ &= - \left[\mathcal{Z} g_V^p + \mathcal{N} g_V^n \right] (p_4^\mu + p_2^\mu) F(q^2). \end{aligned} \quad (2.15)$$

Substituting the following relations for the couplings

$$g_L^u = \frac{1}{2} - \frac{2}{3} \text{sw}^2, \quad g_R^u = -\frac{2}{3} \text{sw}^2, \quad g_L^d = -\frac{1}{2} + \frac{1}{3} \text{sw}^2, \quad g_R^d = \frac{1}{3} \text{sw}^2, \quad (2.16)$$

where $\text{sw}^2 \equiv \sin^2 \theta_W$, we find

$$\begin{aligned} \langle N(p_4) | J_{NC_\mu} | N(p_2) \rangle &= - \left[\mathcal{F}(1/2 - 2\text{sw}^2) + \mathcal{N}(-1/2) \right] (p_4^\mu + p_2^\mu) F(q^2) \\ &= \frac{1}{2} Q_{SM} (p_4^\mu + p_2^\mu) F(q^2), \end{aligned} \quad (2.17)$$

with the weak charge defined by (Scholberg, 2005)

$$Q_{SM} = \mathcal{N} - \mathcal{F}(1 - 4\text{sw}^2). \quad (2.18)$$

Here the subscript indicates that the charge corresponds to the SM current.

The scattering amplitude for the CEvNS in Eq.(2.3) then becomes

$$\mathcal{M} = \frac{G_F}{\sqrt{2}} g_L^v Q_{SM} \bar{v}(p_3) \gamma^\mu (1 - \gamma^5) v(p_1) (p_{4\mu} + p_{2\mu}) F(q^2). \quad (2.19)$$

The average square of this amplitude can be written as

$$\langle |\mathcal{M}|^2 \rangle = \sum_{ss'} |\mathcal{M}|^2 = \frac{1}{2} G_F^2 Q_{SM}^2 |F(q^2)|^2 (g_L^v)^2 L_v^{\mu\nu} W_{\mu\nu}^N \quad (2.20)$$

where we note that neutrino appears only in the left-handed state so that no need for spin averaging factor. We have defined the neutrino tensor $L_v^{\mu\nu}$ and nucleus tensor $W_{\mu\nu}^N$. We can express both of them as

$$\begin{aligned} L_v^{\mu\nu} &= \sum_{ss'} [\bar{v}^s(p_3) \gamma^\mu (1 - \gamma^5) v^{s'}(p_1)] [\bar{v}^s(p_3) \gamma^\nu (1 - \gamma^5) v^{s'}(p_1)]^\dagger \\ &= \text{Tr}[\not{p}_3 \gamma^\mu (1 - \gamma^5) \not{p}_1 \gamma^\nu (1 - \gamma^5)] \\ &= 8(p_1^\mu p_3^\nu + p_1^\nu p_3^\mu - p_1 p_3 g^{\mu\nu} - i\varepsilon^{\alpha\mu\beta\nu} p_{3\alpha} p_{1\beta}), \end{aligned} \quad (2.21)$$

and

$$W_{\mu\nu}^N = (p_{2\mu} + p_{4\mu})(p_{2\nu} + p_{4\nu}). \quad (2.22)$$

Note that the following completeness relations for particle u and antiparticle v have been

implemented

$$\sum_s = u^s(p)\bar{u}^s(p) = \not{p} + m, \quad \sum_s = v^s(p)\bar{v}^s(p) = \not{p} - m. \quad (2.23)$$

Contracting both terms we have

$$L_V^{\mu\nu} W_{\mu\nu}^N = 8 \left[2(p_1 \cdot (p_2 + p_4))(p_3 \cdot (p_2 + p_4)) - (p_1 \cdot p_3)(p_2 + p_4)(p_2 + p_4) \right. \\ \left. - i\varepsilon^{\alpha\mu\beta\nu} p_{3\alpha} p_{1\beta} (p_{2\mu} + p_{4\mu})(p_{2\nu} + p_{4\nu}) \right]. \quad (2.24)$$

The last term is zero due to symmetric-antisymmetric multiplication. Hence we have

$$\langle |\mathcal{M}|^2 \rangle = 4G_F^2 Q_{SM}^2 |F(q^2)|^2 (g_L^V)^2 \left[2(p_1 \cdot p_2 + p_1 \cdot p_4)(p_2 \cdot p_3 + p_3 \cdot p_4) \right. \\ \left. - (p_1 \cdot p_3)(p_2^2 + 2p_2 \cdot p_4 + p_4^2) \right]. \quad (2.25)$$

Implementing the four-vector momentum contractions to the $|\mathcal{M}|^2$, we find

$$\langle |\mathcal{M}|^2 \rangle = 4G_F^2 Q_{SM}^2 |F(q^2)|^2 (g_L^V)^2 2 \left[2m_N^2 E_\nu (E_\nu - T) + m_N^2 E_\nu^2 \right. \\ \left. + m_N^2 (E_\nu - T)^2 - m_N^3 T - m_N^2 T (m_N + T) \right] \\ = 32G_F^2 Q_{SM}^2 |F(q^2)|^2 (g_L^V)^2 m_N^2 E_\nu^2 \left(1 - \frac{T}{E_\nu} - \frac{m_N T}{2E_\nu^2} \right). \quad (2.26)$$

Applying this result to the differential cross-section as in Eq.(A.34), we obtain

$$\left[\frac{d\sigma}{dT} \right]_{SM} = \frac{G_F^2 Q_{SM}^2 m_N |F(q^2)|^2}{4\pi} \left(1 - \frac{m_N T}{2E_\nu^2} - \frac{T}{E_\nu} \right). \quad (2.27)$$

The nuclear form factor $F(q^2)$ approaches to 1 in the coherent limit $q^2 \rightarrow 0$.

2.1.2. Dirac Nucleus

The nucleus can also be considered as a Dirac particle. We can use the usual vector current to replace the scalar of Eq.(2.15), so that

$$\langle N(p_4) | J_{EM}^\mu | N(p_2) \rangle = [\mathcal{L} g_V^p + \mathcal{N} g_V^n] \bar{u}(p_4) \gamma^\mu u(p_2) F(q^2). \quad (2.28)$$

The scattering amplitude then becomes

$$\mathcal{M} = \frac{G_F}{\sqrt{2}} Q_{SM} F(q^2) g_L^V \bar{\nu}(p_3) \gamma^\mu (1 - \gamma^5) \nu(p_1) \bar{u}(p_4) \gamma_\mu u(p_2). \quad (2.29)$$

Note that we could also have antineutrino, but the final result will not be changed with this structure. The contribution of the new nucleus term is the only difference here as we compute the averaged square amplitude, which has the following tensor

$$\begin{aligned} W_{\mu\nu}^N &= \sum_{ss'} [\bar{u}^s(p_4) \gamma_\mu u^{s'}(p_2)] [\bar{u}^s(p_4) \gamma_\nu u^{s'}(p_2)]^\dagger \\ &= \text{Tr}[(\not{p}_4 + m_N) \gamma_\mu (\not{p}_2 + m_N) \gamma_\nu] \\ &= 4(p_{4\mu} p_{2\nu} + p_{4\nu} p_{2\mu} - (p_4 \cdot p_2 - m_N^2) g_{\mu\nu}). \end{aligned} \quad (2.30)$$

Contracting the neutrino and the nucleus tensor, we obtain

$$\begin{aligned} L_\nu^{\mu\nu} W_{\mu\nu}^N &= 32(p_1^\mu p_3^\nu + p_1^\nu p_3^\mu - p_1 p_3 g^{\mu\nu} - i\varepsilon^{\alpha\mu\beta\nu} p_{3\alpha} p_{1\beta}) \\ &\quad \times (p_{4\mu} p_{2\nu} + p_{4\nu} p_{2\mu} - (p_4 \cdot p_2 - m_N^2) g_{\mu\nu}) \\ &= 32[2(p_1 p_4)(p_2 p_3) + 2(p_1 p_2)(p_3 p_4) - 2(p_1 p_3)(p_2 p_4) \\ &\quad + 2(p_1 p_3)(p_2 p_4 - m_N^2)] \\ &= 64[(p_1 p_4)(p_2 p_3) + (p_1 p_2)(p_3 p_4) - (p_1 p_3)m_N^2]. \end{aligned} \quad (2.31)$$

Using the lab frame, the four-vector momentum contraction gives

$$\begin{aligned} L_\nu^{\mu\nu} W_{\mu\nu}^N &= 64[m_N^2(E_\nu - T)^2 + E_\nu^2 m_N^2 - m_N^3 T] \\ &= 128 m_N^2 E_\nu^2 \left[1 - \frac{T}{E_\nu} - \frac{m_N T}{2E_\nu^2} + \frac{T^2}{2E_\nu^2} \right]. \end{aligned} \quad (2.32)$$

The cross section then becomes

$$\left[\frac{d\sigma}{dT} \right]_{SM} = \frac{G_F^2 Q_{SM}^2 m_N |F(q^2)|^2}{4\pi} \left(1 - \frac{m_N T}{2E_\nu^2} - \frac{T}{E_\nu} + \frac{T^2}{2E_\nu^2} \right). \quad (2.33)$$

We notice that only the last term distinguishes this result from the spinless case. In addition, for lower recoil nuclear energy limit, the last two terms can be neglected and we have the same form from both considerations.

The form factor in the differential cross-section (2.27) determines inner structure of

nucleus target. There are many possibilities for choosing it. In this study, we use the Helm parameterization (Helm, 1956) for the form factor:

$$F_{\text{Helm}}(q^2) = 3 \frac{j_1(qR)}{qR} e^{-\frac{1}{2}q^2 s^2}. \quad (2.34)$$

Here, $j_1(x) = \sin x/x^2 - \cos x/x$ is the first order Spherical Bessel function. Nuclear radius is given by $R = \sqrt{c^2 + \frac{7}{3}\pi^2 - 5s^2}$, with the nuclear parameters $c = (1.23\mathcal{A}^{1/3} - 6)$ fm and $s = 0.9$ fm (Duda *et al.*, 2007). Notice that \mathcal{A} is the nucleus mass number. The form factor for proton and neutron are considered equal. Note that relation of the momentum transfer obeys $Q^2 = -q^2 = 2MT$.

2.2. Criteria of Coherency

Coherency interaction occurs in low energy-momentum transfer. Perfect coherency takes place as $q^2 \rightarrow 0$, so that nucleons can be considered as point-like particles (Kerman *et al.*, 2016). The dynamics of the strong interactions can simply be ignored.

Formulation of the criteria of coherency can be obtained from the weak charge in (2.18) by including the proton and neutron form factor as

$$\Gamma(q^2) = (\varepsilon \mathcal{F} F_{\mathcal{F}} - \mathcal{N} F_{\mathcal{N}})^2, \quad \varepsilon \equiv 1 - 4s w^2 \approx 0.045. \quad (2.35)$$

Quantification of the coherency can be utilized by considering alignment of the phase angle, $\phi(q^2)$ that can be from 0° to 90° , from amplitudes of two nonidentical nucleons. Scattering from the center of the involved nucleons leads to quantum mechanics (QM) superpositions. The above formulation then becomes (Sharma *et al.*, 2021)

$$\begin{aligned} \Gamma(q^2) &\equiv \Gamma_{QM}(q^2) = \mathcal{F} \varepsilon^2 [1 + \alpha(\mathcal{F} - 1)] + \mathcal{N} [1 + \alpha(\mathcal{N} - 1)] - 2\alpha \varepsilon \mathcal{F} \mathcal{N} \\ &= (\varepsilon \mathcal{F} - \mathcal{N})^2 \alpha(q^2) + (\varepsilon^2 \mathcal{F} + \mathcal{N}) [1 - \alpha(q^2)]. \end{aligned} \quad (2.36)$$

The parameter $\alpha \equiv \cos \phi(q^2)$ quantifies the degree of coherency. With this relation, full coherency occurs as $\alpha = 1$, while the case of total decoherency is $\alpha = 0$. Furthermore, another parameter has been introduced to directly connect QM coherency and form factor

with the observed cross-section. The former is given by

$$\xi(q^2) = \alpha + (1 - \alpha) \frac{\varepsilon^2 \mathcal{L} + \mathcal{N}}{(\varepsilon \mathcal{L} - \mathcal{N})^2}, \quad (2.37)$$

while the latter is

$$\xi^2(q^2) = \frac{(\varepsilon \mathcal{L} F_{\mathcal{L}} - \mathcal{N} F_{\mathcal{N}})^2}{(\varepsilon \mathcal{L} - \mathcal{N})^2}. \quad (2.38)$$

This parameter is the cross-section reduction fraction.

Behavior of α and ξ , which is equivalent to the Helm form factor denoted F_A^2 in (Sharma *et. al.*, 2021), using several different nucleus target is shown in Figure 10. Fluxes from several neutrino sources were implemented. It can be seen that the full coherency criteria, $\alpha \sim 1$, could be studied better using reactor experiments.

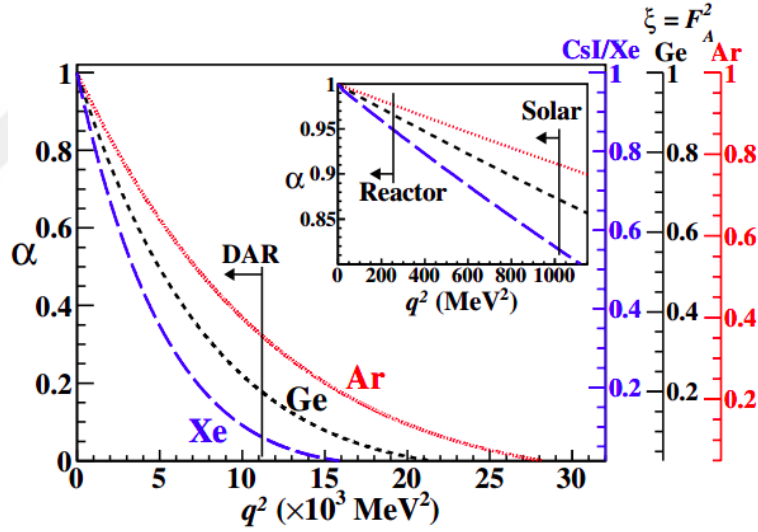


Figure 10. Behavior of α and ξ for several targets with neutrino flux from π -DAR, reactor and solar neutrino (Sharma *et. al.*, 2021).

2.3. Event Rates and Number of Events

The general form of event rate according to nuclear recoil energy is

$$\frac{dR}{dT} = \int_{E_{\nu min}}^{E_{\nu max}} dE_{\nu} \frac{d\Phi(E_{\nu})}{dE_{\nu}} \frac{d\sigma(E_{\nu}, T)}{dT}. \quad (2.39)$$

It is the convolution of neutrino spectrum, $d\Phi/dE_\nu$, and differential cross-section of the process. In the case of a new physics appearance, only the differential cross-section will change. Accordingly, the number of events detected in observation can be written as

$$N_{event} = N_{tar} \int_{T_{th}}^{T_{max}} dT \frac{dR(T, E_\nu)}{dT}, \quad (2.40)$$

where $N_{tar} = 2m_{tar}N_A/m_x$ is the total number of target nucleons with mass target m_{tar} , molar mass of the involved x -atom m_x , and the Avogadro's number $N_A = 6.022 \times 10^{23}$. Uncertainty from observation can not be neglected so that the event numbers must also include the efficiency of an experiment.

2.4. CEvNS Observations

CEvNS gives relatively a large cross-section comparing to other processes involving neutrino so far. An abundance of neutrino sources that meet the detection criteria from terrestrial sources, solar, atmospheric as well as artificial ways like accelerators and detectors would attract scientific activity in near future. The difficulty of detecting the process comes from the nuclear recoil energy that lies in a few keV scales. This challenging objective has finally been witnessed by the advancement of accelerator neutrino technology in recent years by COHERENT collaboration (Akimov *et al.*, 2017).

COHERENT collaboration detected the CEvNS with neutrino energies less than 10 MeV. This collaboration is located at the Spallation Neutron Source (SNS) which runs the most intense neutron pulse have been known. In this experiment, heavy target such as mercury is bombarded by high-energy proton. It then produces a pion-stopped source for fabricating neutrinos (π DAR process) with three types: electron neutrino, muon neutrino, and muon antineutrino. These neutrinos neutrino-energy fluxes satisfy the Michel spectrum (Aki-

mov *et al.*, 2017)

$$\left[\frac{d\Phi(E_\nu)}{dE_\nu} \right]_{\nu_\mu} = \eta \delta \left(E_\nu - \frac{m_\pi^2 - m_\mu^2}{2m_\pi} \right), \quad (2.41)$$

$$\left[\frac{d\Phi(E_\nu)}{dE_\nu} \right]_{\bar{\nu}_\mu} = \eta \frac{64E_\nu^2}{m_\mu^3} \left(\frac{3}{4} - \frac{E_\nu}{m_\mu} \right), \quad (2.42)$$

$$\left[\frac{d\Phi(E_\nu)}{dE_\nu} \right]_{\nu_e} = \eta \frac{192E_\nu^2}{m_\mu^3} \left(\frac{1}{2} - \frac{E_\nu}{m_\mu} \right). \quad (2.43)$$

Here $\eta = rN_{\text{POT}}/4\pi L^2$ is the normalization factor, where according to the COHERENT first detection, the number of neutrinos per flavor produced each proton on target (POT) is $r = 0.08$ with $N_{\text{POT}} = 1.76 \times 10^{23}$, and detector distance from source is $L = 1930$ cm. The data was taken during 308.1 days running. Figure 11 shows the neutrino spectral according to those forms with the η sets to unity. It can be seen that there is an energetic ν_μ flux around

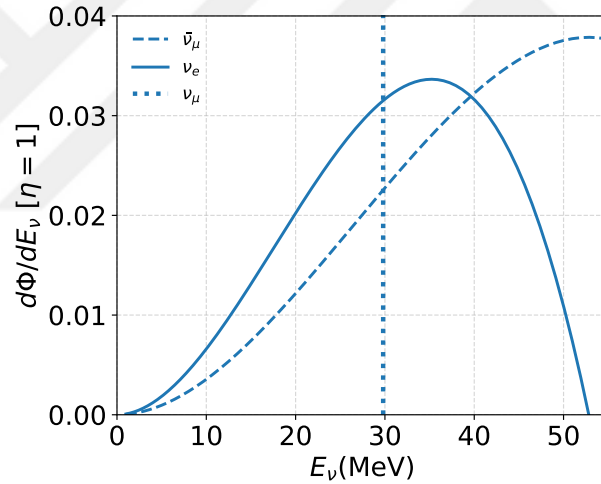


Figure 11. Neutrino flux from π -DAR source with $\eta = 1$.

30 MeV which comes from the direct product of decaying pion at rest. For example, neutrino for two different lifetimes:

$$\pi^+ \rightarrow \nu_\mu + \mu^+ \quad (26 \text{ ns}), \quad \mu^+ \rightarrow \bar{\nu}_\mu + \nu_e + e^+ \quad (2200 \text{ ns}). \quad (2.44)$$

Being a scintillation-based, the COHERENT experiment measures the number of photoelectrons (PE), n_{PE} of CEvNS events. The differential rate that depends on the nuclear recoil energy is related to the electron recoil energy with quenching factor $Q(T)$. This quantity

can then be converted to PE using (Papoulias, 2020)

$$n_{PE} = Q(T)L_Y T, \quad (2.45)$$

with $Q(T) = T_{ee}/T$ is quenching factor, the ratio between emitted scintillation light in nuclear and electron recoils, and $L_Y = 13.348\text{PE}/\text{keV}_{ee}$ is light yield, where keV_{ee} refers to electron recoil energy. For this work, we use the first COHERENT data which gives

$$n_{PE} = 1.17 \left(\frac{T}{\text{keV}} \right). \quad (2.46)$$

The factor 1.17 comes from energy independent Q with $8.78 \pm 1.66\%$ (Akimov *et al.*, 2017). Also from COHERENT, the efficiency function of the observation is

$$\varepsilon(x) = \frac{k_1}{1 + e^{-k_2(x-x_0)}} \Theta(x), \quad (2.47)$$

with $k_1 = 0.6655$ and $k_2 = 0.4942$, and $x_0 = 10.8507$, where the Heaviside function satisfies

$$\Theta(x) = \begin{cases} 0, & x < 5 \\ 0.5, & 5 \leq x < 6 \\ 1, & x \geq 6. \end{cases} \quad (2.48)$$

However, the full coherency was predicted will be achieved from reactors or solar neutrino experiments (Kerman *et. al.*, 2016). During the preparation of this thesis, CONUS Collaboration has announced their result of CEvNS observation from neutrino detector (Bonet *et al.*, 2020). The nowadays active collaborations that suitable for detecting CEvNS are summarized in Table 2, along with their detector target.

Detection of CEvNS will surely offer a new perspective of understanding other phenomena in nature. Any deviation from SM prediction may indicate occurrences of new physics so that it can be used to explain any BSM proposal. The process is also predicted to be dominant in the core-collapse of a supernova (SN), as well as other astrophysical and terrestrial events. The subject of direct detection of weakly interacting massive particle (WIMP) as one of the most probable dark matter candidate has also been affected since their similar

Table 2. Some suitable experiments around the globe for detecting CEvNS.

Experiment	Detector	Source	Location	Reference
COHERENT	CsI, HPGe, etc.	π DAR	USA	(Akimov <i>et al.</i> , 2017)
CONNIE	Si CCDs	Reactor	Brazil	(Aguilar-Arevalo <i>et al.</i> , 2019)
CONUS	HPGe	Reactor	Germany	(Bonet <i>et al.</i> , 2020)
Darshide-LM	LAr	Sun, SN	Italy	(Agnes <i>et al.</i> , 2018)
LUX-ZEPLIN	Dual-phase LXe	Sun, SN	USA	(Akerib <i>et al.</i> , 2020)
MINER	Cryogenic Ge/Si	Reactor	Brazil	(Agnolet <i>et al.</i> , 2016)
NEWS-G	Spherical Counters	Reactor	Canada	(Arnaud <i>et al.</i> , 2018)
NuCLEUS	Cryogenic CaWO ₄	Reactor	Germany	(Rothe <i>et al.</i> , 2020)
RED-100	Dual-phase LXe	Reactor	Russia	(Akimov <i>et al.</i> , 2016)
RICOCHET	Ge, Zn bolometers	Reactor	France	(Billard <i>et al.</i> , 2017)
SuperCDMS	Cryogenic Ge/Si	Sun, SN	Canada	(Asamar <i>et al.</i> , 2019)
TEXONO	p-PCGe	Reactor	Taiwan	(Wong, 2015)
Xenon NT	Dual-phase LXe	Sun, SN	Italy	(Aprile <i>et al.</i> , 2017)

nuclear recoil energy behavior and also from the irreducible neutrino background.

3. GENERAL NEUTRINO INTERACTIONS

Below the electroweak symmetry breaking energy scale, other types of neutrino interactions with other fundamental particles may come into consideration for new physics phenomena. Along with vector and axial-vector types, other Lorentz invariant bilinear combinations may also be introduced at this low scale. From this spirit, we consider a model-independent extension to the SM Lagrangian to accommodate the new mediators for each interactions. Only the interaction of a neutrino with nucleon (proton and neutron), will be focused on in this thesis. Criteria of coherency is considered during the process, so that instead of to each quarks, neutrino is considered to elastically scattered off nucleus.

3.1. Non-standard Interactions of Neutrino

One of the widely studied models in search of new physics BSM is the non-standard interaction (NSI) of neutrinos (Davidson *et al.*, 2003). The model introduces a new type of contact interactions of neutrinos with matter which differs from the SM theory (Miranda and Nunokawa, 2015). In general, it can induce a neutral current (NC) as well as charge current (CC) processes. Both cases suggest the presence of a new mediator with heavier mass (Berezhiani and Rossi, 2002) or in the same order with the EW theory (Farzan and Shoemaker, 2016). Particular to CE ν NS, only the NC case is concerned. Neutrino with the NSI influences quarks inside a nucleus, which could interact either as a non-universal flavor conserving (FC) or flavor violating (FV) process. In general, the model is formulated as

$$\mathcal{L}_{eff}^{NSI} = -2\sqrt{2}G_F \sum_{ab=e,\mu,\tau} \varepsilon_{ab}^{fP(L,R)} (\bar{\nu}_a \gamma^\mu P_L \nu_b) (\bar{f} \gamma_\mu P_{(L,R)} f), \quad (3.1)$$

where f denotes involved fermion, a and b denote neutrino flavors and ε_{ab}^{fP} is the NSI parameterization. This form assumes low-energy interaction below the EW scale, hence neutrino interaction with other particles considered as four fermion point. Considering only the first quark family, we can change f with q that corresponds to u or d quarks, the relevant La-

grangian for CEvNS process can be written as

$$\mathcal{L}_{eff}^{NSI} = \frac{G_F}{\sqrt{2}} \bar{\nu}_a \gamma^\mu (1 - \gamma^5) \nu_b \bar{q} \gamma^\mu (\varepsilon_{ab}^{qV} - \varepsilon_{ab}^{qA} \gamma^5) q. \quad (3.2)$$

This formula describes the NC interaction of neutrino with quarks. We only consider the first generation of quarks, which is the constituent of the nucleon in our hitherto knowledge. The parameter ε_{ab}^{qV} and ε_{ab}^{qA} represent the NSI vector and axial-vector interaction, respectively. These new interactions, if we compare to the Fermi theory, are proportional to $\varepsilon \approx g_X^2 m_W^2 / (g^2 m_X^2)$ where g_X is a coupling constant and m_X the mass of a new mediator.

Consider spinless nucleus, neutral current from the quark case is

$$\begin{aligned} \langle N(p_4) | J_{NSI}^\mu | N(p_2) \rangle &= (\varepsilon_{ab}^{uV} \langle N | \bar{u} \gamma^\mu u | N \rangle + \varepsilon_{ab}^{uV} \langle N | \bar{d} \gamma^\mu d | N \rangle) F(q^2) \\ &= (\varepsilon_{ab}^{uV} (2\mathcal{Z} + \mathcal{N}) + \varepsilon_{ab}^{uV} (2\mathcal{N} + \mathcal{Z})) (p_4^\mu + p_2^\mu) F(q^2). \end{aligned} \quad (3.3)$$

The total neutral current then becomes

$$\begin{aligned} \langle N(p_4) | J_{NC}^\mu | N(p_2) \rangle &= \langle N(p_4) | J_{SM}^\mu + J_{NSI}^\mu | N(p_2) \rangle \\ &= \langle N | \bar{u} \gamma^\mu [(g_V^u + \varepsilon_{ab}^{uV}) - (1 + \varepsilon_{ab}^{uA})] u \\ &\quad + \bar{d} \gamma^\mu [(g_V^d + \varepsilon_{ab}^{dV}) - (1 + \varepsilon_{ab}^{dA})] d | N \rangle (p_4^\mu + p_2^\mu) F(q^2), \end{aligned} \quad (3.4)$$

and hence neglecting the axial-vector case

$$\begin{aligned} \langle N | J_{NC}^\mu | N \rangle &= [(g_V^u + \varepsilon_{ab}^{uV})(2\mathcal{Z} + \mathcal{N}) + (g_V^d + \varepsilon_{ab}^{dV})(\mathcal{Z} + 2\mathcal{N})] (p_4^\mu + p_2^\mu) F(q^2) \\ &= \frac{1}{2} 2 [\mathcal{Z} (1/2 - 2 \sin^2 \theta_W + 2\varepsilon_{ab}^{uV} + \varepsilon_{ab}^{dV}) \\ &\quad + \mathcal{N} (-1/2 + \varepsilon_{ab}^{uV} + 2\varepsilon_{ab}^{dV})] (p_4^\mu + p_2^\mu) F(q^2). \end{aligned} \quad (3.5)$$

Comparing with (2.17), we see the same form. Hence, the different term from the SM differential cross-section is

$$\begin{aligned} Q_{NSI}^2 &= 4 \sum_{a=e,\mu,\tau} \left[\mathcal{N} \left(\frac{1}{2} + \varepsilon_{aa}^{uV} + 2\varepsilon_{aa}^{dV} \right) + \mathcal{Z} \left(\frac{1}{2} - 2s_W^2 + 2\varepsilon_{aa}^{uV} + \varepsilon_{aa}^{dV} \right) \right]^2 \\ &\quad + 4 \sum_{a \neq b=e,\mu,\tau} \left[\mathcal{N} (\varepsilon_{ab}^{uV} + 2\varepsilon_{ab}^{dV}) + \mathcal{Z} (2\varepsilon_{ab}^{uV} + \varepsilon_{ab}^{dV}) \right]^2. \end{aligned} \quad (3.6)$$

As the parameter $\varepsilon_{ab}^{(u,d)V}$ vanishes, we obtain the SM form.

3.2. Simplified Model

A simplified model in general is an alternative type of model in high-energy physics to relate theoretical prediction with experimental data from measurements. It extends the SM with a proposed BSM scenario of new particles. Experimental parameters from this kind of model are considering only new masses and cross-sections as well as branching ratios, while the common full extensions of BSM involve plenty of particles with decay chain accordingly. Hence, it is important to note that simplified models do not represent the actual physics beyond the SM (McCoy and Massimi, 2018). Nevertheless, explaining simplified models still worth consideration such as embedding the model which can be dependent or independent to possible SM extension. Alwall and Toro 2009 for example proposed four simplified models which contain 2-3 masses and 4-5 branching ratios in order to explain data from a collider experiment quantitatively.

From the above explanation, we consider general new neutrino interactions, namely scalar, pseudoscalar, vectorial, axial-vector, (Cerdēno *et al.*, 2016) and tensor (Barranco *et al.*, 2012). Each of these is considered to carry light masses and hence couple to neutrinos and quark constituents of the nucleus. We note that effective neutrino-quark approximation that also consider these types had been conducted recently (Sierra *et. al.*, 2018). The following equations are the corresponding Lagrangians for each considered scenario:

$$\mathcal{L}_S \supset [(g_{vS}\bar{\nu}_R\nu_L + h.c.) + g_{qS}\bar{q}q]\mathcal{S}, \quad (3.7)$$

$$\mathcal{L}_P \supset [(g_{vP}\bar{\nu}_R\nu_L + h.c.) - ig_{qP}\bar{q}\gamma^5 q]\mathcal{P}, \quad (3.8)$$

$$\mathcal{L}_V \supset [g_{vV}\bar{\nu}_L\gamma^\mu\nu_L + g_{qV}\bar{q}\gamma^\mu q]\mathcal{V}_\mu, \quad (3.9)$$

$$\mathcal{L}_A \supset [g_{vA}\bar{\nu}_L\gamma^\mu\nu_L - g_{qA}\bar{q}\gamma^\mu\gamma^5 q]\mathcal{A}_\mu, \quad (3.10)$$

$$\mathcal{L}_T \supset [g_{vT}\bar{\nu}_R\sigma^{\mu\nu}\nu_L - g_{qT}\bar{q}\sigma^{\mu\nu}q]\mathcal{T}_{\mu\nu}, \quad (3.11)$$

where $\sigma_{\mu\nu} = \frac{i}{2}[\gamma_\mu, \gamma_\nu] = \frac{i}{2}(\gamma_\mu\gamma_\nu - \gamma_\nu\gamma_\mu)$. In what follows, we match the quark level current to the nucleus scale. It is performed by first connecting the quark Lagrangian to the nucleon level following (Cirelli *et al.*, 2013), and then the obtained nucleon case to the nucleus level (Kahlhoefer, 2010). After that, we calculate the amplitudes for each possibility to obtain the predicted differential cross-section. Results from this section will be analyzed using the data experiment in the next chapter.

3.2.1. Matching the nucleus current

3.2.1.1. Scalar Interaction

From quark q to nucleon level n (p or n), we have

$$\mathcal{L}_{Sn} = \langle n | \mathcal{L}_S | n \rangle = \sum_{n,q} g_{Sq} \mathcal{S} \langle n | \bar{q}q | n \rangle, \quad (3.12)$$

where

$$\langle n | \bar{q}q | n \rangle = f_{Tq}^n \frac{m_n}{m_q} \bar{n}n. \quad (3.13)$$

The proton, neutron, and quark masses are represented by m_p , m_n , and m_q , respectively. Parameter f_{Tq}^n represents the scalar charge of the quark for $n = p, n$.

From this nucleon level, we may proceed further to the nucleus by $\bar{n}n \rightarrow \langle N | \bar{n}n | N \rangle$. This case needs to consider the momentum transfer $q^\mu = p_4^\mu - p_2^\mu$ as well as the initial and final momentum, p_2^μ and p_4^μ , of the nucleus. Defining the total nucleus momentum as $P^\mu = p_2^\mu + p_4^\mu = 2p_4^\mu - q^\mu = 2p_2^\mu + q^\mu$, the general form of the current can be written as

$$\begin{aligned} \langle N | \bar{n}n | N \rangle = & \bar{N}N F_{S1}(q^2) + \bar{N}\gamma^\mu q_\mu N \frac{F_{S2}(q^2)}{m_N} + \bar{N}\gamma^\mu P_\mu N \frac{F_{S3}(q^2)}{m_N} \\ & + \bar{N}\sigma^{\mu\nu} P_\mu q_\nu N \frac{F_{S4}(q^2)}{m_N^2}. \end{aligned} \quad (3.14)$$

Our ignorance of the inner structure of nucleus is carried in the form factors F_i 's. They are a function of only scalar q^2 in the vertex. We have included the nucleus mass so that all the form factors have the same dimension. Application of the Dirac equation,

$\not{p}_2 N(p_2) = \bar{N}(p_4) \not{p}_4 = m_N N$, gives zero to the second term and $2\bar{N}N$ to the third nucleus currents. To the last term we have

$$\begin{aligned}
\bar{N}(p_4) \sigma^{\mu\nu} P_\mu q_\nu N(p_2) &= \bar{N} \frac{i}{2} (\gamma^\mu (2p_{\mu_4} - q_\mu) \gamma^\nu - \gamma^\nu \gamma^\mu (2p_{\mu_2} + q_\mu)) q_\nu N \\
&= \frac{i}{2} \bar{N} (2\not{p}_4 \gamma^\nu - 2\gamma^\nu \not{p}_2 - (\gamma^\mu \gamma^\nu + \gamma^\nu \gamma^\mu) q_\mu) q_\nu N \\
&= i\bar{N} (\not{p}_4 \gamma^\nu - \gamma^\nu \not{p}_2 - q^\nu) q_\nu N \\
&= i\bar{N} (m_N \gamma^\nu q_\nu - m_N \gamma^\nu q_\nu - q^2) N \\
&= -iq^2 \bar{N}(p_4) N(p_2),
\end{aligned} \tag{3.15}$$

so that we find $\bar{N}N(F_{S1} + 2F_{S3} - iq^2 F_{S4}/m_N^2)$, or simply

$$\langle N | \bar{n} n | N \rangle = \bar{N} N F_S(q^2). \tag{3.16}$$

For the coefficient of the nucleus level, we can define the following expression according to the number of proton \mathcal{Z} and neutron \mathcal{N} of the nucleus as (Cirelli *et al.*, 2013)

$$g_{SN} \equiv \sum_{n,q} g_{Sq} f_{Tq}^n \frac{m_n}{m_q} = \mathcal{Z} \sum_q g_{Sq} f_{Tq}^p \frac{m_p}{m_q} + \mathcal{N} \sum_q g_{Sq} f_{Tq}^n \frac{m_n}{m_q}. \tag{3.17}$$

We only consider the light quarks content of the nucleus in writing this equation. Therefore, the Lagrangian of scalar interaction for nucleus then becomes

$$\mathcal{L}_{SN} = g_{SN} \mathcal{S} \bar{N} N F_S(q^2). \tag{3.18}$$

This form will enter the calculation of the amplitude.

3.2.1.2. Pseudoscalar Interaction

From quark to nucleon level, the relation is

$$\mathcal{L}_{Pn} = \langle n | \mathcal{L}_P | n \rangle = \sum_{n,q} g_{Pq} \mathcal{P} \langle n | \bar{q} (-i\gamma_5) q | n \rangle, \tag{3.19}$$

where the pseudoscalar interaction of quarks satisfy (Ema et. al., 2021)

$$\langle n | \bar{q} i \gamma_5 q | n \rangle = \frac{m_n}{m_q} h_q \bar{n} i \gamma^5 n. \quad (3.20)$$

We emphasize that pseudoscalar form factor was considered zero. This result is a recent result taken from lattice approximation. Matching this to the nucleus level, we have $\bar{n} \gamma^5 n \rightarrow \langle N | \bar{n} \gamma^5 n | N \rangle$. As before, we can write the most general form as

$$\begin{aligned} \langle N | \bar{n} \gamma^5 n | N \rangle = & \bar{N} \gamma^5 N F_{P1}(q^2) + \bar{N} \gamma^\mu \gamma^5 q_\mu N \frac{F_{P2}(q^2)}{m_N} \\ & + \bar{N} \gamma^\mu \gamma^5 P_\mu N \frac{F_{P3}(q^2)}{m_N} + \bar{N} \sigma^{\mu\nu} \gamma^5 P_\mu q_\nu N \frac{F_{P4}(q^2)}{m_N^2}. \end{aligned} \quad (3.21)$$

The second term gives $2\bar{N}N$ and the third is zero. γ^5 gives a little difference to the last term

$$\begin{aligned} \bar{N}(p_4) \sigma^{\mu\nu} \gamma^5 P_\mu q_\nu N(p_2) = & i\bar{N}(p_4) \gamma^5 (\not{p}_4 \gamma^\nu - \not{p}_2 \gamma^\nu - q^\nu) q_\nu N(p_2) \\ = & i\bar{N}(p_4) (-\not{p}_4 \gamma^5 \gamma^\nu q_\nu - \gamma^5 \gamma^\nu q_\nu \not{p}_2 - \gamma^5 q^2) N(p_2) \\ = & i2m_N \bar{N}(p_4) \gamma^\nu \gamma^5 q_\nu N(p_2) - iq^2 \bar{N}(p_4) \gamma^5 N(p_2) \\ = & (4m_N^2 i - q^2 i) \bar{N}(p_4) \gamma^5 N(p_2), \end{aligned} \quad (3.22)$$

where before the last line we implement the same process from the second term. We then obtain $\bar{N} \gamma^5 N (F_{P1} + 2F_{P2} + 4im_N F_{P4} - iq^2 F_{P4}/m_N^2)$, which can be simplified as

$$\langle N | \bar{n} i \gamma_5 n | N \rangle = \bar{N} i \gamma_5 N F_P(q^2). \quad (3.23)$$

Considering the number of protons and neutrons of the nucleus as for the scalar case, we use the following expression for the coefficient which relates new interaction coupling with quarks

$$g_{PN} \equiv \mathcal{L} \sum_q g_{Pq} \frac{m_p}{m_q} h_q^p + \mathcal{N} \sum_q g_{Pq} \frac{m_n}{m_q} h_q^n. \quad (3.24)$$

Then, the Lagrangian for the pseudoscalar interaction becomes

$$\mathcal{L}_{PN} = -ig_{PN} \mathcal{P} \bar{N} \gamma_5 N F_P(q^2). \quad (3.25)$$

3.2.1.3. Vectorial Interaction

From quark to nucleon level, we have

$$\mathcal{L}_{Vn} = \langle n | \mathcal{L}_V | n \rangle = \sum_{n,q} g_{Vq} \mathcal{V}_\mu \langle n | \bar{q} \gamma^\mu q | n \rangle. \quad (3.26)$$

Since we are dealing with proton and neutron and assuming equal coupling to all quarks, we can match the quark current as

$$\begin{aligned} \langle n | g_{Vq} \bar{q} \gamma^\mu q | n \rangle &= \langle n | g_{Vu} \bar{u} \gamma^\mu u | n \rangle + \langle n | g_{Vd} \bar{d} \gamma^\mu d | n \rangle \\ &= g_{Vq} \left[\langle n | \bar{u} \gamma^\mu u | n \rangle + \langle n | \bar{d} \gamma^\mu d | n \rangle \right] \\ &= g_{Vq} \left[(2\mathcal{Z} + \mathcal{N}) \bar{n} \gamma^\mu n + (2\mathcal{N} + \mathcal{Z}) \bar{n} \gamma^\mu n \right] \\ &= g_{VN} \bar{n} \gamma^\mu n, \end{aligned} \quad (3.27)$$

where we have (Cerdēno *et al.*, 2016)

$$g_{VN} = 3g_{Vq} \mathcal{A}. \quad (3.28)$$

Matching this to the nucleus level, we write $\bar{n} \gamma^\mu n \rightarrow \langle N | \bar{n} \gamma^\mu n | N \rangle$. The general form of this term can be written as

$$\begin{aligned} \langle N | \bar{n} \gamma^\mu n | N \rangle &= \bar{N} \gamma^\mu N F_{V1}(q^2) + \bar{N} q^\mu N \frac{F_{V2}(q^2)}{m_N} + \bar{N} P^\mu N \frac{F_{V3}(q^2)}{m_N} \\ &\quad + \bar{N} \sigma^{\mu\nu} q_\nu N \frac{F_{V4}(q^2)}{m_N} + \bar{N} \sigma^{\mu\nu} P_\mu N \frac{F_{V5}(q^2)}{m_N}. \end{aligned} \quad (3.29)$$

We can implement the following Gordon identity

$$\bar{N} \gamma^\mu N = \frac{1}{2m_N} \bar{N} \left((p_4^\mu + p_2^\mu) + i\sigma^{\mu\nu} q_\nu \right) N. \quad (3.30)$$

It can be directly seen that the third term of the general form consists of the sum of $\bar{N} \gamma^\mu N$ and $\bar{N} \sigma^{\mu\nu} q_\nu N$. Moreover, from the process of obtaining Eq.(3.15), the last term proportional to

$\bar{N}q^\mu N$. Consequently, we only left with the following

$$\begin{aligned} \langle N | \bar{n} \gamma^\mu n | N \rangle = & \bar{N} \gamma^\mu N \left(F_{V1}(q^2) + 2F_{V3}(q^2) \right) + \bar{N} q^\mu N \left(\frac{F_{V2}(q^2)}{m_N} \right. \\ & \left. - i \frac{F_{V5}(q^2)}{m_N} \right) + \bar{N} \sigma^{\mu\nu} q_\nu N \left(\frac{F_{V4}(q^2)}{m_N} + i \frac{F_{V3}(q^2)}{m_N} \right). \end{aligned} \quad (3.31)$$

At this point, we should notice that for any covariant current J^μ the Ward identity $q_\mu J^\mu = 0$ applies. With this necessity, the second term must be zero, and hence the general form becomes

$$\langle N | \bar{n} \gamma^\mu n | N \rangle = \bar{N} \left(\gamma^\mu F_V(q^2) + \frac{\sigma^{\mu\nu} q_\nu}{2m_N} G_V(q^2) \right) N, \quad (3.32)$$

where 1/2 at the second term is conventional and form factor corresponds to magnetic dipole moment. Coherent interaction required that the momentum transfer q is small, compared to the nucleus mass. Neglecting the second term then, for coherent criteria, we obtain

$$\langle N | \bar{n} \gamma^\mu n | N \rangle = \bar{N} \gamma^\mu N F_V(q^2). \quad (3.33)$$

The Lagrangian for vectorial interaction then becomes

$$\mathcal{L}_{VN} = g_{VN} \mathcal{V}_\mu \bar{N} \gamma^\mu N F_V(q^2). \quad (3.34)$$

3.2.1.4. Axial-vector Interaction

From quark to nucleon level, we have

$$\mathcal{L}_{An} = \langle n | \mathcal{L}_A | n \rangle = \sum_{n,q} g_{Aq} \mathcal{A}_\mu \langle n | \bar{q} \gamma^\mu \gamma^5 q | n \rangle. \quad (3.35)$$

The nucleon current satisfies the following relation

$$\langle n | \bar{q} \gamma^\mu \gamma^5 q | n \rangle = 2s^\mu \Delta_q^n \bar{n} \gamma^\mu \gamma^5 n = S_n \Delta_q^n \bar{n} \gamma^\mu \gamma^5 n, \quad (3.36)$$

where we have defined $S_n = 2s^\mu$, with s^μ represents the nucleon spin four-vector. The Δ_q^n denotes the axial-vector charge of the quark for $n = p, n$. Matching this to the nucleus level, we need $\bar{n}\gamma^\mu\gamma^5 n \rightarrow \langle N|\bar{n}\gamma^\mu\gamma^5 n|N\rangle$. The general form of this term can be written as

$$\begin{aligned} \langle N|\bar{n}\gamma^\mu\gamma^5 n|N\rangle = & \bar{N}\gamma^\mu\gamma^5 N F_{A1}(q^2) + \bar{N}\gamma^5 q^\mu N \frac{F_{A2}(q^2)}{m_N} + \bar{N}\gamma^5 P^\mu N \frac{F_{A3}(q^2)}{m_N} \\ & + \bar{N}\sigma^{\mu\nu}\gamma^5 q_\nu N \frac{F_{A4}(q^2)}{m_N} + \bar{N}\sigma^{\mu\nu}\gamma^5 P_\nu N \frac{F_{A5}(q^2)}{m_N}. \end{aligned} \quad (3.37)$$

The suitable Gordon identity for this case is

$$\bar{N}\gamma^\mu\gamma^5 N = \frac{1}{2m_N}\bar{N}\left((p_4^\mu - p_2^\mu)\gamma^5 + i\sigma^{\mu\nu}(p_4^\mu + p_2^\mu)\gamma^5\right)N. \quad (3.38)$$

It makes the last term proportional to $\bar{N}\gamma^\mu\gamma^5 N$ and $\bar{N}q^\mu\gamma^5 N$. Moreover, the Dirac equation gives zero to the third term. So that the remaining term is

$$\begin{aligned} \langle N|\bar{n}\gamma^\mu\gamma^5 n|N\rangle = & \bar{N}\gamma^\mu\gamma^5 N \left(F_{A1} + 2iF_{A5}\right) + \bar{N}\gamma^5 q^\mu N \left(\frac{F_{A2}}{m_N} - i\frac{F_{A5}}{m_N}\right) \\ & + \bar{N}\sigma^{\mu\nu}\gamma^5 q_\nu N \frac{F_{A4}}{m_N}. \end{aligned} \quad (3.39)$$

We found no conserved current, so that all terms stay still. The general nucleus current for the axial-vector case can then be written as

$$\langle N|\bar{n}\gamma^\mu\gamma^5 n|N\rangle = \bar{N}\left(\gamma^\mu\gamma^5 F_A(q^2) + \frac{\gamma^5 q^\mu}{m_N} G_A(q^2) + \frac{\sigma^{\mu\nu}\gamma^5 q_\nu}{2m_N} H_A(q^2)\right)N. \quad (3.40)$$

Appearance of the second term is needed to consider the partially conserved axial current (Kurylov and Kamionkowski, 2004). Moreover, the third term accounts for the electric dipole moment. Applying the coherent criteria, the second and the third term can be neglected and we arrive at

$$\langle N|\bar{n}\gamma^\mu\gamma^5 n|N\rangle = \bar{N}\gamma^\mu\gamma^5 N F_A(q^2). \quad (3.41)$$

For the coefficient part, to include all protons and neutrons of the nucleus, we have (Cirelli *et al.*, 2013)

$$g_{AN} \equiv \mathcal{L} \sum_q g_{Aq} S_p \Delta_q^p + \mathcal{N} \sum_q g_{Aq} S_n \Delta_q^n. \quad (3.42)$$

Hence, the nuclear Lagrangian for axial-vector interaction becomes

$$\mathcal{L}_{AN} = g_{AN} \mathcal{A}_\mu \bar{N} \gamma^\mu \gamma^5 N F_A(q^2). \quad (3.43)$$

3.2.1.5. Tensorial Interaction

From the neutrino term, we have

$$\mathcal{L}_{Tn} = \langle n | \mathcal{L}_T | n \rangle = \sum_{n,q} g_{Tq} \mathcal{T}_{\mu\nu} \langle n | \bar{q} \sigma^{\mu\nu} q | n \rangle. \quad (3.44)$$

To the nucleon current, we have

$$\langle n | \bar{q} \sigma^{\mu\nu} q | n \rangle = \delta_q^n \bar{n} \sigma^{\mu\nu} n. \quad (3.45)$$

From nucleon to nucleus current, $\bar{n} \sigma^{\mu\nu} n \rightarrow \langle N | \bar{n} \sigma^{\mu\nu} n | N \rangle$, the general form for tensorial interaction can be expressed as

$$\begin{aligned} \langle N | \bar{n} \sigma^{\mu\nu} n | N \rangle &= \bar{N} \sigma^{\mu\nu} N F_{T_1}(q^2) + \bar{N} (\gamma^\mu P^\nu - \gamma^\nu P^\mu) N \frac{F_{T_2}(q^2)}{m_N} \\ &+ \bar{N} (\gamma^\mu q^\nu - \gamma^\nu q^\mu) N \frac{F_{T_3}(q^2)}{m_N} + \bar{N} (P^\mu q^\nu - P^\nu q^\mu) N \frac{F_{T_4}(q^2)}{m_N^2}. \end{aligned} \quad (3.46)$$

Appropriate Gordon identity for this form is

$$\bar{N} \gamma^\mu \gamma^\nu N = \frac{1}{4m_N} \bar{N} \left(\gamma^\nu (p_4^\mu + p_2^\mu) + q^\mu \gamma^\nu \right) N. \quad (3.47)$$

We can see that the second term will be proportional to

$$i8m_N \bar{N} \sigma^{\mu\nu} N + \bar{N} (\gamma^\mu q^\nu - \gamma^\nu q^\mu) N,$$

which reduces the general form to

$$\begin{aligned} \langle N | \bar{\nu} \sigma^{\mu\nu} \nu | N \rangle &= \bar{N} \sigma^{\mu\nu} N \left(F_{T_1} + 8iF_{T_2} \right) + \bar{N} (\gamma^\mu q^\nu - \gamma^\nu q^\mu) N \left(\frac{F_{T_3}}{m_N} + \frac{F_{T_2}}{m_N} \right) \\ &+ \bar{N} (P^\mu q^\nu - P^\nu q^\mu) N \frac{F_{T_4}}{m_N^2}. \end{aligned} \quad (3.48)$$

Redefining the form factors, we can write the general form as

$$\langle N | \bar{\nu} \sigma^{\mu\nu} \nu | N \rangle = \bar{N} \left(\sigma^{\mu\nu} F_T + \frac{(\gamma^\mu q^\nu - \gamma^\nu q^\mu)}{m_N} G_T + \frac{(P^\mu q^\nu - P^\nu q^\mu)}{m_N^2} H_T \right) N. \quad (3.49)$$

Requirement of coherency lead us to neglecting the second and the third term, so that

$$\langle N | \bar{\nu} \sigma^{\mu\nu} \nu | N \rangle = \bar{N} \sigma^{\mu\nu} N F_T(q^2). \quad (3.50)$$

For the coefficient, we have (Cirelli *et al.*, 2013)

$$g_{TN} = \mathcal{L} \sum_q g_{Tq} \delta_q^p + \mathcal{N} \sum_q g_{Tq} \delta_q^n. \quad (3.51)$$

The Lagrangian for axial-vector interaction at the nuclear level then becomes

$$\mathcal{L}_{TN} = g_{TN} \mathcal{T}_{\mu\nu} \bar{N} \sigma^{\mu\nu} N F_T(q^2). \quad (3.52)$$

3.2.2. Differential cross-section

We calculate the differential cross-section for each of proposed interaction in this section according to the interaction Lagrangians at the nuclear level we have obtained. In doing so, we notice that the neutrino currents for the scalar (pseudoscalar) can be rewritten as

$$\begin{aligned} \bar{\nu}_R \nu_L &= \left(\frac{1}{2} (1 + \gamma_5) \nu \right)^\dagger \gamma^0 \frac{1}{2} (1 - \gamma_5) \nu = \frac{1}{4} \nu^\dagger (1 + \gamma_5) \gamma^0 (1 - \gamma_5) \nu \\ &= \bar{\nu} P_L \nu, \end{aligned} \quad (3.53)$$

while for the vectorial (axial-vector) as

$$\begin{aligned}\bar{\nu}_L \gamma^\mu \nu_L &= \left(\frac{1}{2}(1 - \gamma_5) \nu \right)^\dagger \gamma^0 \gamma^\mu \frac{1}{2}(1 - \gamma_5) \nu = \frac{1}{4} \nu^\dagger (1 - \gamma_5) \gamma^0 \gamma^\mu (1 - \gamma_5) \nu \\ &= \bar{\nu} \gamma^\mu P_L \nu,\end{aligned}\quad (3.54)$$

which is the SM weak current, and for the tensorial as

$$\begin{aligned}\bar{\nu}_R \sigma^{\mu\nu} \nu_L &= \left(\frac{1}{2}(1 - \gamma_5) \nu \right)^\dagger \gamma^0 \sigma^{\mu\nu} \frac{1}{2}(1 - \gamma_5) \nu \\ &= \frac{1}{4} \nu^\dagger (1 - \gamma_5) \gamma^0 \sigma^{\mu\nu} (1 - \gamma_5) \nu = \bar{\nu} \sigma^{\mu\nu} P_L \nu.\end{aligned}\quad (3.55)$$

Moreover, every form factors for every interaction are adapted as the Helm form factor (2.34) from now on.

3.2.2.1. Scalar Contribution

Following the Feynman rules, the amplitude of the process in the Figure 12 can be constructed as

$$-i\mathcal{M}_S = \left[-ig_{S\nu} \bar{\nu}_3 P_L \nu_1 \right] \left[\frac{-i}{q^2 - m_S^2} \right] \left[-ig_{SN} \bar{N}_4 N_2 F(q^2) \right]. \quad (3.56)$$

In the propagator we have used m_S to account the mass of the scalar propagator. We can

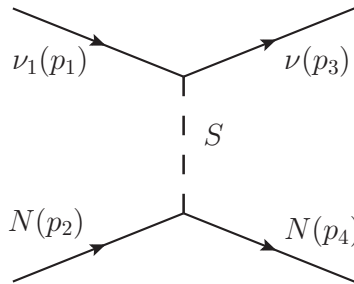


Figure 12. CEvNS with scalar mediator.

then rewrite this form as

$$\mathcal{M}_S = -\frac{1}{2} \frac{G_F Q_S}{q^2 - m_S^2} \bar{\nu}_3 (1 - \gamma_5) \nu_1 \bar{N}_4 N_2 F(q^2), \quad (3.57)$$

where we have defined the scalar coupling as $Q_S = g_{S\nu}g_{SN}/G_F$. The averaged amplitude square then becomes

$$\begin{aligned}
\langle |\mathcal{M}_S^2| \rangle &= \frac{1}{2} \sum |\mathcal{M}^2| \\
&= \frac{1}{2} \frac{G_F^2 Q_S^2 |F(q^2)|^2}{4(q^2 - m_S^2)^2} \sum [\bar{\nu}_3(1 - \gamma_5)\nu_1][\bar{\nu}_1(1 + \gamma_5)\nu_3][\bar{N}_4 N_2][\bar{N}_2 N_4] \\
&= \frac{G_F^2 Q_S^2 |F(q^2)|^2}{8(q^2 - m_S^2)^2} \text{Tr}[\not{p}_3(1 - \gamma_5)\not{p}_1(1 + \gamma_5)] \text{Tr}[(\not{p}_4 + m_N)(\not{p}_2 + m_N)] \\
&= \frac{G_F^2 Q_S^2 |F(q^2)|^2}{4(m_S^2 + 2m_N T)^2} (4p_1 \cdot p_3)(4p_2 \cdot p_4 + 4m_N^2),
\end{aligned} \tag{3.58}$$

and implementing the kinematics we have

$$\begin{aligned}
\langle |\mathcal{M}_S^2| \rangle &= \frac{G_F^2 Q_S^2 |F(q^2)|^2}{4(m_S^2 + 2m_N T)^2} 16(m_N T)(m_N(m_N + T) + m_N^2) \\
&= \frac{4G_F^2 Q_S^2 m_N^3 |F(q^2)|^2}{(m_S^2 + 2m_N T)^2} \left(2T + \frac{T^2}{m_N}\right).
\end{aligned} \tag{3.59}$$

Assuming $T \ll m_N$ and using $d\sigma/dT$, we find the differential cross section as

$$\left[\frac{d\sigma}{dT}\right]_S = \frac{G_F^2 Q_S^2 m_N^2 T |F(q^2)|^2}{4\pi E_\nu^2 (m_S^2 + 2m_N T)^2}. \tag{3.60}$$

3.2.2.2. Pseudoscalar Contribution

The Feynman rules for the process in Figure 13 gives the following amplitude

$$-i\mathcal{M}_P = \left[\bar{\nu}_3(-ig_{P\nu})\frac{1}{2}(1 - \gamma_5)\nu_1\right] \left[\frac{-i}{q^2 - m_P^2}\right] \left[g_{PN}\bar{N}(-i\gamma_5)NF(q^2)\right]. \tag{3.61}$$

This amplitude can be rewritten as

$$\mathcal{M}_P = -\frac{1}{2} \frac{G_F Q_P}{q^2 - m_P^2} F(q^2) \bar{\nu}_3(1 - \gamma_5)\nu_1 \bar{N}_4 i\gamma_5 N_2, \tag{3.62}$$

where the pseudoscalar coupling is $Q_P = g_{P\nu}g_{PN}/G_F$. The averaged amplitude square is

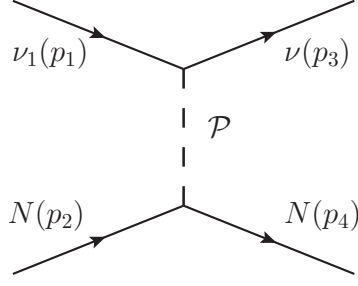


Figure 13. CEvNS with pseudoscalar mediator.

then becomes

$$\begin{aligned}
\langle |\mathcal{M}_P^2| \rangle &= \frac{1}{2} \sum |\mathcal{M}^2| \\
&= \frac{1}{2} \frac{G_F^2 Q_P^2 |F(q^2)|^2}{4(q^2 - m_P^2)^2} \sum [\bar{v}_3(1 - \gamma_5)v_1][\bar{v}_1(1 + \gamma_5)v_3][\bar{N}_4 i \gamma_5 N_2][\bar{N}_2 i \gamma_5 N_4] \\
&= \frac{G_F^2 Q_P^2 |F(q^2)|^2}{8(q^2 - m_P^2)^2} \text{Tr}[\not{p}_3(1 - \gamma_5)\not{p}_1(1 + \gamma_5)] \\
&\quad \times \text{Tr}[(\not{p}_4 + m_N)i\gamma_5(\not{p}_2 + m_N)i\gamma_5] \\
&= \frac{G_F^2 Q_P^2 |F(q^2)|^2}{4(m_P^2 + 2m_N T)^2} (4p_1 \cdot p_3)(4p_2 \cdot p_4 - 4m_N^2),
\end{aligned} \tag{3.63}$$

and after implementing the kinematics we have

$$\begin{aligned}
\langle |\mathcal{M}_P^2| \rangle &= \frac{G_F^2 Q_P^2 |F(q^2)|^2}{4(m_P^2 + 2m_N T)^2} 16(m_N T)(m_N(m_N + T) - m_N^2) \\
&= \frac{4G_F^2 Q_P^2 m_N^2 T^2 |F(q^2)|^2}{(m_P^2 + 2m_N T)^2}.
\end{aligned} \tag{3.64}$$

The differential cross section is then becomes

$$\left[\frac{d\sigma}{dT} \right]_P = \frac{G_F^2 Q_P^2 m_N T^2 |F(q^2)|^2}{8\pi E_\nu^2 (m_P^2 + 2m_N T)^2}. \tag{3.65}$$

3.2.2.3. Vector Contribution

The neutrino current for this case has the same form as the SM. To proceed further, we note that there is an interference of this new proposed Lagrangian with the SM counterpart. We start with the new vector interaction. Amplitude for the process in Figure 14 can be

constructed from the Feynman rules as

$$-i\mathcal{M}_V = \left[-ig_{V\nu}\bar{\nu}_3\gamma^\mu P_L\nu_1 \right] \left[\frac{-ig_{\mu\nu}}{q^2 - m_V^2} \right] \left[-ig_{VN}\bar{N}\gamma^\mu NF(q^2) \right]. \quad (3.66)$$

We have used m_V to denote the mass of the vectorial mediator. We can rewrite this as

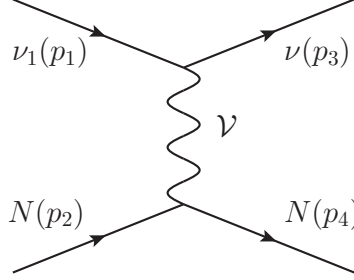


Figure 14. CEvNS with vectorial mediator.

$$\mathcal{M}_V = -\frac{1}{2} \frac{G_F Q_V}{q^2 - m_V^2} \bar{\nu}_3 \gamma^\mu (1 - \gamma_5) \nu_1 \bar{N}_4 \gamma_\mu N_2 F(q^2), \quad (3.67)$$

with $Q_V = g_{V\nu}g_{VN}/G_F$. The averaged amplitude square then becomes

$$\begin{aligned} \langle |\mathcal{M}_V^2| \rangle &= \frac{1}{2} \sum |\mathcal{M}_V^2| \\ &= \frac{1}{2} \frac{G_F^2 Q_V^2 |F(q^2)|^2}{4(q^2 - m_V^2)^2} \sum [\bar{\nu}_3 \gamma^\mu (1 - \gamma_5) \nu_1] [\bar{\nu}_1 \gamma^\nu (1 + \gamma_5) \nu_3] \\ &\quad \times [\bar{N}_4 \gamma_\mu N_2] [\bar{N}_2 \gamma_\nu N_4] \\ &= \frac{G_F^2 Q_V^2 |F(q^2)|^2}{8(q^2 - m_V^2)^2} \text{Tr} \left[\not{p}_3 \gamma^\mu (1 - \gamma_5) \not{p}_1 \gamma^\nu (1 + \gamma_5) \right] \\ &\quad \times \text{Tr} \left[(\not{p}_4 + m_N) \gamma_\mu (\not{p}_2 + m_N) \gamma_\nu \right] \\ &= \frac{G_F^2 Q_V^2 |F(q^2)|^2}{8(q^2 - m_V^2)^2} 2[4(p_1^\mu p_3^\nu + p_1^\nu p_3^\mu - p_1 \cdot p_3 g^{\mu\nu}) \\ &\quad - 4i\varepsilon^{\mu\alpha\nu\beta} p_{3\alpha} p_{1\beta}] \\ &\quad \times [4(p_{2\mu} p_{4\nu} + p_{2\nu} p_{4\mu} - p_2 \cdot p_4 g_{\mu\nu}) + 4g_{\mu\nu} m_N^2] \\ &= \frac{G_F^2 Q_V^2 |F(q^2)|^2}{8(q^2 - m_V^2)^2} 32 \left[2(p_1 \cdot p_2)(p_3 \cdot p_4) + 2(p_1 \cdot p_4)(p_2 \cdot p_3) \right. \\ &\quad \left. - 2(p_1 \cdot p_3) m_N^2 \right] \end{aligned} \quad (3.68)$$

and by implementing the kinematics we have

$$\langle |\mathcal{M}_V^2| \rangle = \frac{1}{8} \frac{G_F^2 Q_V^2 |F(q^2)|^2}{(m_V^2 + 2m_N T)^2} 128 m_N^2 E_V^2 \left[1 - \frac{m_N T}{2E_V^2} - \frac{T}{E_V} + \frac{T^2}{2E_V^2} \right]. \quad (3.69)$$

We can directly use this form to obtain the differential cross-section. But since there is an interference to the SM, we need to consider the sum of both amplitudes $\mathcal{M}_{tot} = \mathcal{M}_{SM} - \mathcal{M}_V$, which is nothing but

$$\mathcal{M}_{tot} = \left[\frac{G_F Q_{SM}}{2\sqrt{2}} + \frac{G_F Q_V}{2(q^2 - m_V^2)} \right] \bar{v}_3 \gamma^\mu (1 - \gamma_5) v_1 \bar{N}_4 \gamma_\mu N_2 F(q^2). \quad (3.70)$$

The averaged amplitude square then becomes

$$\begin{aligned} \langle |\mathcal{M}_{tot}|^2 \rangle &= \frac{1}{2} |\mathcal{M}_{tot}|^2 \\ &= \frac{1}{2} \frac{1}{4} |F(q^2)|^2 \left[\frac{G_F^2 Q_{SM}^2}{2} + \frac{G_F^2 Q_V^2}{(q^2 - m_V^2)^2} + \frac{2G_F^2 Q_{SM} Q_V}{\sqrt{2}(q^2 - m_V^2)} \right] \\ &\quad \times 128 m_N^2 E_V^2 \left[1 - \frac{m_N T}{2E_V^2} - \frac{T}{E_V} + \frac{T^2}{2E_V^2} \right] \\ &= 8 m_N^2 |F(q^2)|^2 \left[\frac{G_F^2 Q_{SM}^2}{2} + \frac{G_F^2 Q_V^2}{(q^2 - m_V^2)^2} + \frac{2G_F^2 Q_{SM} Q_V}{\sqrt{2}(q^2 - m_V^2)} \right] \\ &\quad \times (2E_V^2 - m_N T). \end{aligned} \quad (3.71)$$

The total differential cross section of this process then becomes

$$\begin{aligned} \left[\frac{d\sigma}{dT} \right]_{SM+V} &= \left[\frac{G_F^2 Q_{SM}^2}{2} + \frac{G_F^2 Q_V^2}{(m_V^2 + 2m_N T)^2} - \frac{2G_F^2 Q_V Q_{SM}}{\sqrt{2}(m_V^2 + 2m_N T)} \right] \\ &\quad \times \frac{m_N (2E_V^2 - m_N T) |F(q^2)|^2}{4\pi E_V^2}. \end{aligned} \quad (3.72)$$

Noticing that the first term is nothing but the SM case, the second and the third term respectively gives the new vector and the interference term.

3.2.2.4. Axial-vector Contribution

Feynman rules for the process in Figure 15 gives the following amplitude

$$-i\mathcal{M}_A = \left[-ig_{Av} \bar{\nu}_3 \gamma^\mu P_L \nu_1 \right] \left[\frac{-ig_{\mu\nu}}{q^2 - m_A^2} \right] \left[-ig_{AN} \bar{N} \gamma^\mu \gamma^5 N F(q^2) \right], \quad (3.73)$$

or nothing but

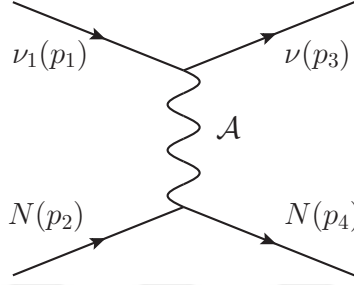


Figure 15. CEvNS with axial-vector mediator.

$$\mathcal{M}_A = -\frac{1}{2} \frac{G_F Q_A}{q^2 - m_A^2} F(q^2) \bar{\nu}_3 \gamma^\mu (1 - \gamma_5) \nu_1 \bar{N}_4 \gamma_\mu \gamma_5 N_2, \quad (3.74)$$

with the axial-vector coupling is $Q_A = g_{Av} g_{AN} / G_F$. The averaged amplitude square then becomes

$$\begin{aligned} \langle |\mathcal{M}_A^2| \rangle &= \frac{1}{2} \sum |\mathcal{M}_A^2| \\ &= \frac{1}{2} \frac{G_F^2 Q_A^2 |F(q^2)|^2}{4(q^2 - m_A^2)^2} \sum [\bar{\nu}_3 \gamma^\mu (1 - \gamma_5) \nu_1] \\ &\quad [\bar{\nu}_1 \gamma^\nu (1 + \gamma_5) \nu_3] [\bar{N}_4 \gamma_\mu \gamma_5 N_2] [\bar{N}_2 \gamma_\nu \gamma_5 N_4] \\ &= \frac{G_F^2 Q_A^2 |F(q^2)|^2}{8(q^2 - m_A^2)^2} \text{Tr} \left[\not{p}_3 \gamma^\mu (1 - \gamma_5) \not{p}_1 \gamma^\nu (1 + \gamma_5) \right] \\ &\quad \times \text{Tr} \left[(\not{p}_4 + m_N) \gamma_\mu \gamma_5 (\not{p}_2 + m_N) \gamma_\nu \gamma_5 \right] \\ &= \frac{G_F^2 Q_A^2 |F(q^2)|^2}{8(q^2 - m_A^2)^2} 2[4(p_1^\mu p_3^\nu + p_1^\nu p_3^\mu - p_1 \cdot p_3 g^{\mu\nu}) \\ &\quad - 4i\varepsilon^{\mu\alpha\nu\beta} p_{3\alpha} p_{1\beta}] \\ &\quad \times [4(p_{2\mu} p_{4\nu} + p_{2\nu} p_{4\mu} - p_2 \cdot p_4 g_{\mu\nu}) - 4g_{\mu\nu} m_N^2]. \end{aligned} \quad (3.75)$$

Implementing the kinematics we have

$$\begin{aligned}
\langle |\mathcal{M}_A^2| \rangle &= \frac{G_F^2 Q_A^2 |F(q^2)|^2}{8(q^2 - m_A^2)^2} 32 \left[2(p_1 \cdot p_2)(p_3 \cdot p_4) + 2(p_1 \cdot p_4)(p_2 \cdot p_3) \right. \\
&\quad \left. + 2(p_1 \cdot p_3)m_N^2 \right] \\
&= \frac{G_F^2 Q_A^2 |F(q^2)|^2}{8(m_A^2 + 2m_N T)^2} 128 m_N^2 E_v^2 \left[1 + \frac{m_N T}{2E_v^2} - \frac{T}{E_v} + \frac{T^2}{2E_v^2} \right].
\end{aligned} \tag{3.76}$$

Similar to the vector case, here we encounter interference with the SM case. The total amplitude then becomes $\mathcal{M}_{tot} = \mathcal{M}_{SM} - \mathcal{M}_A$, where now we consider the SM case also contain axial-vector term

$$\mathcal{M}_{SM} = \frac{G_F}{\sqrt{2}} g_L^V F(q^2) [\bar{\nu}_3 \gamma^\mu (1 - \gamma_5) \nu_1] [\bar{N}_4 \gamma_\mu (Q_{SM} - \gamma_5 Q_a) N_2]. \tag{3.77}$$

We consider the form of Q_a from (Cerdēno *et al.*, 2016)

$$Q_a = S_N (\Delta_u^{(p)} - \Delta_d^{(p)} - \Delta_s^{(p)}). \tag{3.78}$$

The averaged amplitude square, using the kinematic from previous section, then becomes

$$\begin{aligned}
\langle |\mathcal{M}_{tot}|^2 \rangle &= \frac{1}{2} \sum |\mathcal{M}_{tot}|^2 \\
&= \frac{1}{2} |F(q^2)|^2 \left\{ \frac{G_F^2 Q_{SM}^2}{8} 128 m_N^2 E_v^2 \left[1 - \frac{m_N T}{2E_v^2} - \frac{T}{E_v} + \frac{T^2}{2E_v^2} \right] \right. \\
&\quad \left. + \left[\frac{G_F^2 Q_a^2}{8} + \frac{G_F^2 Q_A^2}{4(q^2 - m_A^2)^2} - \frac{G_F^2 Q_a Q_A}{2\sqrt{2}(q^2 - m_A^2)} \right] \right. \\
&\quad \times \left[1 + \frac{m_N T}{2E_v^2} + \frac{T}{E_v} + \frac{T^2}{2E_v^2} \right] + \frac{G_F Q_{SM}}{2\sqrt{2}} \left[\frac{G_F Q_A}{2(q^2 - m_A^2)} - \frac{G_F Q_a}{2\sqrt{2}} \right] \\
&\quad \times [\bar{\nu}_3 \gamma^\mu (1 - \gamma_5) \nu_1] [\bar{\nu}_1 \gamma^\nu (1 - \gamma_5) \nu_3] \\
&\quad \times \left([\bar{N}_4 \gamma_\mu N_2] [\bar{N}_4 \gamma_\nu \gamma_5 N_2] + [\bar{N}_4 \gamma_\mu \gamma_5 N_2] [\bar{N}_4 \gamma_\nu N_2] \right) \left. \right\},
\end{aligned} \tag{3.79}$$

and after calculating the last term, we have

$$\begin{aligned}
\langle |\mathcal{M}_{tot}|^2 \rangle &= \frac{1}{2} |F(q^2)|^2 \left\{ \frac{G_F^2 Q_{SM}^2}{8} 128 m_N^2 E_V^2 \left[1 - \frac{m_N T}{2E_V^2} - \frac{T}{E_V} + \frac{T^2}{2E_V^2} \right] \right. \\
&\quad + \left[\frac{G_F^2 Q_a^2}{8} + \frac{G_F^2 Q_A^2}{4(q^2 - m_A^2)^2} - \frac{G_F^2 Q_a Q_A}{2\sqrt{2}(q^2 - m_A^2)} \right] \\
&\quad \times 128 m_N^2 E_V^2 \left[1 + \frac{m_N T}{2E_V^2} - \frac{T}{E_V} + \frac{T^2}{2E_V^2} \right] \\
&\quad \left. + \frac{G_F Q_{SM}}{2\sqrt{2}} \left[\frac{G_F Q_A}{2(q^2 - m_A^2)} - \frac{G_F Q_a}{2\sqrt{2}} \right] 128 m_N^2 E_V^2 \left[1 - \left(1 - \frac{T}{E_V} \right)^2 \right] \right\}. \tag{3.80}
\end{aligned}$$

Simplifying this we find (and using $q^2 = -2m_N T$)

$$\begin{aligned}
\langle |\mathcal{M}_{tot}|^2 \rangle &= 8 G_F^2 m_N^2 E_V^2 |F(q^2)|^2 \left\{ Q_{SM}^2 \left[1 - \frac{m_N T}{2E_V^2} \right] + Q_a^2 \left[1 + \frac{m_N T}{2E_V^2} \right] \right. \\
&\quad - Q_{SM} Q_a \left[\frac{2E_V T}{E_V^2} \right] + \frac{4Q_a Q_A}{\sqrt{2}(m_A^2 + 2m_N T)} \left[1 + \frac{m_N T}{2E_V^2} \right] \\
&\quad \left. - \frac{Q_{SM} Q_A}{\sqrt{2}(m_A^2 + 2m_N T)} \left[\frac{2E_V T}{E_V^2} \right] + \frac{2Q_A^2}{(m_A^2 + 2m_N T)^2} \left[1 + \frac{m_N T}{2E_V^2} \right] \right\}, \tag{3.81}
\end{aligned}$$

where the first three terms are for the SM with axial-vector only and we have neglected terms with order of (T^2/E_V^2) . Explicitly, the differential cross section of the SM is

$$\begin{aligned}
\left[\frac{d\sigma}{dT} \right]_{SM+a} &= \frac{G_F^2 m_N |F(q^2)|^2}{4\pi} \left[(Q_{SM}^2 + Q_a^2) - (Q_{SM}^2 - Q_a^2) \frac{m_N T}{2E_V^2} \right. \\
&\quad \left. - 2Q_{SM} Q_a \frac{T}{E_V} \right]. \tag{3.82}
\end{aligned}$$

Notice that as $Q_A \rightarrow 0$, we obtain again the SM case. We then find the differential cross section for the new axial-vector as

$$\left[\frac{d\sigma}{dT} \right]_A = \frac{G_F^2 Q_A^2 m_N |F(q^2)|^2 (2E_V^2 + m_N T)}{4\pi E_V^2 (m_A^2 + 2m_N T)^2}, \tag{3.83}$$

and the interference term as

$$\begin{aligned}
\left[\frac{d\sigma}{dT} \right]_{SM+a+A}^{int} &= \frac{G_F^2 Q_a Q_A m_N |F(q^2)|^2 (2E_V^2 + m_N T)}{2\sqrt{2}\pi E_V^2 (m_A^2 + 2m_N T)} \\
&\quad - \frac{G_F^2 Q_{SM} Q_A m_N |F(q^2)|^2 T}{2\sqrt{2}\pi E_V (m_A^2 + 2m_N T)}. \tag{3.84}
\end{aligned}$$

It is however found that the axial-vector term of SM is negligible for heavy nucleus (Papoulias and Kosmas, 2018). Therefore we neglect the Q_a term and hence the new axial-vector directly added with the SM signal in this work.

3.2.2.5. Tensor Contribution

The amplitude of the process in Figure 16 can be obtained from Feynman rules as

$$-i\mathcal{M}_T = \left[-ig_{Tv}\bar{\nu}_3\sigma^{\mu\nu}P_L\nu_1 \right] \left[\frac{-ig_{\mu\mu'}g_{\nu\nu'}}{q^2 - m_T^2} \right] \left[-ig_{TN}\bar{N}\sigma^{\mu'\nu'}NF(q^2) \right], \quad (3.85)$$

where m_T represents mass of the tensorial mediator. Note that here we naively use the

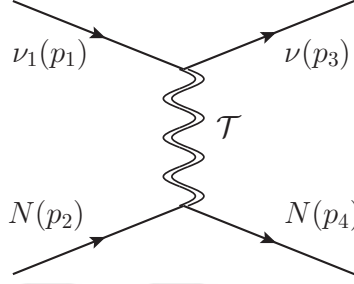


Figure 16. CEvNS with tensorial mediator.

propagator for the tensor field mediator. We can then rewrite the amplitude as

$$\mathcal{M}_T = -\frac{1}{2} \frac{G_F Q_T}{q^2 - m_T^2} F(q^2) \bar{\nu}_3 \sigma^{\mu\nu} (1 - \gamma_5) \nu_1 \bar{N}_4 \sigma_{\mu\nu} N_2, \quad (3.86)$$

where $Q_T = g_{Tv}g_{TN}/G_F$. The averaged amplitude square then becomes

$$\begin{aligned} \langle |\mathcal{M}_T^2| \rangle &= \frac{1}{2} |\mathcal{M}^2| \\ &= \frac{1}{2} \frac{G_F^2 Q_T^2 |F(q^2)|^2}{4(q^2 - m_T^2)^2} \sum \frac{1}{16} [\bar{\nu}_3(\gamma^\mu\gamma^\nu - \gamma^\nu\gamma^\mu)(1 - \gamma_5)\nu_1] \\ &\quad \times [\bar{\nu}_1(1 + \gamma_5)(\gamma^\alpha\gamma^\beta - \gamma^\beta\gamma^\alpha)\nu_3] \\ &\quad \times [\bar{N}_4(\gamma_\mu\gamma_\nu - \gamma_\nu\gamma_\mu)N_2][\bar{N}_2(\gamma_\alpha\gamma_\beta - \gamma_\beta\gamma_\alpha)N_4] \\ &= \frac{1}{128} \frac{G_F^2 Q_T^2 |F(q^2)|^2}{(q^2 - m_T^2)^2} \text{Tr}[\not{p}_3(\gamma^\mu\gamma^\nu - \gamma^\nu\gamma^\mu)(1 - \gamma^5)\not{p}_1(1 + \gamma^5)] \\ &\quad \times (\gamma^\alpha\gamma^\beta - \gamma^\beta\gamma^\alpha) \text{Tr}[\not{p}_4(\gamma_\mu\gamma_\nu - \gamma_\nu\gamma_\mu)\not{p}_2(\gamma_\alpha\gamma_\beta - \gamma_\beta\gamma_\alpha)], \end{aligned} \quad (3.87)$$

and using Mathematica to compute the traces, we find

$$\langle |\mathcal{M}_T^2| \rangle = \frac{256G_F^2 Q_T^2 |F(q^2)|^2}{(m_T^2 + 2m_N T)^2} \left[1 - \frac{T}{E_\nu} + \frac{T^2}{4E_\nu^2} - \frac{m_N T}{4E_\nu^2} \right], \quad (3.88)$$

and for $T \ll E_\nu$, then we have

$$\langle |\mathcal{M}_T^2| \rangle = \frac{256G_F^2 Q_T^2 |F(q^2)|^2}{(m_T^2 + 2m_N T)^2} \left(1 - \frac{m_N T}{4E_\nu^2} \right). \quad (3.89)$$

Therefore, the differential cross section becomes

$$\left[\frac{d\sigma}{dT} \right]_T = \frac{2G_F^2 Q_T^2 m_N |F(q^2)|^2 (4E_\nu^2 - m_N T)}{\pi E_\nu^2 (m_T^2 + 2m_N T)^2}. \quad (3.90)$$

3.3. Summary of Generalized Interactions

The NSI gives a factor correction to the SM which come from the NSI charge Q_{NSI} . The charge provides deviation from the SM according to how neutrinos interact with quarks inside the nucleus. There are two terms in general which consist of the FC plus the FV case of neutrino. The FC case would change value of the SM factor if the same neutrino flavor observed from initial and final state (i.e. $\epsilon_{ee}, \epsilon_{\mu\mu}, \epsilon_{\tau,tau}$), while the FV case would add an additional term if neutrino flavor changes (i.e. $\epsilon_{e\mu}, \epsilon_{e\tau}, \epsilon_{\mu e}, \epsilon_{\mu\tau}, \epsilon_{e,tau}, \epsilon_{\mu,tau}$).

The simplified model provides five possible new interactions that come from the most general bilinear combination. Each of which proposes a light new mediator with the corresponding coupling to the neutrino and quark constituent of the nucleus. In general, the differential cross-section of each interaction can be summarized as in Table 3.

Table 3. Summary of quantities from simplified model.

New Lagrangian	Nucleus-coupling	Differential Cross-section
(3.7)	(3.17)	(3.60)
(3.8)	(3.24)	(3.65)
(3.9)	(3.28)	(3.72)
(3.10)	(3.42)	(3.83)
(3.11)	(3.51)	(3.90)

4. NUMERICAL RESULTS AND DISCUSSIONS

In this chapter, we present phenomenological predictions of the CE ν NS in the framework of general neutrino interactions. We assign benchmarks in accordance with the COHERENT (Akimov *et al.*, 2017), and also from detector such as the TEXONO (Kerman *et al.*, 2016), CONUS (Bonet *et al.*, 2020), and CONNIE (Aguilar-Arevalo *et al.*, 2019). Some properties of these experiments that we utilize in this work are given in Table.4.

Table 4. Key properties from several experiments.

Experiment	ν Type	Nuclear threshold	Energy Range	Detector
COHERENT	$\nu_e, \nu_\mu, \bar{\nu}_\mu$	20 keV	50, 100 MeV	CsI, Ar, Xe
TEXONO	$\bar{\nu}_e$	0.1 keV	2 – 8 MeV	Ge
CONUS	$\bar{\nu}_e$	0.1 keV	< 10 MeV	Ge
CONNIE	ν_α	1 keV	< 60 MeV	Si

In what follows, we present the kinematics of the CE ν NS, its SM prediction, and possible new physics from the NSI and the simplified model. We also provide an effect of the mass on cross section from the new interactions. Finally, the bound as mass-coupling planes for each case is presented from χ^2 -analysis focusing on COHERENT 2017 data.

4.1. Kinematics and Form Factor Effect

The maximum nuclear recoil energy

$$T_{max} = \frac{2E_\nu^2}{m_N + 2E_\nu} \approx \frac{2E_\nu^2}{m_N} \quad (4.1)$$

as of initial neutrino energy in the CE ν NS process for nuclei mentioned in the Tab.4 is given in Figure 17 (left-panel). We can see that a lighter nucleus has larger recoil energy. Here, we have taken the averaged mass number of the composite CsI target. If the maximum threshold energy is large, such as approaching the initial neutrino energy, we obtain a linear behavior. This case for Ge target is shown in Figure 17 (right-panel), where the linearity meets at

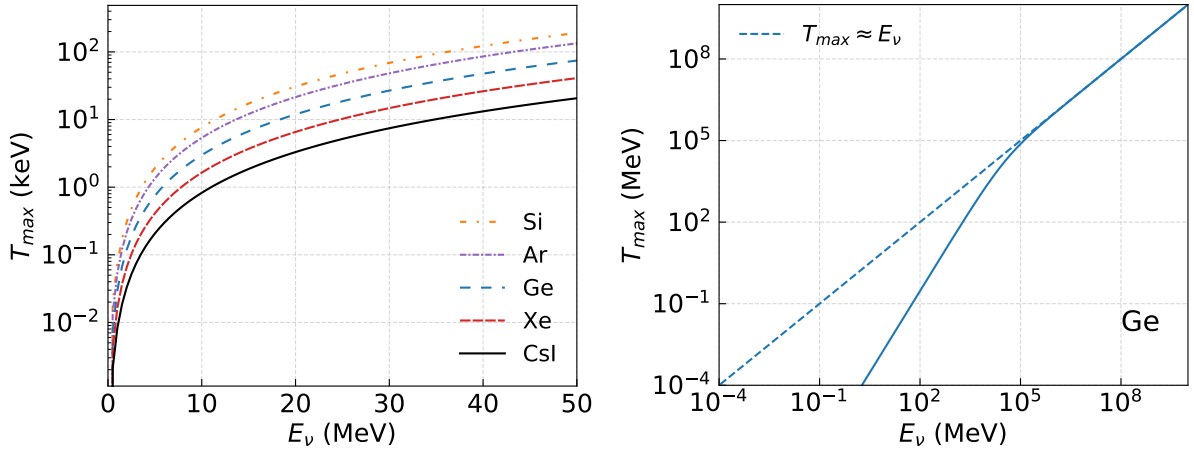


Figure 17. Behavior of T_{max} for some different nucleus (left). Effect of T_{max} for high E_ν (right).

around 10^5 GeV neutrino energy. In this limit, coherent interaction is not relevant.

The behavior of form factors, using the Helm parameterization, from the considered nuclei are shown in Figure 18 (left) as a function of nuclear recoil energy. It indicates that criteria of full coherency occur in the low nuclear recoil energy. We may also obtain the

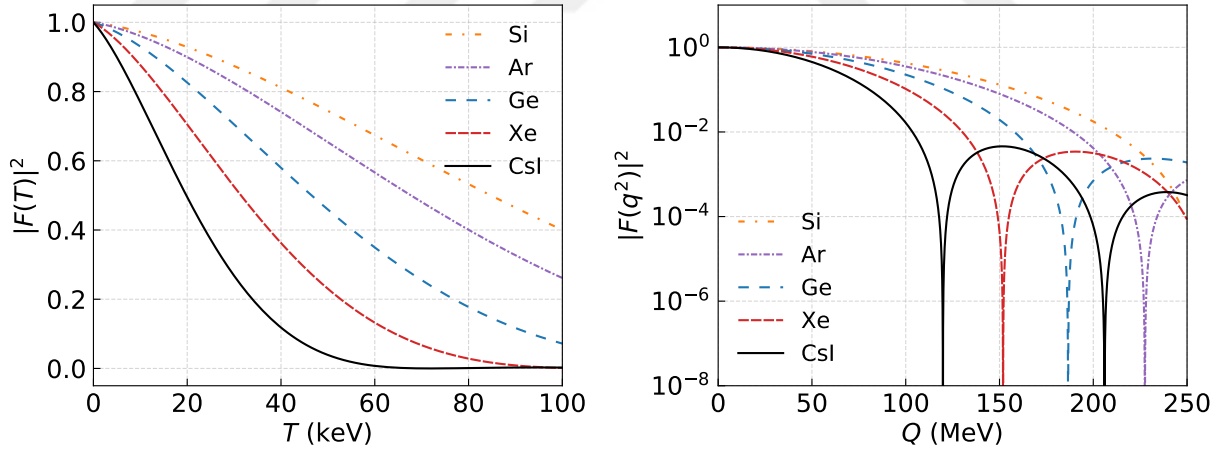


Figure 18. T -dependent (left) and Q -dependent of the Helm form factor (right).

behavior for momentum transfer dependent Q in Figure 18 (right). For this purpose we use $Q = \sqrt{2m_N T}$. From this result, it can be considered that we may take the form factor as 1 below 50 MeV momentum transfer. The Helm form factor is commonly used for spin-independent nucleon (Engel, 1991). It is then obvious that CEvNS is a low energy phenomenon.

4.2. Standard Model

We present the SM CE ν NS T -dependent differential cross-section in Figure 19 for the considered nuclei in Table 4. Two initial neutrino energies are chosen, 5 MeV and 50 MeV. The mass of the nuclei is in an atomic mass unit (amu). In this calculation, we have implemented the form factor effect. It shows that a heavier nucleus gives a larger spectrum and fall earlier than the lighter nucleus for both considered neutrino energy. The CsI target is calculated by separating its constituent, Cs and I, and then adding them up. With this treatment, even though has a larger spectrum, the CsI falls nearly at the same recoil energy as the Xe target.

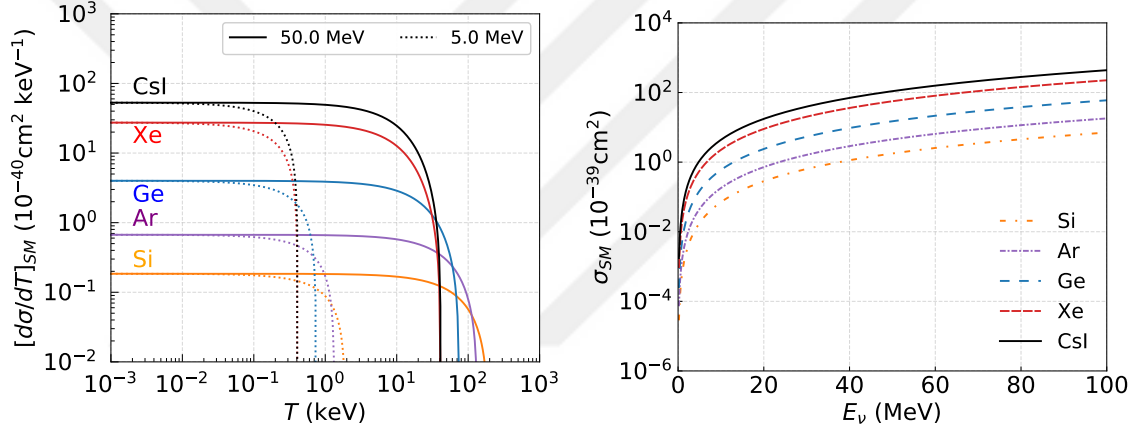


Figure 19. SM CE ν NS differential (left) and its total cross-section spectrum (right) for five nucleus targets.

The total cross-section of CE ν NS can be found by integrating the differential cross section. In general we have

$$\sigma = \int_{T_{th}}^{T_{max}} dT \frac{d\sigma}{dT}. \quad (4.2)$$

By integrating from $0 < E_\nu < 100$ MeV, we show the total cross-section spectrum of the process in Figure 19 (right). The CsI, being the heaviest target, provides the higher value among concerning targets, followed by Xe, Ge, Ar, and then Si. Using the properties of the first COHERENT experiment for 308 days running time, we also show the differential rate of CE ν NS in Figure 20 for the five considered target. It is obtained by convoluting the differential cross section with the neutrino flux. It indicates that lightest target gives smaller

spectrum with long T dependency. Note that for the CsI, we have added the contribution of Cs and I nucleus separately.

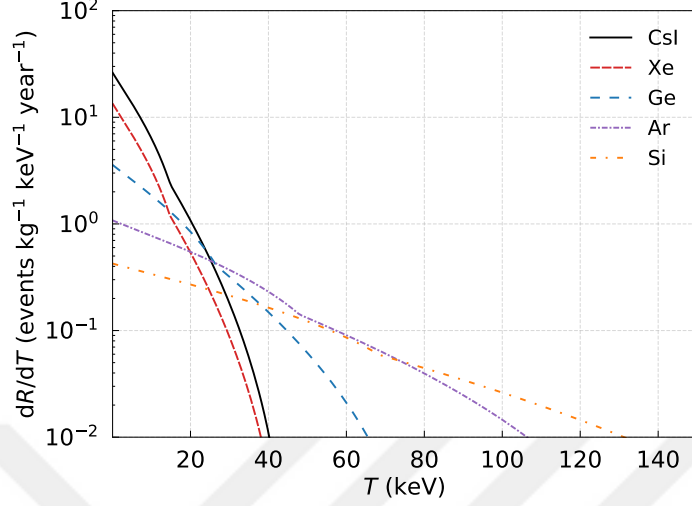


Figure 20. Differential rate of SM CEvNS for five nucleus targets.

4.3. Non-Standard Interactions

We present differential cross-section from different targets correspond to an accelerator (CsI, Xe, Ar) and detector (Ge, Si) neutrino properties in Figure 21. From the former, we choose 100 and 50 MeV neutrino energy which is criteria from the COHERENT, and for the latter 8 and 5 MeV, appropriate to TEXONO, CONUS and CONNIE. Recent parameter values of NSI interaction strength from Ref.(Giunti, 2020), given in Table 5, are used to see the NSI behavior. With these values, the NSI spectrum (blue line) is expected to be

Table 5. Considered NSI parameters for plotting.

FC:	$\varepsilon_{ee}^{uV} = 0.02$	$\varepsilon_{ee}^{dV} = 0.17$	$\varepsilon_{\mu\mu}^{uV} = 0.18$	$\varepsilon_{\mu\mu}^{dV} = 0.17$	$\varepsilon_{\mu e}^{uV} = 0.04$
FV:	$\varepsilon_{\mu e}^{dV} = 0.04$	$\varepsilon_{\tau e}^{uV} = 0.16$	$\varepsilon_{\tau e}^{dV} = 0.16$	$\varepsilon_{\tau\mu}^{uV} = 0.04$	$\varepsilon_{\tau\mu}^{dV} = 0.04$

approximately ~ 10 orders larger than the SM (green line). The grey region represents the minimum nuclear threshold energy, taken from relevant observation of the chosen nucleus target. For Si, the threshold is 1 keV, for Ge is 0.1 keV, and for Ar, Xe, and CsI is 20 keV. The spectrum of each cases fall-off after reaching this value even for the CsI with 50 MeV

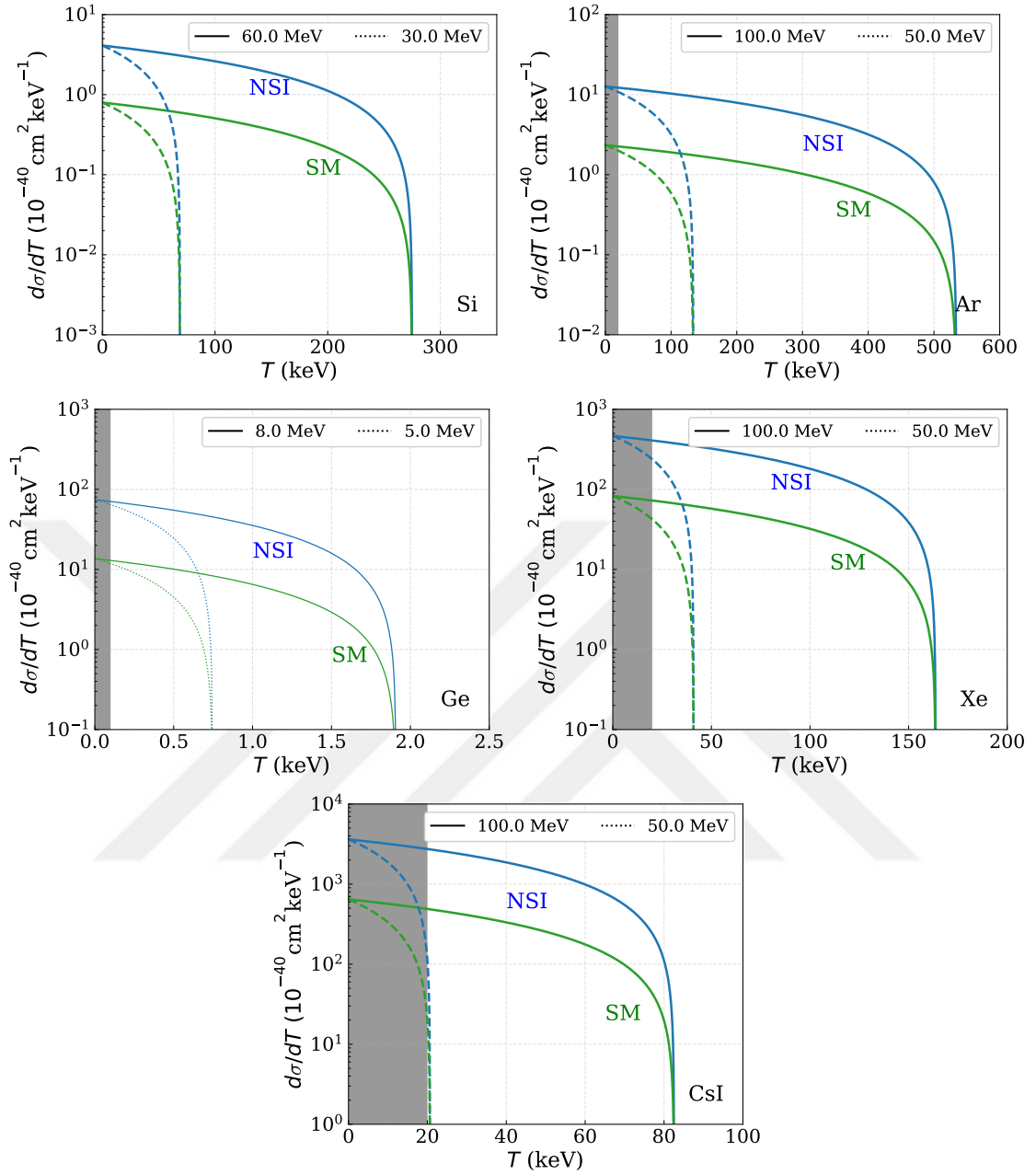


Figure 21. CEvNS differential cross section for Si, Ar, Ge, Xe, and CsI with threshold criteria from experiment using recent NSI parameters.

neutrino energy before the spectrum reaches 25 keV. Notice that for the Si, its spectra reaches over 250 keV T so that the threshold region is hardly seen.

Bound prediction of NSI parameters on the CEvNS process is shown in Figure 22, which is extracted from $\sigma_0^{NSI}/\sigma_0^{SM}$ (Mustamin and Demirci, 2021). This ratio shows that the NSI effect to the SM is independent with the considered target nuclei. here, we assume $\epsilon_{ab}^{uV} \approx -\epsilon_{ab}^{dV}$ and $N/Z \approx 1$. In obtaining these results, two preferred parameters are taken and

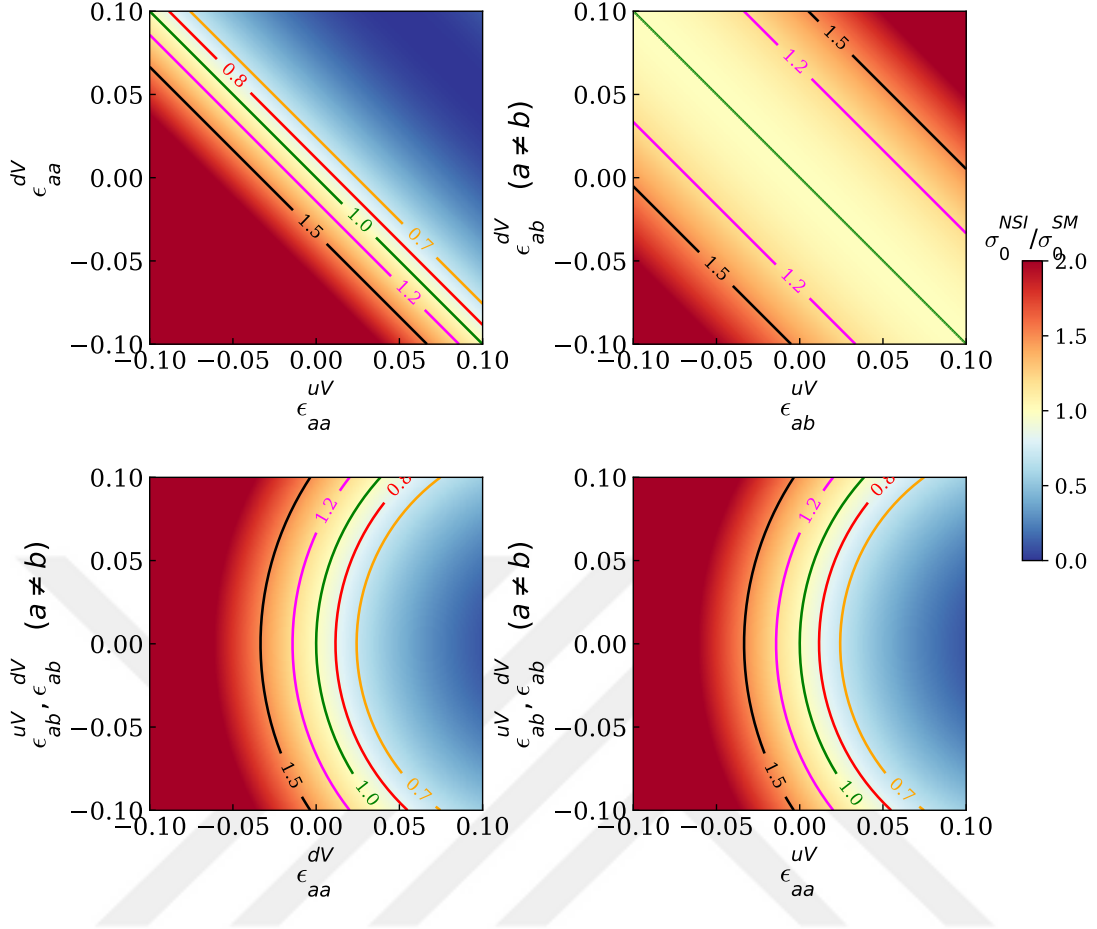


Figure 22. Bound prediction of the NSI parameters in CEvNS process.

the others are set to be zero. We show the case of the SM, in other words no new physics appears, as the green line where the ratio is equal to one. The other lines are taken to indicate deviation if a new interaction takes place. The range has been set within $(-0.1, 0.1)$ interval so that the deviation can be clearly seen even for a small range of ϵ .

The ratio can be 0, indicated by the vanishing contours, or increase two times larger than the SM as indicated by the color bar. The left-top figure shows the case of "non-universal" FC, as $a = b = e, \mu, \tau$. A small deviation from the SM, either the NSI is larger or lower, has been presented by the other four possibilities. The significance region of the NSI lies in the lower part of this case. The right-top indicates the FV case when $a \neq b$. Only the $\sigma_0^{NSI}/\sigma_0^{SM} > 1$ case appears here, which indicates that if we observe a lower value of deviation, the other parameters would be responsible for explanation. In other words, the FV case could not be explained if we have a lower cross-section value. Also note the deviation distance from the SM is relatively larger than the FC case. The two bottom panels show a

combination of FC and FV. The bottom-left is the combination of FC on the d (ϵ_{aa}^{dV}) and the bottom-right for the u (ϵ_{aa}^{uV}) with the FV cases ($\epsilon_{ab}^{u,dV}$, where $a \neq b$). These two indicate the same behaviors would appear from these considerations. The significant effect of NSI is indicated to occur in the negative region of ϵ_{aa}^{dV} and ϵ_{aa}^{uV} , at least for the > 1.5 line. Our obtained predictions can be used for further analysis of the NSI status using experimental data from observation.

4.4. Simplified Model

The general neutrino interaction here corresponds to the model on explaining solar neutrino with possible dark matter interaction (Cerděno *et al.*, 2016). With the analytical results in the previous chapter, their differential cross-sections are shown in Figure 23 for scalar, pseudoscalar, vectorial, axial-vector, and tensorial interactions. In obtaining these results, we have considered universal coupling from every new interaction with either neutrino or quark, with $g_{\nu S} = g_{qS} = 10^{-6}$. This value is taken for representative, from typical new mediator consideration which predicted to be even smaller (Farzan *et al.*, 2018). Values of the coupling parameters for each case are given in Table 6. We set all the possible new medi-

Table 6. Values of the simplified parameters.

Parameter	Value	Reference
$f_{T_u}^p$	0.0208	(Hoferichter <i>et al.</i> , 2015)
$f_{T_u}^n$	0.0189	
$f_{T_d}^p$	0.0411	
$f_{T_d}^n$	0.0451	
$\Delta_u^p = \Delta_u^n$	0.842	
$\Delta_d^p = \Delta_d^n$	-0.427	
$h_u^p = h_u^n$	1.65	(Ema <i>et al.</i> , 2021)
$h_d^p = h_d^n$	0.375	
$\delta_u^p = \delta_d^n$	0.84	(Belanger <i>et al.</i> , 2009)
$\delta_d^p = \delta_u^n$	-0.23	

ators to carry 100 MeV mass. We also consider two neutrino energies, 5 MeV and 50 MeV, corresponding to the energy criteria from a neutrino accelerator and detector respectively.

As in the previous section, we also provide five different nuclei as the target. Regarding

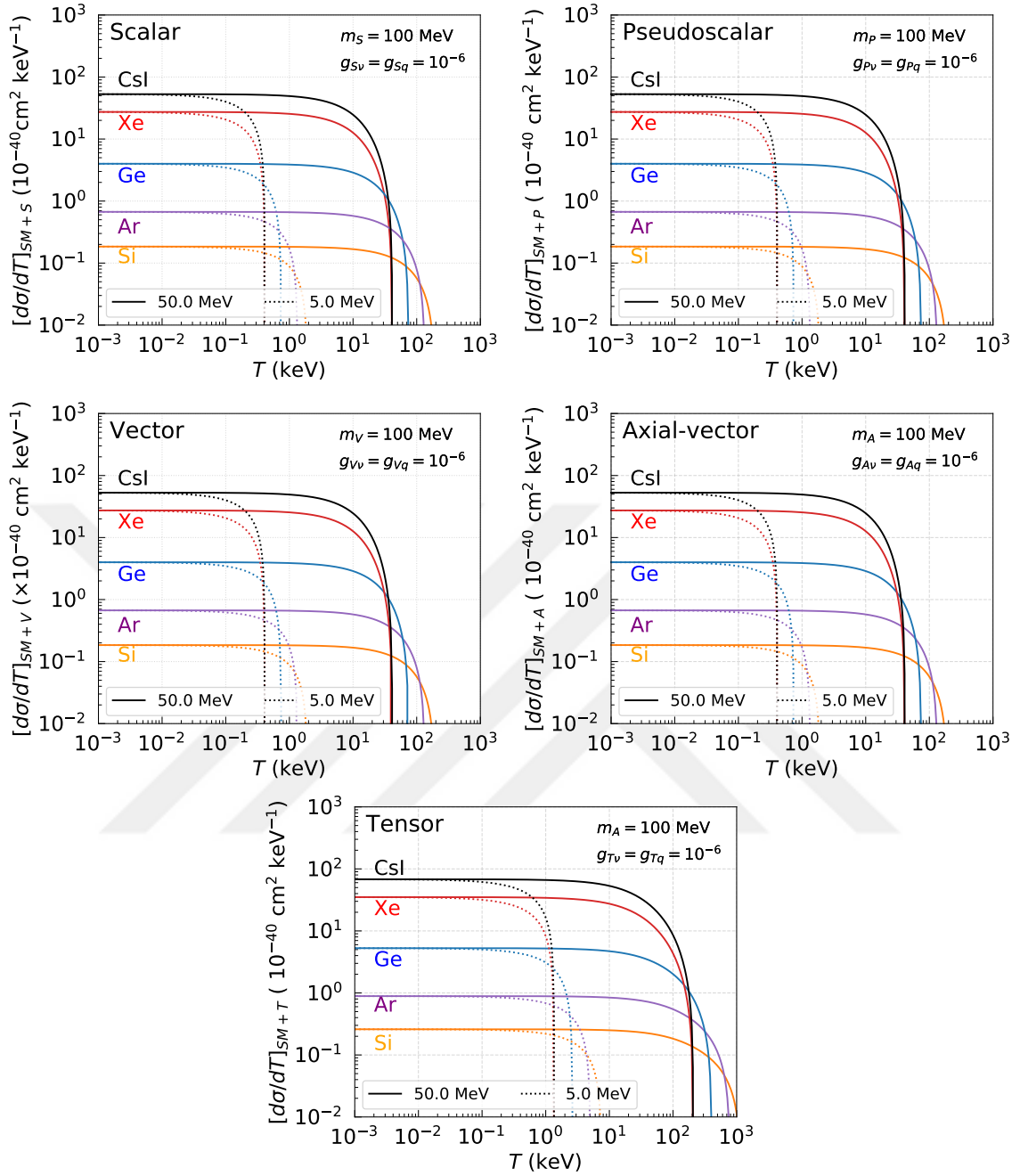


Figure 23. The differential cross-section for CEvNS process with the simplified model.

these choices, we can see that a heavier target gives a larger differential cross-section. The scale of neutrino energy indicates that the spectrum goes off earlier for a smaller value. For the CsI target, we separate the differential cross-section for each constituent target. All of the possible new interactions provide a well-behaved spectrum for the two considered energies. Considering the nuclear threshold, differential cross sections fall after reaching 0.1 keV. This behavior indicates the importance of having equipment with low-energy sensitivity.

4.5. Analysis of COHERENT Data

We constraint the parameter of the NSI and the simplified model using minimum χ^2 -method (Fieldman and Cousins, 1998). Published data from experiments consist of uncertainty in the best value observed. With this technique, we may put a confident level (CL) bound on the parameter. In this work, we consider 68% and 90% CL limits from the con-

Table 7. Significance value and its corresponding degree of freedom.

CL (%)	degree of freedom				
	1	2	3	4	5
68.30	1.00	2.30	3.53	4.72	5.89
90.00	2.71	4.61	6.25	7.78	9.24
95.40	4.00	6.17	8.02	9.70	11.3
99.00	6.63	9.21	11.3	13.3	15.1
99.73	9.00	11.8	14.2	16.3	18.2
99.99	15.1	18.4	21.1	23.5	25.7

sidered model. Prescription values for the number of degree of freedom (dof) to the CL are given in Table 7. As we have two free parameters from the NSI and the simplified model, the corresponding value for 68% is $\chi_{min}^2 + 2.30$ and for 90% is $\chi_{min}^2 + 4.61$.

We analyze the COHERENT data in the first publication (Akimov *et al.*, 2017) using the 1-bin analysis. The χ^2 function for this aim is

$$\chi^2 = \left(\frac{N_{obs} - N_{pre}(1 + \alpha) - N_{bkg}(1 + \beta)}{\sigma} \right)^2 + \left(\frac{\alpha}{\sigma_\alpha} \right)^2 + \left(\frac{\beta}{\sigma_\beta} \right)^2, \quad (4.3)$$

with statistical uncertainty

$$\sigma = \sqrt{N_{obs} + N_{bkg} + 2N_{ss}}. \quad (4.4)$$

In the above equation, $N_{obs} = 142$, $N_{pre}, N_{bkg} = 6$, and $N_{ss} = 405$ are the number of events for observed, predicted, prompt neutron background, and steady state background, respectively. There are two systematic parameters, α and β . The first corresponds to the signal rate uncertainty and the latter to the background. These two have fractional uncertainty $\sigma_\alpha = 0.28$ and $\sigma_\beta = 0.25$. We extract the constraint by minimizing this function.

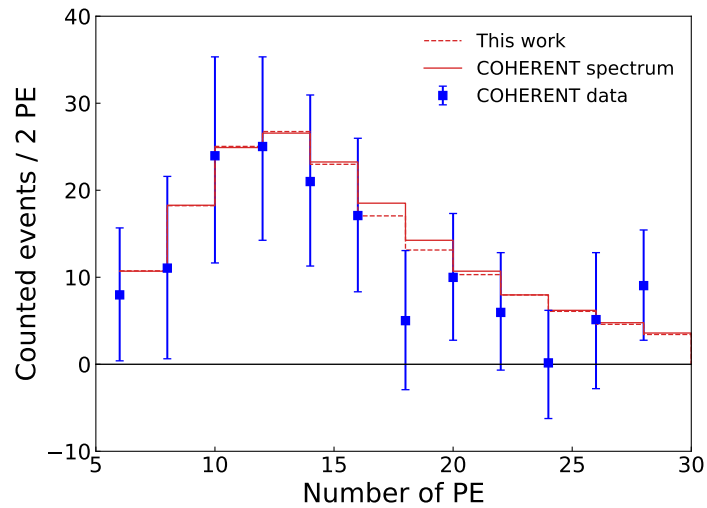


Figure 24. Predicted CEvNS event per 2 PE at COHERENT.

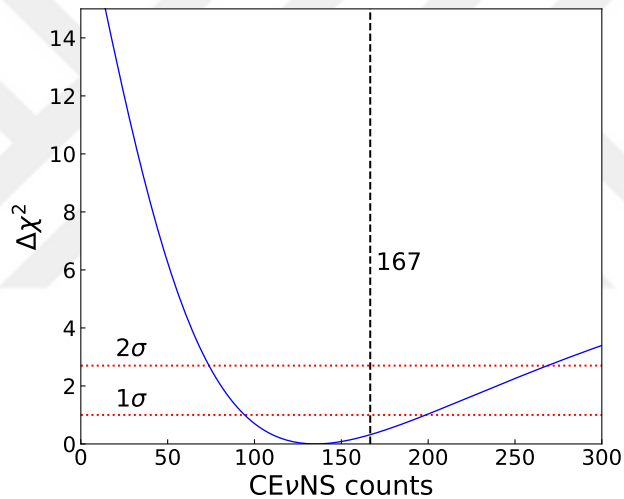


Figure 25. $\Delta\chi^2$ corresponds to 1-bin analysis of COHERENT data.

The considered spectrum we study is given in Figure 24. Here we show the predicted event per 2 PE, relevant with COHERENT collaboration. Event from this work is presented as dashed red line while the predicted spectrum from COHERENT is in the solid red line. Observed data, the square blue points, can be seen fitted proportionally with the predictions. The $\Delta\chi^2$ behavior of the analyzed data is given in Figure 25. The dashed black line indicates 166 the CEvNS expected events while the dotted red lines the confidence levels.

4.5.1. Non-Standard Neutrino Interactions

We provide the 68% CL (red) and 90% CL (blue) allowed region for the NSI parameter in Figure 26 from COHERENT data both for FC and FV case. According to the neutrino

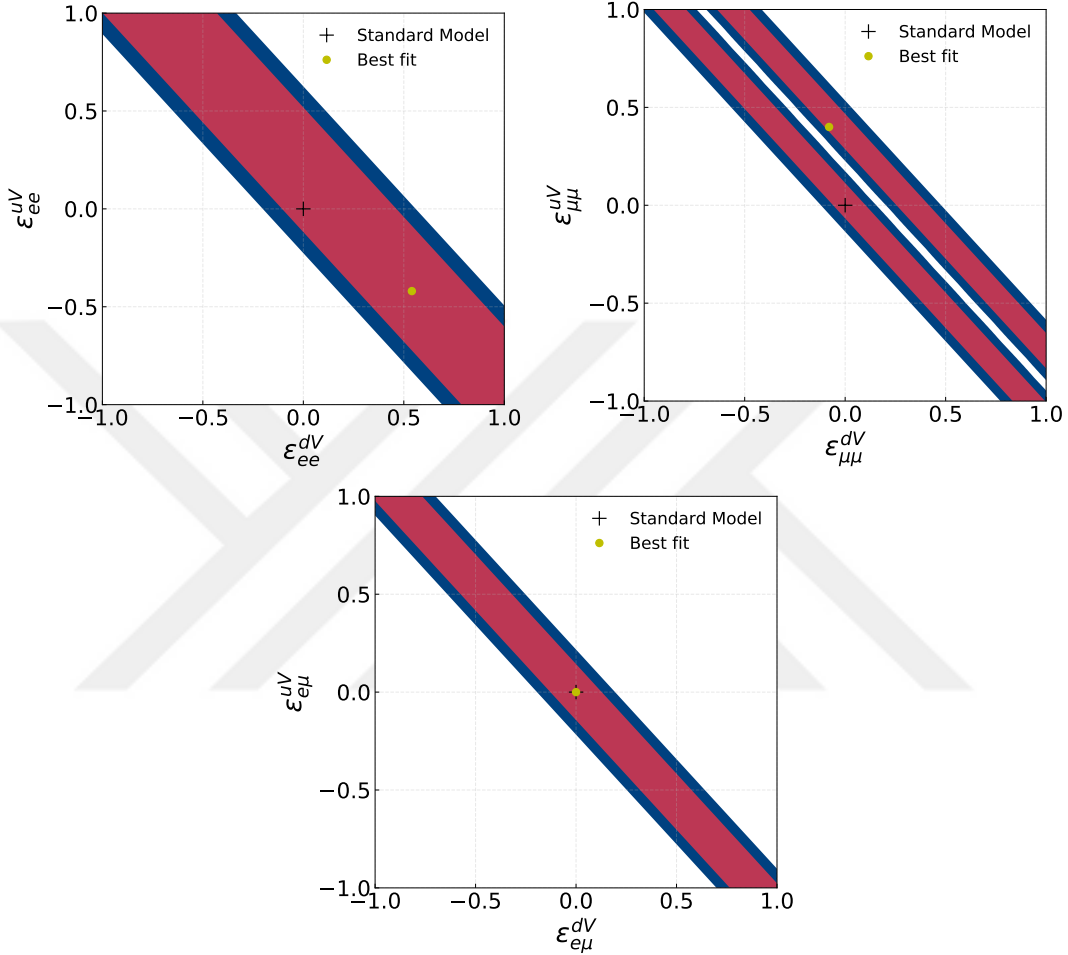


Figure 26. Allowed regions of the NSI FC (upper) and FV (lower) parameter space with 68% (red) and 90% (blue) CL from COHERENT data.

type from the SNS facility, the COHERENT experiment consider a prompt ν_μ and delayed $\bar{\nu}_\mu$ and ν_e . Therefore only e and μ flavor of neutrino can be analyzed. The best-fit values are $(0.54, -0.42)$ for the $\epsilon_{ee}^{dV}, \epsilon_{ee}^{uV}$, $(-0.08, 0.40)$ for the $\epsilon_{\mu\mu}^{dV}, \epsilon_{\mu\mu}^{uV}$, and $(0.0, 0.0)$ for the $\epsilon_{e\mu}^{dV}, \epsilon_{e\mu}^{uV}$, indicated by a yellow dot in each case.

4.5.2. Simplified Model

We present the lower bound of the coupling and mass from each considered new interaction with 68% CL (red) and 90% CL (blue) exclusion region from the simplified model in this section. We take the non-universal case of the coupling, in which the new interaction to the neutrino and to the quarks are the same. We emphasize that our results for the scalar and vectorial case are in agreement with recent works (Billard *et al.*, 2018; Papoulias and Kosmas, 2018).

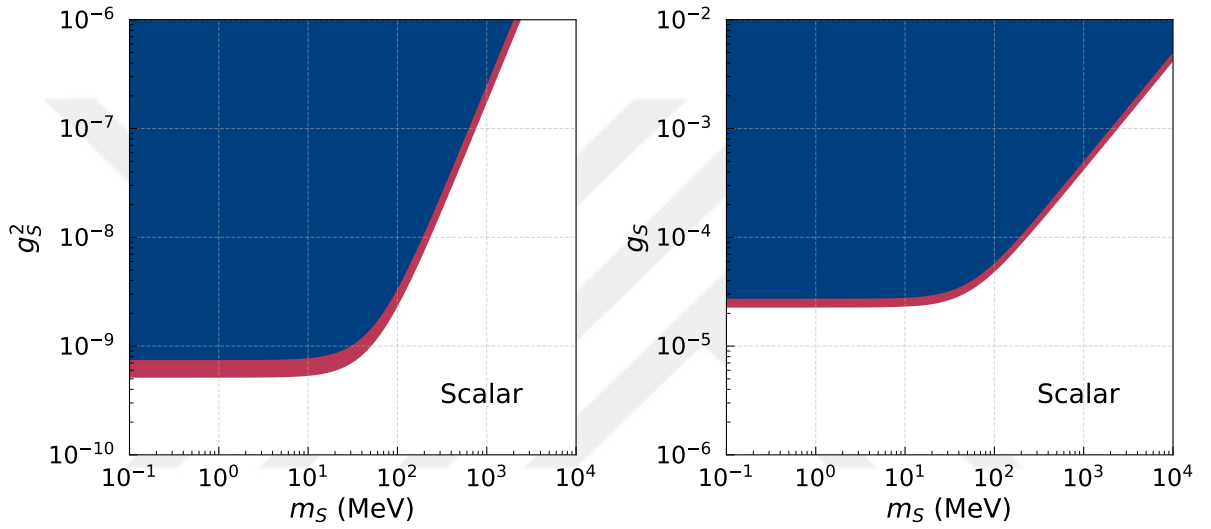


Figure 27. Lower exclusion bound on parameter space of $g_S^2 - m_S$ (left) and $g_S - m_S$ (right) with 68% (red) and 90% (blue) CL.

Figure 27 shows the exclusion region from the new scalar mediator. The lower bound of g_S^2 reaches 5.09×10^{-10} (68% CL) 7.40×10^{-10} (90% CL), while the g_S reaches 2.26×10^{-5} (68% CL) and 2.69×10^{-5} (90% CL). The mass is steady for $m_S < 10$ MeV. After that, the coupling dependency occurs for both cases.

Figure 28 is the exclusion region of the new pseudoscalar interactions. We have used the non-zero form factor and keep the T^2 term. The lower bound of g_P^2 reaches 3.15×10^{-11} (68% CL) and 4.51×10^{-11} (90% CL), while the g_P reaches 5.61×10^{-6} (68% CL) and 6.77×10^{-6} (90% CL). Again, the behavior of the mediator mass is the same as the previous case.

Figure 29 shows exclusion region from the vector mediator. We emphasize that this

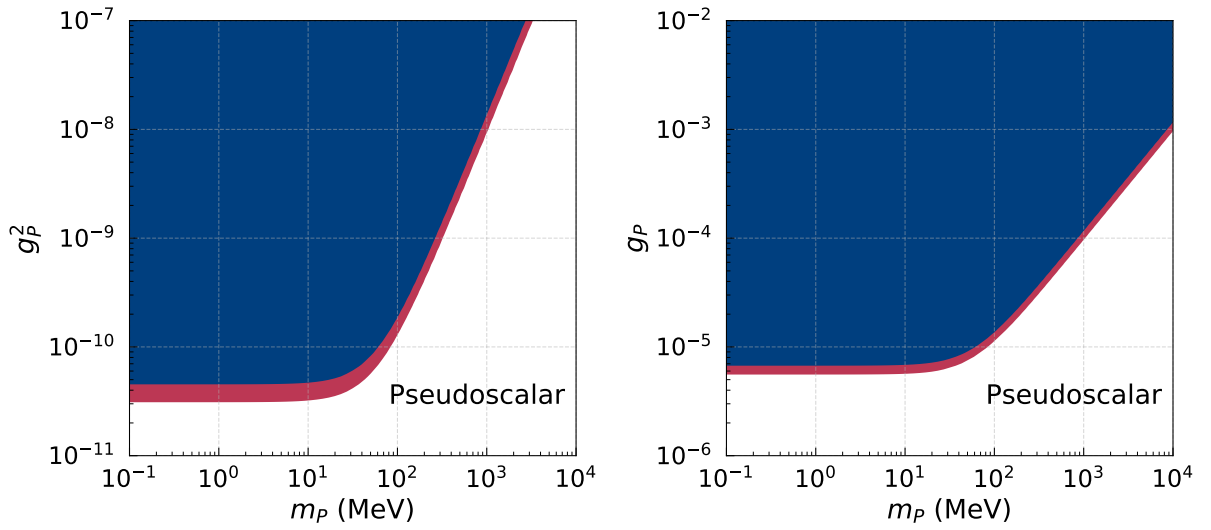


Figure 28. Same as Figure 27 for pseudoscalar mediator.

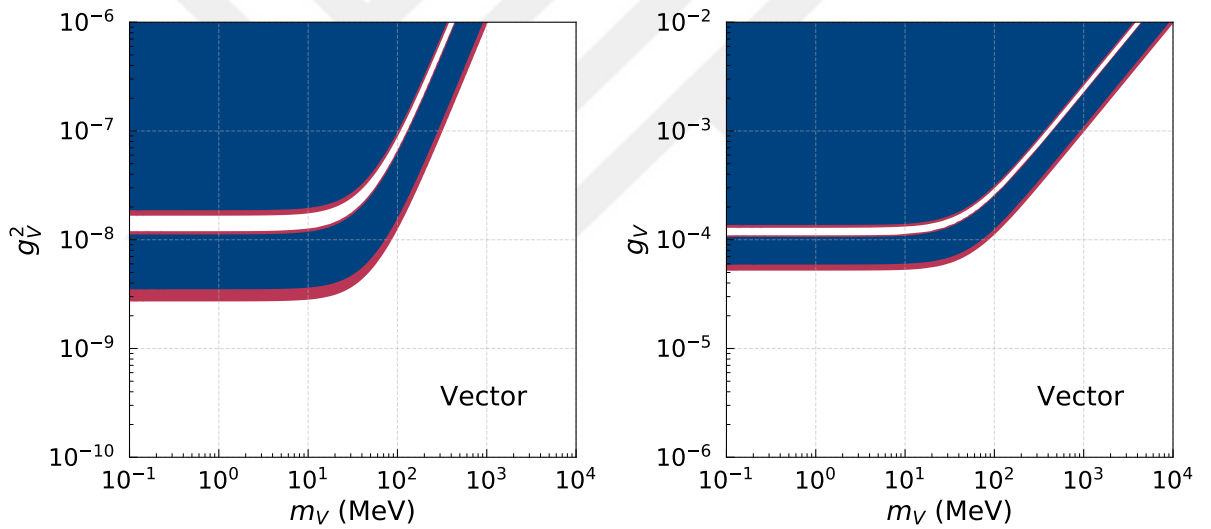


Figure 29. Same as Figure 27 for vector mediator.

case has interference term with the SM. The degeneracy region is obtained, which happens as the interference term has the same with the SM. The lower bound of g_V^2 reaches 2.72×10^{-9} (68% CL) and 3.52×10^{-9} (90% CL), while for the g_V reaches 5.22×10^{-5} (68% CL) and 5.93×10^{-5} (90% CL).

Figure 30 shows bound of the axial-vector mediator. Here we simply neglect the interference term of the new mediator with the SM. The lower bound of g_A^2 reaches 1.44×10^{-8} (68% CL) and 2.03×10^{-8} (90% CL), while the g_A reaches 1.20×10^{-4} (68% CL) and

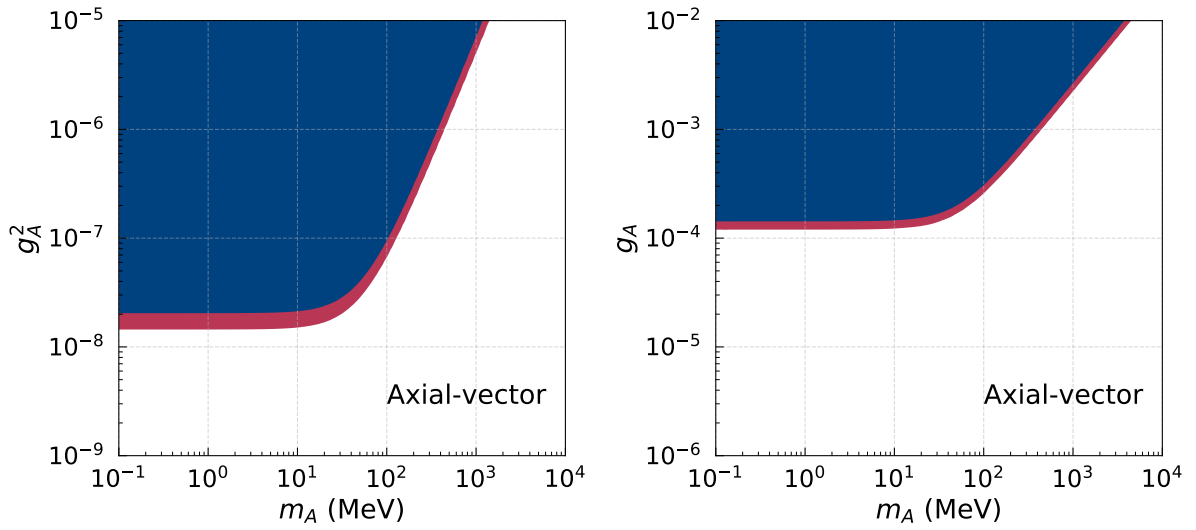


Figure 30. Same as Figure 27 for axial-vector mediator.

1.42×10^{-4} (90% CL). We can see that the mass of the axial-vector mediator is relatively constant up to 10 MeV, same as the previous case.

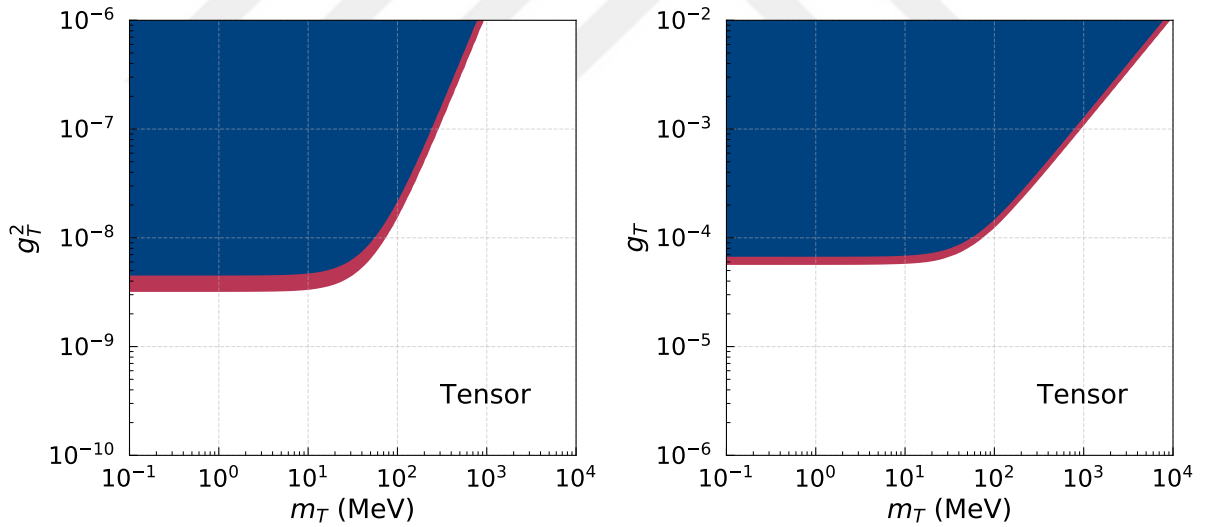


Figure 31. Same as Figure 27 for tensor mediator.

Lastly, Figure 31 gives the exclusion bound for the appearance of tensor interaction. The lower bound of g_T^2 reaches 3.17×10^{-9} (68% CL) and 4.47×10^{-9} (90% CL), while the g_T reaches 5.61×10^{-5} (68% CL) and 6.64×10^{-5} (90% CL). The mass of the tensor mediator, again, behaves the same as the previous cases.

5. CONCLUSIONS

In this work, we have shown the formulation of the CE ν NS process within the SM and the effect of general neutrino interactions. We have considered the NSI and the simplified model for this purpose. Before discussing our objectives, we have briefly introduced neutrino physics and then examined CE ν NS theoretically as well as how to detect this phenomenon. For the latter, the first successful observation of the COHERENT experiment has been reviewed. In addition, effect of coherency has also been discussed where it is found that the best way to study this process is by using reactor neutrino.

The NSI effect simply changes the form of the weak charge, which is different from the possible FC and FV of neutrino flavor. For the simplified model case, we have used model-independent parameterization with new interactions that correspond to the possible bilinear combinations: scalar, pseudoscalar, vector, axial-vector, and tensor. Differential cross-section of each case has been computed in which the effect of new interactions are induced from the strength of the considered model with its coupling to quark content of nucleus.

We have used five target nucleus to show behavior of some physical quantities: T_{max} , form factor, differential cross-section and total cross-section. It is found that the maximum recoil energy for heavier nuclei is slightly small than the lighter ones. As the initial energy of neutrino increases, the maximum recoil energy follows the same trend. For Ge target, we have shown that the case of large neutrino energy would give approximately the same T_{max} . This is important for choosing sources and building the CE ν NS detector. From the form factor plots, we have shown that large T , which also implies large Q would penetrate the nucleus structure. So to observe coherent criteria, equipment sensitive to small T is necessary. For the differential and the total cross-section, heavier targets provide larger spectrum.

The NSI model only changes the overall strength from predicted SM. Hence the shape of the cross-section is not affected as indicated in the given result. Using the updated values of the free parameters, we have shown that NSI provides a larger spectrum than the SM case. Analyzing COHERENT data, we have shown the 68% and the 90% CL parameter

constraint for the FC as well as the FV case, correspond to the produced neutrinos of the π -DAR experiment at the SNS. Updating these values from future experimental data will surely improve our understanding of the model.

The phenomenology of the simplified model has been discussed. Five different types of new interactions are considered: scalar, pseudoscalar, vector, axial-vector, tensor. The pseudoscalar case in literature is considered zero from the form factor effect but taken otherwise here. Our result of differential cross-section considers at least T order, except for the pseudoscalar case where the lowest is T^2 . In general, the vector-type interaction estimated the largest spectrum than other types. The source is expected from the extra term from the interference with the SM. Lower-exclusion bound are obtained from the COHERENT data within 68% and 90% CL.

Predictions of both the NSI and the simplified model can be further improved from the future advancement of CEvNS experiments. These beyond SM cases open a new perspective for investigating new physics, especially in low energy neutrino scale. Including in this area are astrophysical, solar, atmospheric, or geoneutrino. Connection with DM-matter interaction is also an interesting subject to be explored since CEvNS has a similar formulation, either theoretical calculation or experimental equipment, with the direct detection of DM.

6. REFERENCES

- Aartsen, M.G., *et al.* (IceCube), 2015. Constraints on ultrahigh-energy cosmic-ray sources from a search for neutrinos above 10 PeV with IceCube, Phys. Rev. Lett., 117, 241101.
- Abe, Y., *et al.* (Double CHOOZ), 2012. Indication of reactor $\bar{\nu}_e$ disappearance in the Double Chooz experiment, Phys. Rev. Lett., 108, 131801.
- Agnes, P., *et al.* (DarkSide), 2018. Low-Mass Dark Matter Search with the DarkSide-50 Experiment, Phys.Rev.Lett., 121(8), 081307.
- Agnolet, G., *et al.*, 2016. Background Studies for the MINER Coherent Neutrino Scattering Reactor Experiment, Nucl.Instrum.Meth.A, 853, 53-60.
- Aguilar-Arevalo, A., *et al.* (CONNIE Collaboration), 2019. Exploring low-energy neutrino physics with the Coherent Neutrino Nucleus Interaction Experiment, Phys. Rev. D, 100, 092005.
- Ahmad, Q.R., *et al.* (SNO), 2002. Direct evidence for neutrino flavor transformation from neutral current interactions in the Sudbury Neutrino Observatory, Phys. Rev. Lett., 89, 011301.
- Ahn, J.K., *et al.* (RENO), 2012. Observation of reactor electron antineutrinos disappearance in the RENO experiment, Phys. Rev. Lett., 108, 191802.
- Akerib, D.S., *et al.* (LUX-ZEPLIN), 2020. The LUX-ZEPLIN (LZ) Experiment, Nucl.Instrum.Meth.A, 953, 953.
- Akimov, D., *et al.*, 2016. RED-100 detector for the first observation of the elastic coherent neutrino scattering off xenon nuclei, Jour. Phys. : Conf. Ser., 675, 012016.
- Akimov, D., *et al.* (COHERENT), 2017. Observation of coherent elastic neutrino-nucleus scattering, Science, 357, 1123–1126.
- Alekseev, E.N., *et al.*, 1987. Possible Detection of a Neutrino Signal on 23 February 1987 at the Baksan Underground Scintillation Telescope of the Institute of Nuclear Research, JETP Lett., 45, 589-592.
- Alwall, J. and Toro, N., 2009. Simplified Models for a First Characterization of New Physics at the LHC, Phys.Rev.D, 79, 075020.
- An, F.P., *et al.* (Daya Bay), 2012. Observation of electron-antineutrino disappearance at Daya Bay, Phys. Rev. Lett., 108, 171803.
- Aprile, E., *et al.*, 2017. The XENON1T Dark Matter Experiment, Eur. Phys. J. C, 77, 12, 881.
- Armbruster, B., *et al.* (KARMEN), 2002. Upper limits for neutrino oscillations $\bar{\nu}_\mu \rightarrow \bar{\nu}_e$ from muon decay at rest, Phys.Rev.D, 65, 112001.

- Arnaud, Q., *et al.* (NEWS-G), 2018. First results from the NEWS-G direct dark matter search experiment at the LSM, *Astropart.Phys.*, 97, 54-62.
- Asamar, E.L., *et al.* (SuperCDMS), 2019. SuperCDMS SNOLAB: status and prospects for measuring the coherent neutrino scattering, *J.Phys.Conf.Ser.*, 1216(1), 012020.
- Athanassopoulos, C., *et al.* (LSND), 1997. The Liquid scintillator neutrino detector and LAMPF neutrino source, *Nucl.Instrum.Meth.A*, 388, 149-172.
- Bahcall, J.N., Pinsonneault, M.H., and Basu, S., 2000. Solar models: Current epoch and time dependences, neutrinos, and helioseismological properties, *Astrophys.J.*, 555, 990-1012.
- Barranco, J., *et al.*, 2012. Tensorial NSI and Unparticle physics in neutrino scattering, *Int. J. Mod. Phys. A*, 27, 1250147.
- Barwick, S.W., *et al.* (ARIANNA), 2015. A first search for cosmogenic neutrinos with the ARIANNA Hexagonal Radio Array, *Astropart. Phys.*, 70, 12.
- Belanger, G. *et al.*, 2009. Dark matter direct detection rate in a generic model with micrOMEGAs 2.2, *Comput. Phys. Commun.*, 180, 747-767.
- Berezhiani, Z. and Rossi, A., 2002. Limits on the non-standard interactions of neutrinos from e^+e^- colliders, *Phys. Lett. B*, 535, 207-218.
- Bethe, H. and Critchfield, C.L., 1938. The formation of deuterium by proton combination, *Phys.Rev.*, 54, 248-254.
- Bethe, H., 1939. Energy production in stars, *Phys.Rev.*, 55, 434-456.
- Bethe, H. and Peierls, R., 1934. The 'Neutrino', *Nature*, 133, 532.
- Billard, J., *et al.*, 2017. Coherent Neutrino Scattering with Low Temperature Bolometers at Chooz Reactor Complex, *J.Phys.G*, 44(10), 105101.
- Billard, J., Johnston, J., and Kavanagh, B., 2018. Prospects for exploring New Physics in Coherent Elastic Neutrino-Nucleus Scattering, *Jour. Cos. and Astr. Phys.*, 2018, 16.
- Bionta, R.M., *et al.* (IMB), Observation of a Neutrino Burst in Coincidence with Supernova SN 1987a in the Large Magellanic Cloud, *Phys. Rev. Lett.*, 58, 1494.
- Bird, D.J., *et al.*, 1994. Detection of a cosmic ray with measured energy well beyond the expected spectral cutoff due to cosmic microwave radiation, *Astrophys.J.*, 441, 144-150.
- Bonet, H., *et al.*, 2020. First constraints on elastic neutrino nucleus scattering in the fully coherent regime from the Conus experiment, *Phys.Rev.Lett.*, 126(4), 041804.
- Cerděno, D. G., *et al.*, 2016. Physics from solar neutrinos in dark matter direct detection experiments, *JHEP*, 05, 118.

- Cirelli, M., *et al.*, 2013. Tools for model-independent bounds in direct dark matter searches, JCAP, 04, 019.
- Cowan, C.L., *et al.*, 1956. Detection of the free neutrino: A Confirmation, Science, 124, 103–104.
- Davidson, S., Pena-Garay, C., Rius, N., and Santamaria, A., 2003. Present and future bounds on non-standard neutrino interactions, JHEP, 03, 011.
- Duda, G., Kemper, A., and Gondolo, P., 2007. Model-independent form factors for spin-independent neutralinonucleon scattering from elastic electron scattering data, JCAP, 4, 12.
- Ellis, J., Olive, K.A., and Savage, C., 2008. Hadronic Uncertainties in the Elastic Scattering of Supersymmetric Dark Matter, Phys. Rev. D, 77, 065026.
- Ema, Y., Sala, F., and Sato, R., 2021. Neutrino experiments probe hadrophilic light dark matter, SciPost Phys., 10, 072.
- Engel, J., 1991. Nuclear form-factors for the scattering of weakly interacting massive particles, Phys. Let. B, 264, 114-119.
- Englert, F. and Brout, R., 1964. Broken symmetry and the mass of gauge vector mesons, Phys.Rev.Lett., 13, 321-323.
- Farzan, Y. and Shoemaker, I.M., 2016. Lepton flavor violating non-standard interactions via light mediators, JHEP, 07, 33(2016).
- Farzan, Y., Lindner, M., Rodejohann, W., and Xu, X., 2018. Probing neutrino coupling to a light scalar with coherent neutrino scattering, JHEP, 05, 66(2018).
- Fermi, E., 1934. Trends to a Theory of beta Radiation. (In Italian), Nuovo Cim., 11, 1-19.
- Feynman, R. P. and Gell-Mann, M., 1958. Theory of the Fermi Interaction, Phys. Rev., 109, 193-198.
- Fieldman, G. J. and Cousins, R.D., 1998. Unified approach to the classical statistical analysis of small signals, Phys. Rev. D, 57, 3873.
- Fiorentini, G., Lissia, M., and Mantovani, F., 2007. Geo-neutrinos and Earth's interior, Phys.Rept., 453, 117-172.
- Freedman, D., 1974. Coherent Neutrino-Nucleus Scattering as a Probe of the Weak Neutral Current, Phys. Rev. D, 9, 1389-1392.
- Fukuda, Y., *et.al.* (Super-Kamiokande), 1998. Evidence for oscillation of atmospheric neutrinos, Phys.Rev.Lett., 81, 1562-1567.
- Gaisser, T.K. and Honda, M., 2002. Flux of atmospheric neutrinos, Ann.Rev.Nucl.Part.Sci., 52, 153-199.
- Gelmini, G. B., 2004. Prospect for relic neutrino searches, Phys.Scripta, T121, 131-136.

- Giunti, C., 2020. General COHERENT constraints on neutrino nonstandard interactions, Phys. Rev. D, 101, 035039.
- Glashow, S.L., 1961. Partial Symmetries of Weak Interactions, Nucl.Phys., 22, 579-588.
- Greisen, K., 1966. End to the cosmic ray spectrum?, Phys.Rev.Lett., 16, 748-750.
- Guralnik, G.S., Hagen, C.R., and Kibble, T.W.B., 1964. Global Conservation Laws and Massless Particles, Phys.Rev.Lett., 13, 585-587.
- Helm, R. H., 1956. Inelastic and Elastic Scattering of 187-Mev Electrons from Selected Even-Even Nuclei, Phys. Rev., 104, 1466.
- Hernandez, P., 2015. Neutrino Physics, CERN Yellow Report, 5, 85-142.
- Higgs, P.W., 1964. Broken Symmetries and the Masses of Gauge Bosons, Phys.Rev.Lett., 13, 508-509.
- Hirata, K., *et al.* (Kamiokande-II), 1987. Observation of a Neutrino Burst from the Supernova SN 1987a, Phys. Rev. Lett., 58, 1490.
- Hoferichter, M., *et al.*, 2015. Matching pionnucleon RoySteiner equations to chiral perturbation theory, Phys.Rev.Lett., 115(19), 192301.
- Horiuchi, S., *et al.*, 2018. Diffuse supernova neutrino background from extensive core-collapse simulations of 8-100 M_{\odot} 100 progenitors, Mon.Not.Roy.Astron.Soc., 475, 1363-1374.
- Junnarkar, P. and Walker-Loud, A., 2013. Scalar strange content of the nucleon from lattice QCD, Phys.Rev.D, 87, 114510.
- Kahlhoefer, F., 2010. Sensitivity of Liquid Xenon Detectors for Low Mass Dark Matter Unpublished diploma thesis, University of Heidelberg, Heidelberg, Germany.
- Kerman, S., *et al.* (TEXONO), 2016. Coherency in Neutrino-Nucleus Elastic Scattering, Phys. Rev. D, 93, 113006.
- Kurylov, A. and Kamionkowski, M., 2004. Generalized analysis of weakly interacting massive particle searches, Phy. Rev. D, 69, 063503.
- Lindner, M., Rodejohann, W., and Xu, X., 2017. Coherent neutrino-nucleus scattering and new neutrino interactions, JHEP, 03, 097.
- Maki, Z., Nakagawa, M., and Sakata, S., 1962. Remarks on the unified model of elementary particles, Prog. Theor. Phys., 28, 870-880.
- McCoy, C.D. and Massimi, M., 2018. Simplified models: a different perspective on models as mediators, Euro. Jnl. Phil. Sci., 8, 99-123.
- Miranda, O.G. and Nunokawa, H., 2015. Non standard neutrino interactions: current status and future prospects, New J. Phys., 17(9), 095002.

- Mustamin, M.F. and Demirci, M., 2021. Study of Non-standard Neutrino Interactions in Future Coherent Elastic Neutrino-Nucleus Scattering Experiments, Braz. J. Phys., 51(3), 813-819.
- Naumov, D.V., 2011. Introduction to Neutrino Physics, Phys.Part.Nucl.Lett., 8, 717-742.
- Papoulias, D.K., 2020. COHERENT constraints after the COHERENT-2020 quenching factor measurement, Phys. Rev. D, 102, 113004.
- Papoulias, D.K. and Kosmas, T.S., 2018. COHERENT constraints to conventional and exotic neutrino physics, Phys.Rev.D, 97(3), 033003.
- Pauli, W., 1930. Dear radioactive ladies and gentlemen, Phys. Today, 156.
- Pontecorvo, B., 1957. Mesonium and anti-mesonium, Sov.Phys.JETP, 33, 549-551.
- Rothe, J., *et al.* (NUCLEUS Collaboration), 2020. NUCLEUS: Exploring Coherent Neutrino-Nucleus Scattering with Cryogenic Detectors, Jour. Low Temp. Phys., 7, 191.
- Sakurai, J.J., 1958. Mass reversal and weak interactions, Nuovo Cim., 7, 649-660.
- Salam, A., 1968. Weak and Electromagnetic Interactions, Proc. of the 8th Nobel Symposium, 680519, 367-377.
- Schael, S. (ALEPH, DELPHI, L3, OPAL, SLD, LEP Electroweak Working Group, SLD Electroweak Group, SLD Heavy Flavour Group), 2006. Precision electroweak measurements on the Z resonance, Phys. Rept., 427, 257-454.
- Scholberg, K., 2005. Prospects for measuring coherent neutrino-nucleus elastic scattering at a stopped-pion neutrino source, Phys. Rev. D, 73, 033005.
- Sharma, V., *et al.* (TEXONO), 2021. Studies of quantum-mechanical coherency effects in neutrino-nucleus elastic scattering, Phys. Rev. D, 103, 092002.
- Sierra, D. A., Romeri, V. D., and Rojas, N., 2018. COHERENT analysis of neutrino generalized interactions, Phys. Rev. D, 98, 075018.
- Sinev, G., 2020. Constraining Non-Standard Neutrino Interactions and Estimating Future Neutrino-Magnetic-Moment Sensitivity With COHERENT, Duke University, ProQuest Dissertations Publishing, 27744578.
- Sudarshan, E.C.G. and Marshak, R.E., 1958. Chirality invariance and the universal Fermi interaction, Phys. Rev., 109, 1860.
- Thomson, M., 2013. Modern Particle Physics, Cambridge University Press.
- Vitagliano, E., Tamborra, E., and Raffelt, G., 2019. Grand Unified Neutrino Spectrum at Earth: Sources and Spectral Components, Rev. Mod. Phys., 92, 45006.
- Weinberg, S., 1967. A Model of Leptons, Phys.Rev.Lett., 19, 1264-1266.
- Wong, H., 2015. Taiwan EXperiment On Neutrino, The Universe, 3, 4, 22-37.

Wu, C.S., *et al.*, 1957. Experimental Test of Parity Conservation in β Decay, Phys. Rev., 105, 1413–1414.

Zatsepin, G.T. and Kuzmin, V.A., 1966. Review of Particle Physics, JETP Lett., 4, 78-80.

Zyla, P. A., *et al.* (Particle Data Group), 2020. Review of Particle Physics, Prog. Theor. Exp. Phys., 2020, 083C01.



7. APPENDICES

7.1. CONVENTION AND NOTATION

The γ^μ sandwiched between particle fields is the Dirac gamma-matrices. They obey the Clifford algebra

$$\{\gamma^\mu, \gamma^\nu\} = 2g^{\mu\nu}, \quad (\text{A.1})$$

with metric tensor $g^{\mu\nu}$ is defined as

$$g^{\mu\nu} = \begin{pmatrix} 1 & 0 & 0 & 0 \\ 0 & -1 & 0 & 0 \\ 0 & 0 & -1 & 0 \\ 0 & 0 & 0 & -1 \end{pmatrix}. \quad (\text{A.2})$$

Explicitly, the gamma-matrices are

$$\gamma^0 = \begin{pmatrix} \mathbb{1} & 0 \\ 0 & -\mathbb{1} \end{pmatrix}, \quad \gamma^j = \begin{pmatrix} 0 & \sigma^j \\ -\sigma^j & 0 \end{pmatrix}, \quad (\text{A.3})$$

where $\mathbb{1}$ is a 2×2 identity matrix while σ^i , with $i = 1, 2, 3$, are the Pauli matrices

$$\sigma^1 = \begin{pmatrix} 0 & 1 \\ 1 & 0 \end{pmatrix}, \quad \sigma^2 = \begin{pmatrix} 0 & -i \\ i & 0 \end{pmatrix}, \quad \sigma^3 = \begin{pmatrix} 0 & 1 \\ -1 & 0 \end{pmatrix}. \quad (\text{A.4})$$

These matrices are Hermitian and satisfy the following relations

$$[\sigma^i, \sigma^j] = 2i\varepsilon^{ijk}\sigma^k, \quad \{\sigma^i, \sigma^j\} = 2\delta^{ij}, \quad (\text{A.5})$$

where ε^{ijk} and δ^{ij} are the Levi-Civita symbol and Kronecker delta, respectively.

The matrix appears in the Lagrangian density of the Dirac fields

$$\mathcal{L}_{Dirac} = \bar{\psi}(i\rlap{\not{D}} + m)\psi, \quad (\text{A.6})$$

with Feynman slashed $\rlap{\not{D}} = \gamma^\mu \partial_\mu$ have been used. The equation of motion of this Lagrangian is

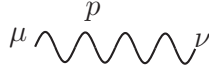
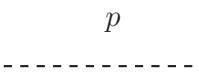
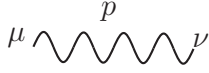
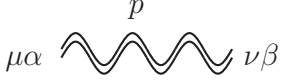
$$(i\gamma^\mu \partial_\mu - m)\psi = 0, \quad (\text{A.7})$$

which is the Dirac equation.

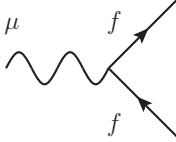
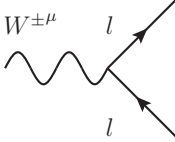
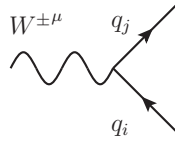
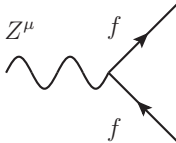
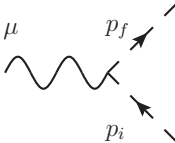
7.2. RELATED FEYNMAN RULES

The following give summary of Feynman rules related to process involved in this work.

- Propagators

			
Photon (γ)	Scalar (S, P)	Vectorial (W, Z, V, A)	Tensorial (T)
$\frac{-ig_{\mu\nu}}{p^2+i\epsilon}$	$\frac{i}{p^2-m^2+i\epsilon}$	$\frac{-ig_{\mu\nu}}{p^2-m^2+i\epsilon}$	$\frac{-ig_{\mu\alpha}g_{\nu\beta}}{p^2-m^2+i\epsilon}$

- Vertex

		
$ff\gamma: -iQe\gamma^\mu$	$llW^\pm: -i\frac{g_W}{2\sqrt{2}}\gamma^\mu(1-\gamma^5)$	$qqW^\pm: -i\frac{g_W}{2\sqrt{2}}\gamma^\mu(1-\gamma^5)V_{ji}$
		
$ffZ: -i\frac{g_Z}{2}\gamma^\mu(g_V - g_A\gamma^5)$	$\phi\phi\gamma: -ie(p_\mu^i + p_\mu^f)$	

Where $g_W = \frac{e}{\sin\theta_W}$, $g_Z = \frac{g_W}{\cos\theta_W}$, $g_V = g_L + g_R = I_3 - 2Q\sin^2\theta_W$, and $g_A = g_L - g_R = I_3$. The V_{ji} denotes the CKM matrix. The Feynman gauge have been used for the W^\pm and Z mediator.

7.3. KINEMATICS

The kinematic of the $\nu(p_1) + N(p_2) \rightarrow \nu(p_3) + N(p_4)$ in the rest frame of initial nucleus is shown in Figure 32. In this process the initial and final mass for the target nucleus and incoming neutrino is the same. Particularly, $m_1 = m_3 = m_\nu$ for neutrino and $m_2 = m_4 = m_N$ for nucleus. Relations between four-vector momentum $p_i = (E_i, \vec{p}_i)$ with $i = 1, 2, 3, 4$ can be proceed further. Since $\vec{p}_2 = 0$, we can clearly see that

$$p_2 \cdot p_4 = E_2 E_4 - \vec{p}_2 \vec{p}_4 = m_N E_4. \quad (\text{A.8})$$

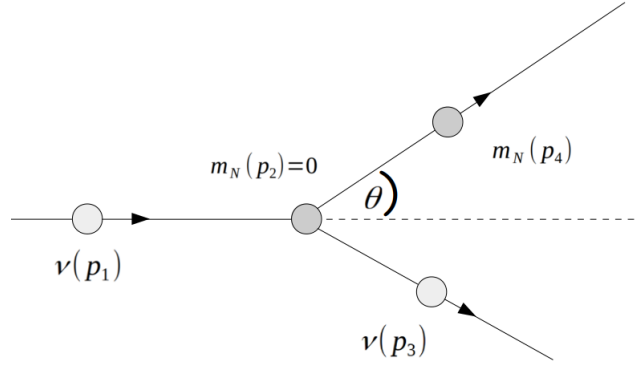


Figure 32. Framework of kinematics for CEvNS process.

From $p_i^2 = m_i^2$ and conservation of momentum $p_1 + p_2 = p_3 + p_4$, squaring this equation gives

$$\begin{aligned} p_1^2 + p_2^2 + 2p_1 \cdot p_2 &= p_3^2 + p_4^2 + 2p_3 \cdot p_4 \\ m_v^2 + m_N^2 + 2p_1 \cdot p_2 &= m_v^2 + m_N^2 + 2p_3 \cdot p_4 \\ p_1 \cdot p_2 &= p_3 \cdot p_4. \end{aligned} \quad (\text{A.9})$$

Contracting the left hand side we find

$$p_1 \cdot p_2 = E_1 E_2 - \vec{p}_1 \vec{p}_2 = E_v m_N. \quad (\text{A.10})$$

We can also have $p_1 - p_4 = p_3 - p_2$ from the momentum conservation. Squaring this we obtain

$$\begin{aligned} p_1^2 + p_4^2 - 2p_1 \cdot p_4 &= p_3^2 + p_2^2 - 2p_2 \cdot p_3 \\ m_v^2 + m_N^2 - 2p_1 \cdot p_4 &= m_N^2 + m_v^2 - 2p_2 \cdot p_3 \\ p_1 \cdot p_4 &= p_2 \cdot p_3. \end{aligned} \quad (\text{A.11})$$

Hence applying energy conservation $E_3 = E_1 + E_2 - E_4$ and recoil energy transfer

$$T = E_3 - E_1 = E_4 - E_2, \quad (\text{A.12})$$

hence

$$p_2 \cdot p_3 = E_2 E_3 - \vec{p}_2 \vec{p}_3 = M_N (E_1 + M_N - E_4) = M_N (E_1 - T). \quad (\text{A.13})$$

We can also work out the square of $p_1 - p_3 = p_4 - p_2$ to get

$$\begin{aligned} p_1^2 + p_3^2 - 2p_1 \cdot p_3 &= p_4^2 + p_2^2 - 2p_2 \cdot p_4 \\ 2m_v^2 - 2p_1 \cdot p_3 &= 2m_N^2 - 2p_2 \cdot p_4 \\ p_1 \cdot p_3 &= m_v^2 - m_N^2 + m_N \cdot E_4 = m_v^2 + m_N (E_4 - m_N) \\ p_1 \cdot p_3 &= m_v^2 + m_N T \approx m_N T \end{aligned} \quad (\text{A.14})$$

since neutrino is considered massless in the SM.

We can also extract the maximum nuclear recoil energy of the process. This is achieved as the angle between the two final particles θ is 180° . Starting with $p_1 \cdot p_2 = p_3 \cdot p_4$ we get

$$\begin{aligned} E_1 E_2 - \vec{p}_1 \vec{p}_2 &= E_3 E_4 - \vec{p}_3 \vec{p}_4 \\ E_1 m_N &= E_3 E_4 - |\vec{p}_3| |\vec{p}_4| \cos 180^\circ \\ E_1 m_N &= E_3 E_4 + |\vec{p}_3| |\vec{p}_4|. \end{aligned} \quad (\text{A.15})$$

Since $T = E_4 - E_2 = E_4 - m_N$ then $E_4 = T + m_N$. From conservation of energy we also have $E_3 = E_1 + E_2 - E_4 = E_1 + m_N - (T + m_N)$ or $E_3 = E_1 - T$. Neglecting neutrino mass, then $p_3^2 = E_3^2 - |\vec{p}_3|^2 = 0$, and hence

$$|\vec{p}_3| = E_3 = E_1 - T. \quad (\text{A.16})$$

From the p_4 , squaring it we get

$$\begin{aligned} E_4^2 - |\vec{p}_4|^2 &= m_N^2 \\ |\vec{p}_4|^2 &= E_4^2 - m_N^2 = (E_4 - m_N)(E_4 + m_N) \\ |\vec{p}_4|^2 &= (T + m_N - m_N)(T + m_N + m_N) \\ |\vec{p}_4|^2 &= T(T + 2m_N) \\ |\vec{p}_4| &= \sqrt{T(T + 2m_N)}. \end{aligned} \quad (\text{A.17})$$

With $E_3, E_4, |\vec{p}_3|$ and $|\vec{p}_4|$ while setting $E_1 \rightarrow E_\nu$, then

$$\begin{aligned} E_\nu m_N &= (E_\nu - T)(T + m_N) + (E_\nu - T)(\sqrt{T(T + 2m_N)}) \\ E_\nu m_N &= E_\nu T + E_\nu m_N - T^2 - T m_N + (E_\nu - T)\sqrt{T(T + 2m_N)} \\ T m_N - T(E_\nu - T) &= (E_\nu - T)\sqrt{T(T + 2m_N)} \\ \left(\frac{m_N}{E_\nu - T} - 1\right) T &= \sqrt{T(T + 2m_N)}, \end{aligned} \quad (\text{A.18})$$

and squaring this equation

$$\begin{aligned} \left[\frac{m_N^2}{(E_\nu - T)^2} - \frac{2m_N}{E_\nu - T} + 1 \right] T^2 &= T(T + 2m_N) \\ m_N^2 T - 2m_N T(E_\nu - T) &= 2m_N (E_\nu - T)^2 \\ m_N T - 2T(E_\nu - T) &= 2(E_\nu^2 - 2E_\nu T + T^2) \\ m_N T + 2E_\nu T &= 2E_\nu^2 \end{aligned} \quad (\text{A.19})$$

so that, denoting $T \rightarrow T_{\max}$, we obtain

$$T_{\max} = \frac{2E_\nu}{m_N + 2E_\nu}, \quad (\text{A.20})$$

the maximum nuclear recoil energy of the process.

From this relation, it is also possible to obtain the minimum neutrino energy that can

trigger threshold recoil energy, denoted as T_{th} . This threshold depends on the detector properties. From the above relation, we can write

$$\begin{aligned} m_N T + 2E_\nu T &= 2E_\nu \\ 2m_N T + T^2 &= (2E_\nu - T)^2 \\ \sqrt{2m_N T + T^2} &= 2E_\nu - T, \end{aligned} \quad (\text{A.21})$$

where we have multiplied by 2 and added T^2 for completing square. Using $T \rightarrow T_{\text{th}}$, the minimum neutrino energy can then be written as

$$E_{\nu_{\text{min}}} = \frac{1}{2} \left[\sqrt{2m_N T_{\text{th}} + T_{\text{th}}^2} + T_{\text{th}} \right]. \quad (\text{A.22})$$

We may also develop the relevant differential cross-section for the $\nu + N \rightarrow \nu + N$ elastic process. The general form obeys (Thomson, 2013)

$$d\sigma = \frac{\langle |\mathcal{M}^2| \rangle}{2E_1 2E_2 |\vec{v}_1 - \vec{v}_2|} \frac{d^3 \vec{p}_3}{(2\pi^3) 2E_4} \frac{d^3 \vec{p}_4}{(2\pi^3) 2E_4} (2\pi)^4 \delta^4(p_1 + p_2 - p_3 - p_4). \quad (\text{A.23})$$

Using the velocity relation $\vec{v} = \vec{p}/E$, the incident flux can be written as

$$2E_1 2E_2 |\vec{v}_1 - \vec{v}_2| = 4(E_2 |\vec{p}_1| - E_1 |\vec{p}_2|), \quad (\text{A.24})$$

where in the center of mass frame, $\vec{p}_1 = -\vec{p}_2$ and $\vec{p}_3 = -\vec{p}_4$, so we can integrate

$$\begin{aligned} \int \int \frac{d^3 \vec{p}_3}{(2\pi)^3 2E_4} \frac{d^3 \vec{p}_4}{(2\pi)^3 2E_4} (2\pi)^4 \delta(E_1 + E_2 - E_3 - E_4) \delta^3(\vec{p}_1 + \vec{p}_2 - \vec{p}_3 - \vec{p}_4) \\ = \frac{|\vec{p}_3|^2 d\Omega}{16\pi^2 E_3 E_4} \int d|\vec{p}_3| \delta(E_{CM} - E_3 - E_4), \end{aligned} \quad (\text{A.25})$$

where now $E_3 = \sqrt{|\vec{p}_3|^2 + m_3^2}$ and $E_4 = \sqrt{|\vec{p}_3|^2 + m_4^2}$, while we have defined $E_{CM} = E_1 + E_2$. Note also that the solid angle is $d\Omega = \sin\theta d\theta d\phi$. The Jacobian of the last line for $x = E_{CM} - E_3(\vec{p}_3) - E_4(\vec{p}_3)$

$$J = \left| \frac{dx}{dp_3} \right| = |\vec{p}_3| \frac{E_3 + E_4}{E_3 E_4}, \quad (\text{A.26})$$

changing variable $dp_3 = dx|J|^{-1}$ leads us to

$$\frac{|\vec{p}_3|^2 d\Omega}{16\pi^2 E_3 E_4} \int dx \delta(x) \left(\frac{E_3 E_4}{|\vec{p}_3| (E_3 + E_4)} \right) = \frac{|\vec{p}_3| d\Omega}{16\pi^2 E_{CM}} \theta(E_{CM} - m_3 - m_4) \quad (\text{A.27})$$

where the delta function gives $E_{CM} = E_3 + E_4$ and note that $\theta(x)$ is a Heaviside function. The differential cross-section then becomes

$$\frac{d\sigma}{d\Omega} = \frac{\langle |\mathcal{M}^2| \rangle}{64\pi^2 E_{CM}^2} \frac{|\vec{p}_3|}{|\vec{p}_1|}. \quad (\text{A.28})$$

Instead of solid angle $d\Omega$, we aim to convert this into nuclear recoil energy dT . We note that $q = p_3 - p_1$, hence $q^2 = p_1^2 + p_3^2 - 2|\vec{p}_1||\vec{p}_3|\cos\theta$ or for massless case $dq^2 = -2|\vec{p}_1||\vec{p}_3|d(\cos\theta)$. So that

$$\frac{d\sigma}{dq^2} = -\frac{d\phi}{2|\vec{p}_1||\vec{p}_3|} \frac{\langle |\mathcal{M}^2| \rangle}{64\pi^2 E_{CM}^2} = -\frac{1}{|\vec{p}_1||\vec{p}_3|} \frac{\langle |\mathcal{M}^2| \rangle}{64\pi E_{CM}^2}. \quad (\text{A.29})$$

Since $q^2 = -2m_N T \rightarrow dq^2 = -2m_N dT$, then

$$\frac{d\sigma}{dT} \frac{dT}{dq^2} = -\frac{1}{2m_N} \frac{d\sigma}{dT}, \quad (\text{A.30})$$

then, since in the center of mass frame $|\vec{p}_1| = |\vec{p}_3|$, we obtain

$$\frac{d\sigma}{dT} = \frac{m_N \langle |\mathcal{M}^2| \rangle}{32\pi E_{CM}^2 |\vec{p}_1|^2}. \quad (\text{A.31})$$

Next, we may square the incident flux of Eq.(A.24) to obtain $(E_2|\vec{p}_1| - E_1|\vec{p}_2|)^2 = E_2^2|\vec{p}_1|^2 + E_1^2|\vec{p}_2|^2 - 2E_2|\vec{p}_1|E_1|\vec{p}_2|$, where the last term can be replaced from relation $(p_1 \cdot p_2)^2 = E_1^2 E_2^2 + |\vec{p}_1|^2 |\vec{p}_2|^2 - 2E_1 E_2 |\vec{p}_1| |\vec{p}_2|$, hence

$$\begin{aligned} (E_2|\vec{p}_1| - E_1|\vec{p}_2|)^2 &= E_2^2|\vec{p}_1|^2 + E_1^2|\vec{p}_2|^2 + (p_1 \cdot p_2)^2 - E_1^2 E_2^2 - |\vec{p}_1|^2 |\vec{p}_2|^2 \\ &= (p_1 \cdot p_2)^2 - (E_1^2 - |\vec{p}_1|^2)(E_2^2 - |\vec{p}_2|^2) \\ &= (p_1 \cdot p_2)^2 - m_1 m_2. \end{aligned} \quad (\text{A.32})$$

Since from the kinematic $p_1 \cdot p_2 = m_N E_V$ and set $m_1 = m_V \approx 0$, $m_2 = m_N$, in the center of mass frame $\vec{p}_1 = -\vec{p}_2$ we obtain the following relation

$$E_{CM}^2 |\vec{p}_1|^2 = m_N^2 E_V^2. \quad (\text{A.33})$$

Hence, the general form of the differential cross-section becomes

$$\frac{d\sigma}{dT} = \frac{\langle |\mathcal{M}^2| \rangle}{32\pi m_N E_V^2}. \quad (\text{A.34})$$

CURRICULUM VITAE

The author was born in Ujung Pandang (now Makassar), South Sulawesi Indonesia. After finishing his undergraduate degree at the Department of Physics, Hasanuddin University, he spent one year as a lecture assistant at the same university. During the undergraduate degree, he became the best student at the Faculty of Mathematics and Natural Sciences. He had chosen as one of the university's delegations to Hiroshima University for a short course. He attends two particle physics school at the University of Malaya, Malaysia and Chulalongkorn University, Thailand. He spent three months short study at the Center of Physics Research at the Indonesian Institute of Sciences (LIPI). For his master degree, he has been awarded a fully-funded scholarship from the Turkish government by the YTB program at Karadeniz Technical University. During the master program, he participated in two short courses: Istanbul Theoretical Physics Days (Mimar Sinan Fine Arts University) and School of Computer Applications in Particle Physics (Istanbul University). He also contributes to three conferences: The 36th International Physics Conference (Turkish Physical Society); Beyond Standard Model: From Theory to Experiment, BSM-2021 (Zewail City of Science and Technology, Sabanc University); The 28th International Workshop on Weak Interactions and Neutrinos, WIN2021 (University of Minnesota). During his master level, the author contributed in four SCI publications. He knows Bahasa Indonesia, English, Turkish, and Bahasa Bugis.